Experimental Analysis of Bed Load Sediment Motions Using High-Speed Imagery in Support of Statistical Mechanics Theory

By

Siobhan L. Fathel

Dissertation

Submitted to the Faculty of the

Graduate School of Vanderbilt University

in partial fulfillment of the requirements

for the degree of

DOCTOR OF PHILOSOPHY

in

Environmental Engineering

December, 2016

Nashville, Tennessee

Approved:

David J. Furbish, Ph.D.

James H. Clarke, Ph.D.

George M. Hornberger, Ph.D.

Calvin F. Miller, Ph.D.

To Austin, who has followed and supported me on this journey.

ACKNOWLEDGMENTS

This work would not have been possible without the support and guidance of so many wonderful people. First, I would like to thank my advisor, David Jon Furbish, who strengthened my love of science, provided direction and guidance for this thesis, and helped make this project something that I am truly proud of. I owe him heaping piles of gratitude! Special thanks to Stacey Worman, who not only helped to provide a solid foundation, modeling wizardry, and thoughtful insights for this thesis, but who also spent a week, shrub-diving and rattler-dodging, in the field with me. Furthermore, I'd like to thank all the predecessors on this project, your valuable insights, work, and discoveries made my work possible.

On a more personal note, I'd like to thank my closest friends and family members for listening to frequent (and sometimes long-winded) descriptions of my work, your support is something I truly appreciate. I would like to especially thank my mother and sister for truly embracing my science-nerd side. Also, to everyone who provided a listening ear or bounced ideas around with me- Thank you.

In large part my success is strongly tied to my working environment. It is for this reason that I would like to thank the EES faculty, students, and staff, who have made the last two years a truly cool and special place to work. In particular, I'd like to thank my fellow graduate students for fun distractions, intellectual conversations, and steadfast support.

And finally, this work would not have been possible without the support of Vanderbilt University, the Earth and Environmental Sciences department, the Civil and Environmental Engineering Department, and funding provided by a National Science Foundation grant #EAR0744934.

TABLE OF CONTENTS

LIST OF TABLES

LIST OF FIGURES

CHAPTER 1

Introduction

1.1 Overview and Motivation

Bed load sediment transport in turbulent shear flows is a topic with broad implications for problems in ecology, river geomorphology, and river engineering. Sediment transport is an essential component of bed form development and, more generally, river morphodynamics. Despite the importance of this topic, we do not fully understand how sediment moves. Bed load sediment transported within a turbulent shear flow experiences complex motions in response to forces associated with near-bed fluid motions, particle-particle interactions, and particle-bed interactions. These particles move in a combination of rolling, sliding, and low saltating motions. Given the complexity of coupled particle-fluid physics contributing to sediment transport, there is value in gaining a clearer understanding of sediment motions at the grain scale in relation to near-bed turbulence. Many current descriptions of bed load sediment transport largely involve semi-empirical formulations that attempt to relate sediment motions to macroscopic quantities such as the bed stress (e.g., *Stelczer*, 1981; *Seminara et al.*, 2002; *Parker et al.*, 2000a; *Lajeunesse et al.*, 2010). Numerous formulae of this type are available, but typically involve large uncertainties. These formulations tend to perform well only under controlled laboratory conditions and are difficult to apply to field conditions (e.g., *Wilcock*, 2001; *Frey and Church*, 2009). We turn to probabilistic descriptions of sediment transport as an alternative to current methods, with the aim of gaining a clearer understanding of the statistically expected particle behavior.

Bed load transport is inherently a stochastic process (*Paintal*, 1971; *Nikora et al.*, 2002; *Furbish et al.*, 2012a), which merits probabilistic descriptions of sediment motions. We cannot predict the motion of an individual particle, but we can expect to gain a clearer understanding of statistically expected particle behavior based on high-resolution experi-

mental measurements. We build on ideas first presented by *Einstein* (1937, 1942, 1950), wherein we adopt concepts and language from probability to describe bed load particle motions and transport. Indeed, there has been a recent, renewed interest in probabilistic descriptions of bed load particle motions pertaining to the ingredients of the particle flux (e.g., *Parker et al.*, 2000b; *Ancey*, 2010; *Furbish et al.*, 2012a,b; *Furbish and Schmeeckle*, 2013; *Ancey and Heyman*, 2014; *Armanini et al.*, 2014; *Heyman et al.*, 2014) as well as the behavior of tracer particles (e.g., *Nikora et al.*, 2002; *Schumer et al.*, 2009; *Foufoula-Georgiou and Stark*, 2010; *Bradley and Tucker*, 2010; *Ganti et al.*, 2010; *Voller and Paola*, 2010; *Hill et al.*, 2010; *Ball*, 2012; *Martin et al.*, 2014; *Lajeunesse et al.*, 2013; *Hassan et al.*, 2013; *Pelosi et al.*, 2014; *Martin et al.*, 2014). This renewed interest by the scientific community in recent years has been combined with advances in laboratory measurement techniques. Namely, the use of high-speed videos of particle motions has allowed for increased resolution in the measurement of sediment particle motions (*Lajeunesse et al.*, 2010; *Roseberry et al.*, 2012; *Martin et al.*, 2012; *Radice et al.*, 2013; *Campagnol et al.*, 2013; *Heyman et al.*, 2014; *Ancey and Heyman*, 2014). These data allow for an improved understanding of bed load sediment motions and transport. However, even with advances in imaging, we still lack macroscopic descriptions of sediment transport that are consistent with features of particle scale motions. Probabilistic theories are emerging, but these need to be supported by detailed observations.

Of particular interest to us is the possibility of integrating certain concepts from classical statistical mechanics into probabilistic descriptions of bed load particle motions and transport. I will use data sets from experiments, which are incomparable in terms of precision, resolution, and the total number of observations of particle motions, to support this probabilistic approach. Herein, I build on the work of *Ancey et al.* (2006), *Ancey and Heyman* (2014), *Furbish et al.* (2012a,b), and *Furbish and Schmeeckle* (2013), wherein the authors provide a foundation to apply ideas from statistical mechanics to describe sediment behavior, where the details of sediment motions are revealed by high speed imagery.

Within this context, the work acts as a step to better define the probabilistic behavior of sediment transport, and thereby contributes to a broader theory to describe expected particle behaviors for specific bed and flow conditions.

1.2 Structure of Dissertation

The chapters of this dissertation are written as standalone manuscripts, with the exception of this chapter (Chapter 1), which serves as an introduction, and the final chapter (Chapter 5), which provides a summary of the findings within this dissertation and offers ideas for future work. The manuscript-style chapters (2 through 4) address three primary aspects of bed load sediment transport. (1) We characterize the underlying ensemble distributions of key measures of particle motions (particle velocities, accelerations, hop distances, and travel times) from measurements obtained from high speed imagery, in order to better inform the stochastic process of bed load sediment transport. (2) We then work to reinforce and elaborate key elements of previous results reported by *Furbish et al.* (2012c) and *Furbish et al.* (2012b). Specifically, we apply several methods to determine the nature of bed load particle diffusion using sizable data sets. (3) Finally, we analyze patterns and controls on sediment entrainment and disentrainment. Here we focus on sediment entrainment and disentrainment in relation to near-bed fluid velocity measurements. Throughout this dissertation, I use a probabilistic approach to describe the processes that control sediment motions, the entrainment and disentrainment of sediment particles, and the associated patterns of particle motions in relation to turbulence structures. Specific objectives and findings from Chapters 2 through Chapter 4 are described below.

Chapter 2 presents the work reported in *Fathel et al.* (2015), which uses a high-resolution data set of particle motions to define the forms and qualities of the ensemble distributions of particle velocities, accelerations, hop distances and travel times. The size and resolution of the data sets presented in this chapter allow us to confidently describe the forms and qualities of the ensemble distributions of these particle motions under specific experimen-

tal conditions. The autocorrelation functions of frame-averaged values (and the decay of these functions) support the idea that the forms of these distributions become time-invariant within the five second imaging interval. Additionally, we consider the effects of experimental censorship associated with a finite sampling window and show that the experimental results may indeed be biased by the window size. Overall, these ensemble distributions best represent the probabilistically expected behavior of particle motions consistent with the macroscopic sediment and flow conditions, and thus provide a clear target for further analyses of transport, including statistical mechanics theory and numerical simulations.

In Chapter 3, we investigate the diffusive contribution to the sediment flux, as elaborated in *Fathel et al.* (2016). The start-and-stop motions of sediment particles on a streambed mimic aspects of the Einstein-Smoluchowski description of the random-walk motions of Brownian particles, where particles diffuse normally. However, recent work suggests that the spreading rate of sediment particles differs from Brownian behavior. We use measurements of particle motions obtained from high-speed imaging of bed load transport to demonstrate that conventional measures of particle spreading reveal different attributes of bed load particle behavior depending on details of the calculation. We find ballistic-like behavior at the shortest (10^{-2} s) timescale, followed by apparent anomalous behavior due to correlated random walks in transition to normal diffusion ($>10^{-1}$ s) — similar to Brownian particle behavior but involving distinctly different physics. However, when treated as a 'virtual plume' over this timescale range, particles exhibit inhomogeneous diffusive behavior because both the mean and the variance of particle travel distances increase nonlinearly with increasing travel times, a behavior that is unrelated to anomalous diffusion or to Brownian-like behavior. Our results indicate that while there are similarities between bed load transport and Brownian systems, care is needed in suggesting anomalous behavior when appealing to conventional measures of diffusion formulated for ideal particle systems.

Chapter 4 acts to provide a clearer understanding of the transport and spreading be-

havior of bed load particles and tracers by providing detailed descriptions of key features associated with the processes of particle entrainment and disentrainment. Here we address the "initial motion problem" by analyzing the initial direction and magnitude of activated particles along with the spatial distribution of entrainment. We also provide an analysis of simultaneous measurements of near-bed fluid velocities and particle motions, which indicates that fluid velocities are not necessarily higher near entrainment events. This further suggests that the connection between the fluid and particle entrainment is complex and will require attention to detail to better define this relationship. Furthermore, the high resolution of the data presented, which contains positions of particles measured start-to-stop, allows us to measure the distributions of particle wait times (the duration of time between successive particle motions in an area) and of particle rest times (the duration of time between the disentrainment of a particle and the reentrainment of that particle). Wait times in combination with the particle entrainment determines the intensity of transport. In turn, rest times, following disentrainment, bear on descriptions of particle spreading during transport. More specifically, particle disentrainment determines the distance that particle move following entrainment, that is, the distribution of hop distances, and together with intervening rest times, influence the virtual velocity and spreading of tracer particles. This work provides an important step towards empirically defining the distribution of rest times, yet we also highlight the experimental limitations of these measurements. The combination of the work contained in this chapter acts to highlight and reveal important aspects of the mechanical behavior of particles during entrainment and disentrainment, and ultimately shows that these processes involve more than 'starting' and 'stopping'. At the time of writing this dissertation this manuscript is "in preparation" (*Fathel et al.*, in prep.).

In addition to these chapters, I have contributed substantively as coauthor on two separate published papers, and one manuscript, that are closely related to the material presented in this dissertation, and which make use of the data sets described below. The first paper (*Furbish et al.*, 2016a) concerns theoretical aspects of the entrainment form of the particle

flux and the Exner equation, and appeals to the ensemble distributions of particle motions described in Chapter 2, specifically the relationship between particle hop distances and travel times. The second paper (*Furbish et al.*, 2016b) builds directly from my work presented in Chapter 2. We describe the most likely forms of the probability distribution of bed load particle velocities, accelerations, hop distances and travel times based on E. Jayness principle of maximum entropy — honoring mechanical and kinematic constraints imposed by equilibrium transport conditions — to show that the most likely distributions are consistent with the distributions reported in Chapter 2. We also have prepared a paper for publication (*Furbish et al.* in prep.) that places concepts raised in Chapter 3 concerning bed load sediment diffusion within a broader context. This manuscript is written as a "State of Sciences" article for the journal Earth Surfaces Processes and Landforms, and therefore provides a more general description of the essential elements of particle diffusion during sediment transport, clarifying important details not usually covered in descriptions of diffusive behavior in sediment systems.

CHAPTER 2

Experimental Evidence of Statistical Ensemble Behavior in Bed Load Sediment Transport

2.1 Abstract

A high-resolution data set obtained from high-speed imaging of coarse sand particles transported as bed load allows us to confidently describe the forms and qualities of the ensemble distributions of particle velocities, accelerations, hop distances and travel times. Autocorrelation functions of frame-averaged values (and the decay of these functions) support the idea that the forms of these distributions become time-invariant within the five second imaging interval. Distributions of streamwise and cross-stream particle velocities are exponential, consistent with previous experiments and theory. Importantly, streamwise particle velocities possess a "light" tail, where the largest velocities are limited by near-bed fluid velocities. Distributions of streamwise and cross-stream particle accelerations are Laplace in form and are centered on zero, consistent with equilibrium transport conditions. The majority of particle hops, measured start-to-stop, involve short displacements, and streamwise hop distances possess a Weibull distribution. In contrast to previous work, the distribution of travel times is exponential, consistent with a fixed temporal disentrainment rate. The Weibull distribution of hop distances is consistent with a decreasing spatial disentrainment rate, and is related to the exponential distribution of travel times. By taking into account the effects of experimental censorship associated with a finite sampling window, the relationship between streamwise hop distances and travel times, $L_x \sim T_p^{\alpha}$, likely involves an exponent of $\alpha \sim 2$. These experimental results — an exponential distribution of travel times T_p and a Weibull distribution of hop distances L_x with shape parameter $k < 1$ — are consistent with a nonlinear relationship between these quantities with $\alpha > 1$.

2.2 Introduction

Sediment particles transported as bed load within a turbulent shear flow experience complex motions in response to forces exerted on them by near-bed fluid motions, and in response to forces associated with particle-particle interactions and particle-bed interactions. Individual particle motions involve combinations of rolling, sliding and low saltations. Particles hops — measured start-to-stop — may be brief and short, involving displacements of only one or a few particle diameters, or involve relatively long displacements during which particles experience a few to tens of collisions with the bed between the onset and cessation of motion, or consist of motions intermediate to these. Some particles may move upstream.

When viewed at timescales longer than that associated with the ballistic-like behavior of particles between successive particle-bed collisions (*Nikora et al.*, 2002; *Furbish et al.*, 2012b), bed load particle motions are inherently stochastic. Herein, probabilistic descriptions of bed load particle motions and transport, building from ideas introduced by *Einstein* (1937, 1942, 1950), become valuable inasmuch as the concepts and language of probability are particularly well suited to the problem of describing these motions. Indeed, there has been a recent, renewed interest in probabilistic descriptions of bed load particle motions pertaining to the ingredients of the particle flux (e.g., *Parker et al.*, 2000b; *Ancey*, 2010; *Furbish et al.*, 2012a,b; *Ancey and Heyman*, 2014; *Armanini et al.*, 2014; *Heyman et al.*, 2014; *Heyman*, 2014) as well as the behavior of tracer particles (e.g., *Nikora et al.*, 2002; *Schumer et al.*, 2009; *Foufoula-Georgiou and Stark*, 2010; *Bradley and Tucker*, 2010; *Ganti et al.*, 2010; *Voller and Paola*, 2010; *Hill et al.*, 2010; *Ball*, 2012; *Martin et al.*, 2012; *Lajeunesse et al.*, 2013; *Hassan et al.*, 2013; *Pelosi et al.*, 2014; *Martin et al.*, 2014). This effort is aimed at a deeper understanding of the transport of sediment and sediment-borne substances, the influence of stochastic motions on bedform evolution, and, in turn, the effect of changes in streambed elevation on tracer particle motions. In addition, new measurement techniques, including high-speed imaging, are providing an unprecedented opportunity to observe and measure particle motions, and to test and constrain theories of particle be-

havior during transport, including advanced numerical renditions of this behavior (e.g., *Schmeeckle*, 2014a,b; *Kidanemariam and Uhlmann*, 2014).

Of particular interest to us is the possibility of integrating certain concepts from classical statistical mechanics into probabilistic descriptions of bed load particle motions and transport. As outlined in *Furbish et al.* (2012a) and *Furbish and Schmeeckle* (2013), this effort is aimed at describing the probabilistically expected behavior of particles, subject to mechanical constraints imposed on the particle system. A central element of this approach involves appealing to the idea of ensemble behavior, wherein we envision an ensemble of configurations of particle positions and velocities, much as *Gibbs* (1902) described for gas particles. To be clear, 'ensemble behavior' is not to be misinterpreted as the collective behavior of a group (an 'ensemble') of particles. Rather, 'ensemble' refers to the statistical mechanics idea of a Gibbs-like ensemble of independent but nominally identical systems of particles, so that 'ensemble behavior' means the statistically expected states of particles as reflected by the forms and moments of the distributions of these states measured over the ensemble — an idea that we elaborate in Section 2. The approach then focuses on the ensemble distributions of particle velocities, accelerations, hop distances and associated travel times as a basis for describing ingredients of, say, the particle flux or particle diffusion, notably pertaining to the rarefied (versus continuum) conditions that occur at low to moderate transport stages (*Schmeeckle and Furbish*, 2007; *Furbish and Schmeeckle*, 2013; *Heyman et al.*, 2014; *Heyman*, 2014). Of critical importance in support of this approach are experimental measurements of particle motions that can be used to reveal, with high fidelity, the forms and parametric values of these distributions, together with associated levels of particle activity (the number of particles in motion per unit streambed area).

The experiments reported by *Roseberry et al.* (2012) involving high-speed imaging of particle motions under four different transport stages provided important initial insights regarding details of particle motions and activity pertaining to ensemble behavior. As noted by *Furbish et al.* (2012b), however, these measurements were not entirely satisfactory. Sev-

eral of the sets of measurements had sufficiently large imaging windows to sample a suite of particle hop distances, but suffered from short sampling times. In contrast, several of the sets of measurements involved sufficient sampling times, but suffered from small imaging windows. Keeping this in mind, the experimental data indicated that the distributions of streamwise and cross-stream particle velocities are exponential, and that the probability distribution of streamwise velocities has a "light" tail. The results also suggested that hop distances vary nonlinearly with associated travel times. Furthermore, the measurements indicated that the particle activity exhibits quasi-periodic variations over multiple timescales, a behavior that is related to turbulent sweep events as well as higher frequency variations that reflect the response of particles to small-scale near-bed turbulence and particle-bed interactions (see auxiliary video of particle motions). The measurements, involving sub-pixel resolution of particle displacements, importantly revealed that particle motions are dominated by small displacements and small velocities, and moreover, that particle motions are intrinsically periodic (*Furbish et al.*, 2012b).

The purpose of this paper is to reinforce, and elaborate, key elements of the measurements and results reported by *Roseberry et al.* (2012), and to clarify uncertain results presented therein. Specifically, we present results from an unusually large, high-quality data set obtained from tracking individual particle motions from the high-speed imaging of five consecutive seconds of bed load sediment transport. This rich data set provides the basis for defining the underlying forms of the ensemble distributions of particle motions, in particular, the distributions of streamwise and cross-stream particle velocities and accelerations, and the distributions of particle hop distances and associated travel times. We appeal to features of the autocorrelation functions of frame-averaged values to suggest that these distributions quickly approach their time-invariant (ensemble) forms compatible with the experimental conditions. Similar to the experimental results of *Lajeunesse et al.* (2010) and *Roseberry et al.* (2012), we find that the probability density functions of both the streamwise and cross-stream velocities have exponential forms. The data set allows us to confirm

that the streamwise velocity distribution possesses a "light" tail, consistent with the idea that the largest particle velocities are limited by the magnitude of near-bed fluid velocities (*Roseberry et al.*, 2012; *Furbish and Schmeeckle*, 2013; *Schmeeckle*, 2014b). The distributions of the streamwise and cross-stream particle accelerations are Laplace in form and are centered on zero, consistent with the concept of equilibrium transport (*Furbish and Schmeeckle*, 2013). The data also reveal that the probability density $f_{L_x}(L_x)$ [L^{-1}] of particle hop distances L_x [L] has the form of a Weibull distribution that is physically related to the exponential form of the associated density $f_{T_p}(T_p)$ [T^{-1}] of travel times T_p [T]. A plot of measured values of L_x versus T_p represents a sample drawn from the joint probability distribution $f_{L_x,T_p}(L_x,T_p)$. On average L_x varies with T_p as $L_x \sim T^{\alpha}$. Whereas *Roseberry et al.* (2012) suggested that $\alpha \sim 5/3$, a value reproduced by the simulations of *Fan et al.* (2014), here we illustrate that this value likely reflects bias due to experimental censorship (e.g., *Furbish et al.*, 1990) associated with the sampling window size, and that more likely $L_x \sim T_p^2$.

As described in the Methods and Measurements section below, our measurements of particle motions (particle tracking) are quite laborious, given the level of precision to which we aspire. Indeed, one of our points in the Conclusions section involves an appeal for improving automated (high-fidelity) particle-tracking methods. Whereas we report one set of measurements here, we note that our results and conclusions are entirely consistent with those pertaining to a second set of measurements involving a higher transport stage, for which we have simultaneous measurements of near-bed fluid velocities (to be reported separately). Given the significance of the idea of ensemble distributions of quantities describing particle motions (i.e., particle velocities, accelerations, hop distances and travel times), we start by elaborating the idea of a sediment particle ensemble, adding key points to previous descriptions (*Furbish et al.*, 2012a; *Furbish and Schmeeckle*, 2013).

2.3 Theoretical Basis of Ensemble Distributions of Particle Velocities, Hop Distances and Travel Times

As described in *Furbish et al.* (2012a) and *Furbish and Schmeeckle* (2013), we start by envisioning an ensemble of particle configurations and velocities in a manner similar to that outlined by *Gibbs* (1902) for gas particle systems. As *Kittel* (1958) notes... "The scheme introduced by Gibbs is to replace *time averages* over a single system by *ensemble averages*, which are averages at a fixed time over all systems in an ensemble... It may be argued, as Tolman (*Tolman*, 1938) has done, that the ensemble average really corresponds better to the actual situation than does the time average." Specifically, we envision bed load particles moving over an area B on a streambed subjected to steady macroscopic flow conditions, and assume that the streambed is planar (e.g., *Lajeunesse et al.*, 2010; *Roseberry et al.*, 2012), albeit possibly involving small, stationary fluctuations in elevation (e.g., *Wong et al.*, 2007). Here we are focusing on motions of particles that are entrained from the streambed and then return to it after traveling some distance. Thus, of particular interest are motions measured parallel to the surface; of less concern are the details of motions normal to the surface. This is intrinsically a two-dimensional problem.

We initially choose B to be sufficiently large that, during any small interval of time $\mathrm{d}t$, any difference in the number of particles leaving B and the number arriving is negligibly small relative to the total number N_a of active particles within B. Similarly, any difference in the number of particles that stop and start within B during $\mathrm{d}t$ is negligibly small relative to the total number N_a. Then, N_a may be considered fixed from one instant to the next. We now envision all possible instantaneous configurations of the N_a active particles as defined by their xy-coordinate positions within B at a fixed time, with the understanding that this set of configurations need not represent the same set of particles, only that N_a is fixed. This imagined set of possible configurations constitutes an ensemble of active particle positions. Moreover, each active particle in each possible configuration possesses an instantaneous velocity $\mathbf{u}_p = \mathbf{i}u_p + \mathbf{j}v_p$. We now envision the ensemble as consisting of

all possible instantaneous states defined by the joint occurrence of particle positions and velocities u_p and v_p.

Here we emphasize that each instantaneous state satisfies the physics of coupled fluid-particle motions compatible with the macroscopic flow conditions. Let us therefore imagine randomizing the time series of particle states in order to remove any temporal correlation in particle configurations and velocities from one instant to the next. At this point we may imagine that each of the states represents an instant in an independent system subjected to the same macroscopic flow conditions. Indeed, we may imagine that the great number of states represents a great number of independent but nominally identical systems at a fixed time, in which case the ensemble of configurations and velocities is like that envisioned by Gibbs. To be clear, we are referring to an ensemble of systems, not an ensemble of particles nor, as yet, an ensemble distribution. As Kittel [1958, p. 8] notes, "The word *ensemble* is used in a special sense in statistical mechanics, a sense unrecognized by most lexicologists."

Focusing on particle velocities, suppose that we calculate the average streamwise velocity of the N_a active particles for each member of the ensemble, then, in turn, calculate the "grand" average of these averages. This is an ensemble averaged velocity (e.g., *Kittel*, 1958). Let us now reassemble the members of the ensemble into their original serial order. We can again calculate the average streamwise velocity of the N_a active particles at each instant in the time series, then, in turn, calculate the grand average of these averages. This is a time averaged velocity. But noting that we are using the same average for each of the systems in both calculations, by definition the time average is equal to the ensemble average. Hence, we are in this example justified in concluding that the ergodic hypothesis is satisfied (e.g., *Tolman*, 1938). Also note that we are interested in higher statistical moments, for example, the variance of the particle velocities. Such moments are statistically expected (averaged) quantities, so this example concerning ensemble and time averages also applies to the calculation of these higher moments.

We also are interested in the distribution of particle velocities. This distribution may vary from one member of the ensemble to another. Our objective, therefore, is to describe the most probable velocity states of the particles compatible with the extant fluid-particle physics, leading to the ensemble distribution of velocities whose moments coincide with the expected ensemble values (*Furbish and Schmeeckle*, 2013). In this point of view, each member of the ensemble represents a sample drawn from the ensemble distribution. Moreover, the form of each distribution and its parametric quantities, being consistent with the physics of coupled fluid-particle motions, therefore are considered to be a signature of the transport process for specified sediment and macroscopic flow conditions.

We now broaden our view of an ensemble of independent systems at a fixed time to one that allows these systems to evolve over a specified period. This is important for conceptualizing an ensemble involving quantities that are not instantaneous, namely, particle hop distances and associated travel times. Specifically, we envision an ensemble of independent systems wherein particle motions begin within an area $b\mathrm{d}x$ during the interval from t to $t+\mathrm{d}t$ at the fixed time t, allowing each independent system to evolve long enough for the N particles starting during $\mathrm{d}t$ to complete their motions. As in the example above involving particle velocities, we may consider this set of travel distances L_x for each system as being a sample of size N drawn from an ensemble distribution $f_{L_x}(L_x)$. For a given width b, N varies from one system of the ensemble to the next. Moreover, in general any one sample has the appearance of an irregular histogram of hop distances rather than a smooth distribution. Then, upon collecting all such samples from all members of the ensemble and pooling them, the resulting distribution converges to its ensemble form. Or, with respect to time, we may imagine letting an individual system evolve. During successive intervals $\mathrm{d}t$, successive sets of N particles begin their hops from within $b\mathrm{d}x$, each set leading after a period of time to a histogram of travel distances L_x. Assuming the process acting on the particles does not change over time, then with sufficient time T we may assume the accumulated samples converge to the ensemble distribution $f_{L_x}(L_x)$, which is invariant with respect to

time. Similarly we may assume these accumulated samples yield the ensemble distribution $f_{T_p}(T_p)$ of travel times T_p. As with ensemble distributions of instantaneous quantities (e.g., velocities), these ensemble distributions are to be considered a signature of the transport process for specified sediment and macroscopic flow conditions.

For reference below we can relate this idea of an ensemble distribution of hop distances and associated travel times to instantaneous quantities. Specifically, let t_p [T] denote the travel time ('age') of a particle measured from the instant that its motion begins, and let $l_x(t_p)$ [L] denote the associated travel distance. If $f_{t_p}(t_p,t)$ [T^{-1}] denotes the probability distribution of particle ages t_p at time t, then at any instant conservation of probability requires that

$$\frac{\partial f_{t_p}(t_p,t)}{\partial t} = -\frac{\partial f_{t_p}}{\partial t_p} - D_f\,, \tag{2.1}$$

which is a simple rendering of the Master equation, a general expression of conservation of probability (Appendix A). The first term on the right side describes 'advection' of probability over the domain t_p due to particle aging at a rate $\mathrm{d}t_p/\mathrm{d}t = 1$, and D_f [T^{-2}] denotes a 'failure rate' associated with deposition of particles with age $t_p = T_p$; note that D_f may be a function of t_p or f_{t_p}, or both. Note that $t_p \leq T_p$ and $l_x \leq L_x$, where $t_p \longrightarrow T_p$ and $l_x(T_p) \longrightarrow L_x$ only when motion ceases. With steady conditions where entrainment and deposition are balanced, then at any fixed time, $\mathrm{d}f_{t_p}/\mathrm{d}t_p = -D_f$. The solution of this requires a fixed boundary condition $f_{t_p}(0) = E_f$ [T^{-1}] associated with steady entrainment of particles with starting age $t_p = 0$. Moreover, in this situation $f_{t_p}(t_p) \rightarrow f_{T_p}(T_p)$ represents the distribution of expected age states of the particles compatible with the extant fluid-particle physics, that is, the ensemble distribution of particle travel times. By a similar development we may assert that the steady distribution $f_{l_x}(l_x) \rightarrow f_{L_x}(L_x)$ represents the ensemble distribution of hop distances. These quantities are jointly distributed as $f_{L_x,T_P}(L_x,T_p)$.

There is a practical task of estimating, from experimental measurements, the forms and parametric values of ensemble distributions. To do this we must appeal to the ergodic hypothesis to assess whether the estimated distributions represent ensemble distributions. The

key is determining whether the measured time series of quantities characterizing particle motions are of sufficient duration that estimated distributions are approximately time invariant. As described below (Section 2.4), our principal diagnostics involve assessing whether time series of frame-averaged quantities are approximately stationary, and whether the total sampling time exceeds the time in which the autocorrelation function decays to zero for these quantities.

Note that sediment transport involves a significant serial correlation in motions as turbulent flow structures move over the bed. We expect that when persistence (i.e., memory or temporal correlation) is present in the time-series data, statistical convergence generally requires a larger sample size (more frames) relative to the convergence time of a weakly correlated series.

2.4 Methods and Measurements

The experimental data presented here were collected in the River Dynamics Laboratory at Arizona State University using an 8.5×0.3 m recirculating flume. Flow velocities were measured using an acoustic Doppler velocimeter (ADV) positioned approximately 1 cm above the bed. As reported by *Roseberry et al.* (2012) and *Furbish et al.* (2012b), these experiments involved four flow conditions. (The Froude number varied from 0.30 to 0.35, and the Shields number varied from 0.034 to 0.063.) Here we present a reanalysis of Run 3, in which the time-averaged velocity near the bed was 31.0 cm sec^{-1} with a flow depth of 12.5 cm. The bed material used in this experiment is a uniform, coarse sand with an average diameter D_{50} of 0.05 cm. The stream bed was prepared by smoothing it flat prior to the start of the experiment.

The sediment bed is photographed through a plexiglass "sled" window placed on the surface of the water. This provides a clear view of the bed, preventing distortion of the images caused by light refraction from fluctuations in the water surface. The flow is sufficiently deep that the plexiglass window does not interfere with the flow at the bed surface.

The high-speed imagery captures an area of the sediment bed that is 7.57 cm long (streamwise) and 6.05 cm wide (cross-stream), with a corresponding resolution of 1280 $\times$ 1024 pixels. The set of images, taken at a rate of 250 frames per second, spans a total of 19.4 seconds (4912 frames). We analyzed five consecutive seconds (1250 frames) of the imagery, where virtually every moving particle was tracked.

Particle tracking was performed using the open-source software ImageJ. This involved marking the centroid of each particle as it moves through successive frames. ImageJ provides sub-pixel resolution of the centroid coordinates. The software records the pixel coordinates for each particle throughout the set of consecutive images as individual particle "tracks." The pixel coordinates from each particle track were then converted into streamwise x_p [L] and cross-stream y_p [L] coordinate positions. Within the video, approximately 95% of the particles in motion were tracked, amounting to more than 150,000 unique spatial positions from more than 10,000 active particles. The 5% of particles that were not tracked either left the field of view early or proved too difficult to follow through the course of the video. Particle hops, counted only if the particles started and stopped within the field of view, represent a subset ($\sim$65%) of the tracked motions.

Particles were tracked only after they began to move. We did not track the motions of particles that "wiggled" back and forth within their pockets, but otherwise did not move or hop. All particle motions were manually tracked by one individual to maintain consistency. This manual method provides accurate measurements of all motions without a bias towards short or long displacements. Individual hops were measured from incipient motion to a stopped position such that both streamwise and cross-stream velocities are zero. We also note that 0.4 seconds (100 frames) of imagery from this same experiment is presented as the data for Run R3B in *Roseberry et al.* (2012). Whereas we use these data for comparison to our own, we do not pool these data with the set described here.

2.5 Time Series of Features of Particle Motions

Here we describe the experimental time series of key features of particle motions (Figure 2.1) as context for our descriptions of the probability distributions of particle velocities, accelerations, hop distances and travel times presented in the next section. These series include: 1) the particle activity (the number of particles in motion within each frame); 2) the frame-averaged streamwise and cross-stream velocities of active particles; and 3) the frame-averaged streamwise and cross-stream accelerations of active particles. These quantities are based on all particle motions that occurred during the measurement period. Note that the 'instantaneous' velocity of an individual particle is estimated as the displacement between successive frames divided by the time interval (0.004 sec in this case), and its acceleration is similarly estimated by differencing successive velocities and dividing by the time interval. In addition we calculate the frame-averaged travel time ('age') and the frame-averaged travel distance of active particles, measured from the times and positions of initial motion. These quantities are based only on those particles ($N \sim 4,000$) that completed full hops (start-to-stop) within the imaging area. We also consider the autocorrelation functions (Figure 2.2) of these time series.

The particle activity fluctuates over more than an order of magnitude, from a low of about 20 particles to more than 330 particles, with an average of 118 and a coefficient of variation CV = 0.56 (Table 2.1). Consistent with previous measurements (e.g., *Roseberry et al.*, 2012; *Heyman and Ancey*, 2014), this series reflects the effects of patchy, intermittent turbulent sweeps and smaller structures over the scale of the imaging window, and the associated balance between entrainment and deposition, and the intervening travel times of particles (see auxiliary video). The fluctuations involve multiple frequencies, noticeably at approximately one-second intervals, and are reflected in the irregularly oscillating autocorrelation function (Figure 2.2). The time in which the autocorrelation function decays is several ($\sim$3) seconds. Note that, based on the birth-death Markov model of particle-bed exchanges provided by *Ancey et al.* (2008) involving particle entrainment with particle-bed

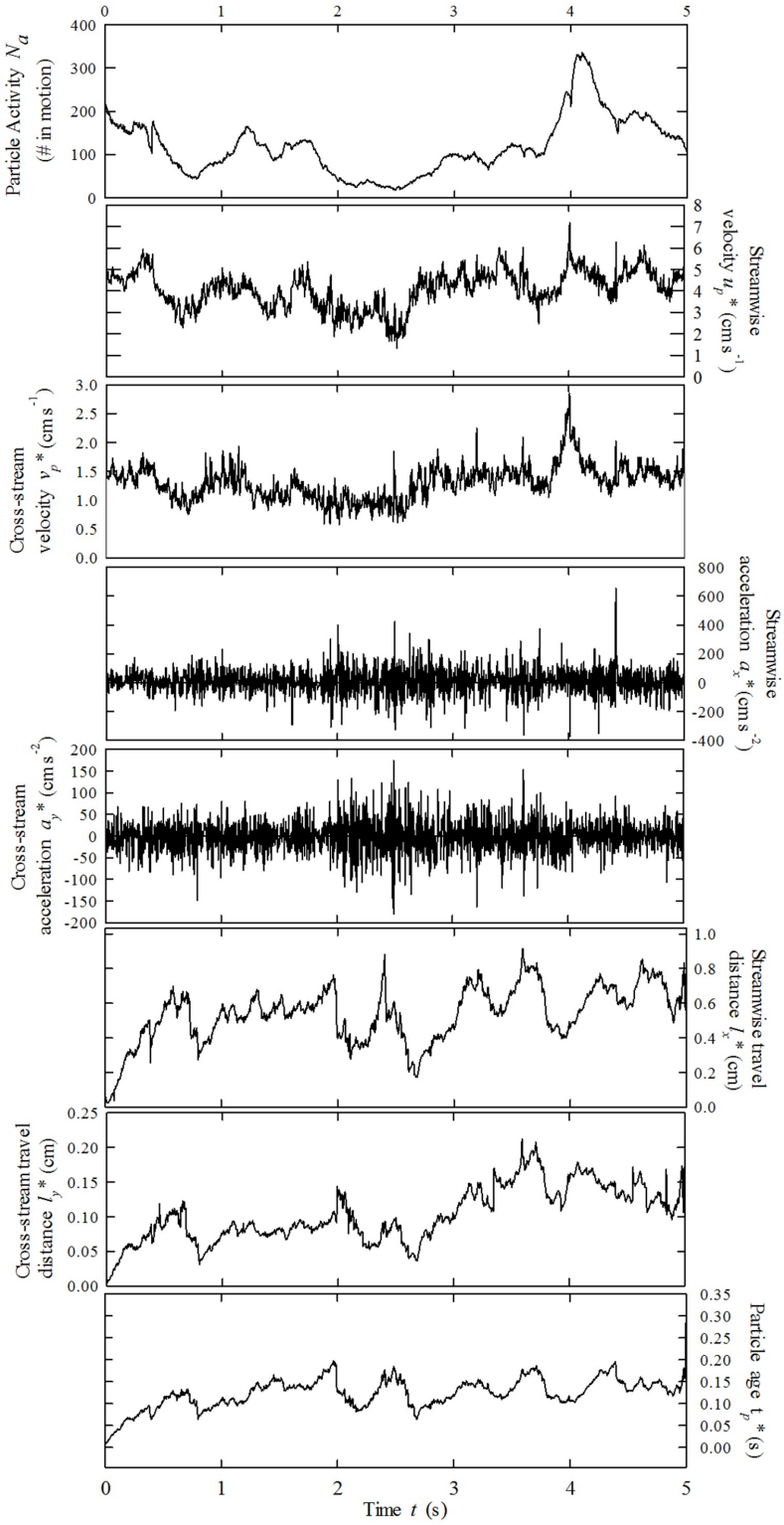

Figure 2.1: Time series of frame-averaged key particle motions.

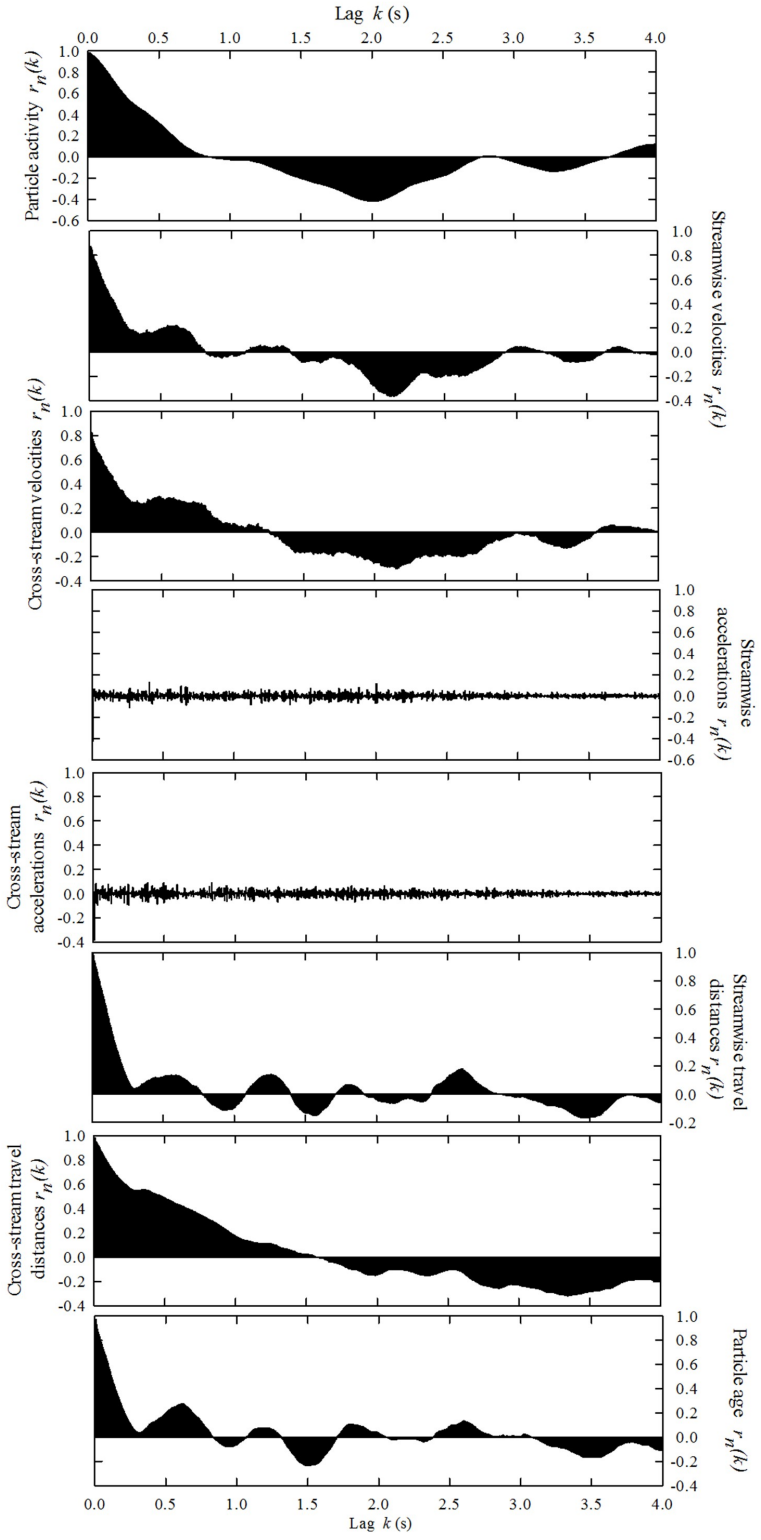

Figure 2.2: Autocorrelation functions of the frame-averaged time series presented in Figure 2.1.

collisions ('collective entrainment'), *Heyman* (2014) suggests that the variance of the activity systematically varies with window size in relation to the correlation length associated with particle-bed exchanges.

Note that the frame-averaged velocities and accelerations described next involve the particle activity. That is, these averages are based on the varying numbers of active particles.

Table 2.1: This table contains the minimum, maximum, mean, and standard deviation for each of the calculated quantities in Figure 2.1. The coefficient of variation is calculated as the ratio of the standard deviation to the mean.

	N_a	u_p^*	v_p^*	a_x^*	a_y^*	l_x^*	l_y^*	t_p^*
Minimum	17	1.33	0.58	246.09	140	0.023	0.005	0.008
Maximum	335	7.18	2.85	1195.39	524.88	0.98	0.21	0.34
Mean	118.08	4.08	1.30	557.76	263.51	0.54	0.10	0.12
St. Dev.	65.91	0.87	0.30	150.66	52.22	0.16	0.039	0.035
Coeff. Var.	0.56	0.21	0.23	0.27	0.20	0.30	0.38	0.28

The frame-averaged streamwise velocity and the frame-average of the magnitudes of cross-stream velocities each fluctuate by a factor of about four, with CV = 0.21 and CV = 0.23, respectively. These series co-vary with each other as well as with the particle activity, and involve high-frequency fluctuations superimposed on lower frequencies present in the activity series. The time it takes for the autocorrelation functions to decay to zero are similar to that of the particle activity.

In contrast, the frame-averaged streamwise and cross-stream particle accelerations are dominated by high-frequency fluctuations about zero means. The magnitudes of the streamwise and cross-stream accelerations have CV = 0.27 and CV = 0.20, respectively. The autocorrelation functions reveal that these effectively are white noise signals. At any instant, accelerations and decelerations are approximately balanced, and short-lived imbalances are quickly damped (*Furbish and Schmeeckle*, 2013). The averaged accelerations are relatively insensitive to the number of particles in motion. Note that our calculations of accelerations effectively represent a first-differencing of the velocities (e.g., *Box and Jenkins*, 1976), the

effect of which is to reduce serial correlation relative to that associated with the velocities.

The frame-averaged streamwise travel distance, the frame-average of the magnitudes of cross-stream travel distances, and the frame-averaged particle age, are all approximately stationary signals, and have CV = 0.30, CV = 0.38, and CV = 0.28, respectively. Notice that there is a lag of approximately 0.5 sec before each of these signals reaches a steady level following the start of the signal Figure 2.1. This lag reflects the growing travel distances and ages of the subset of motions representing complete hops early in the series as these converge to the average total hop distances and associated travel times. The fluctuations within the particle 'age' signal result from the balance between entrainment and disentrainment (and intervening particle aging). Here, the autocorrelation functions reveal that these series are much like the particle activity and frame-averaged velocities, in both the form and the time for the function to decay.

These time series and their autocorrelation functions indicate that the measurement interval of five seconds is sufficiently long to assert that the forms of the distributions of particle velocities, accelerations, hop distances and travel times, as described in the next section, are approximately time-invariant and representative of the ensemble conditions in the experiments. Of the series, the particle activity exhibits the strongest persistence. The variance is dominated by intermediate frequencies (relative to the record length); high-frequency fluctuations are notably absent in comparison with the other signals. We cannot guarantee that the experimental conditions do not involve lower frequency variations not sampled by the five-second record, which may influence the behavior of these time series. Nonetheless, for comparison a much longer (96 second) time series of streamwise velocity measurements using an acoustic Doppler velocimeter (50 Hz) at positions $\sim$1 cm above the bed possesses an autocorrelation function that decays well within (i.e., $\sim$2 s) a five second interval (as opposed to exhibiting a slowly decaying signature of a non-stationary signal). Inasmuch as the particle activity is responding to near-bed turbulence fluctuations, we therefore may assume that the autocovariance structure of this series is

reasonably steady and representative of the macroscopic flow conditions. Moreover, the autocorrelation functions of the other signals, with shorter decay times, are consistent with the idea that these features of sediment motions (particularly particle accelerations) become statistically steady relatively quickly. We also note that there are two dominant periodicities present within the first (lag) second of the autocorrelation functions of the velocities, travel distances, particle ages, and (more subtly) particle activity.

Longer time series could possibly lead to changes in the estimated parametric values of the distributions, but less likely in their forms, if these series involved lower-frequency variations, or strong intermittent variations, that are significantly different from the measured sampling interval. We suspect that this would be more likely for series (e.g., particle activity) with significant persistence than with series (e.g., particle accelerations) with little persistence — assuming steady macroscopic flow conditions.

2.6 Probability Distributions of Features of Particle Motions

2.6.1 Particle Velocities

The data presented here represent a large sample ($\sim$148,000) of particle velocities that occur under the flow conditions of the experiment. We pool the measurements for the streamwise velocities u_p and the cross-stream velocities v_p in the distributions presented below.

Streamwise particle velocities, neglecting the small proportion of small negative velocities, are well approximated by an exponential distribution (Figure 2.3), namely,

$$f_{u_p}(u_p) = \frac{1}{\overline{u_p}} e^{-u_p/\overline{u_p}} \qquad u_p \geq 0\,, \tag{2.2}$$

where $\overline{u_p}$ is the average velocity. This result is consistent with similar experiments (*Lajeunesse et al.*, 2010; *Roseberry et al.*, 2012) and with theory (*Furbish and Schmeeckle*, 2013). High velocity values fall below the exponential fit, and the highest measured values

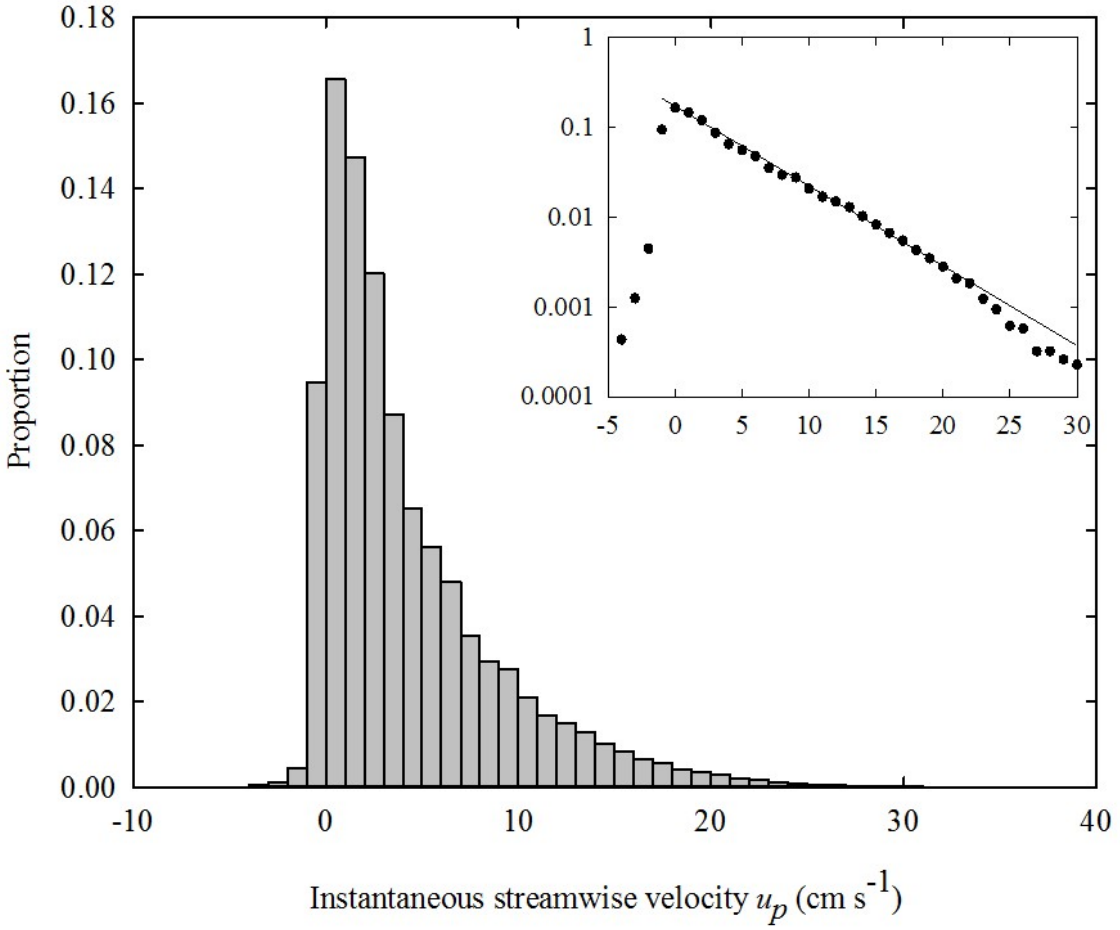

Figure 2.3: Discrete probability density of streamwise velocities u_p, and semi-log plot (inset) of probability density versus u_p, with straight-line fit to data illustrating exponential form of distribution.

(Figure 2.3) are less than the average fluid velocity measured by the ADV positioned 1 cm above the bed. The richness of this data set, including a significant number of values in the largest histogram bins, allows us to reinforce the idea that the streamwise velocity distribution indeed exhibits a light tail under these experimental conditions, and that near-bed fluid velocities act as a control on the maximum particle velocity, where particles generally do not move faster than the fluid (*Roseberry et al.*, 2012; *Furbish and Schmeeckle*, 2013).

This presence of a light tail, for physical reasons, means that the particle velocity distribution is not strictly exponential, as probability is repartitioned (in an unknown manner)

from the tail area to lower velocity states. For this reason we previously have correctly referred to this as being an 'exponential-like' distribution [*Roseberry et al.*, 2012; *Furbish and Schmeeckle*, 2013], although for simplicity we use the shorter wording in reference to this and other distributions.

The cross-stream velocity distribution is approximately symmetrical about $v_p = 0$ (Figure 2.4). The form of this distribution is a two-sided exponential distribution, or Laplace distribution (inset, Figure 2.4), with the form,

$$f_{v_p}(|v_p|) = \frac{1}{\overline{|v_p|}} e^{-|v_p|/\overline{|v_p|}}, \tag{2.3}$$

where $\overline{|v_p|}$ is the mean magnitude of the cross-stream velocity. This result also is consistent with previous measurements (*Lajeunesse et al.*, 2010; *Roseberry et al.*, 2012) and with theory (*Furbish and Schmeeckle*, 2013).

2.6.2 Particle Accelerations

Uniform, quasi-steady ('equilibrium') transport requires that the ensemble averaged particle acceleration be zero (*Furbish et al.*, 2012c; *Furbish and Schmeeckle*, 2013), which in turn means that the average force on the particles must equal zero. Specifically, if $f_{a_x}(a_x)$ [$\mathrm{L}^{-1}\ \mathrm{T}^2$] denotes the distribution of streamwise particle accelerations a_x [$\mathrm{L}\ \mathrm{T}^{-2}$], then

$$\int_{-\infty}^{\infty} a_x f_{a_x}(a_x)\, \mathrm{d}a_x = 0\,. \tag{2.4}$$

A similar expression pertains to the distribution $f_{a_y}(a_y)$ [$\mathrm{L}^{-1}\ \mathrm{T}^2$] of cross-stream accelerations a_y [$\mathrm{L}\ \mathrm{T}^{-2}$].

We plot the distributions of the streamwise (Figure 2.5) and cross-stream (Figure 2.6) particle accelerations a_x and a_y. The distributions are both centered on zero, such that the positive and negative accelerations are balanced. These distributions have a Laplace form,

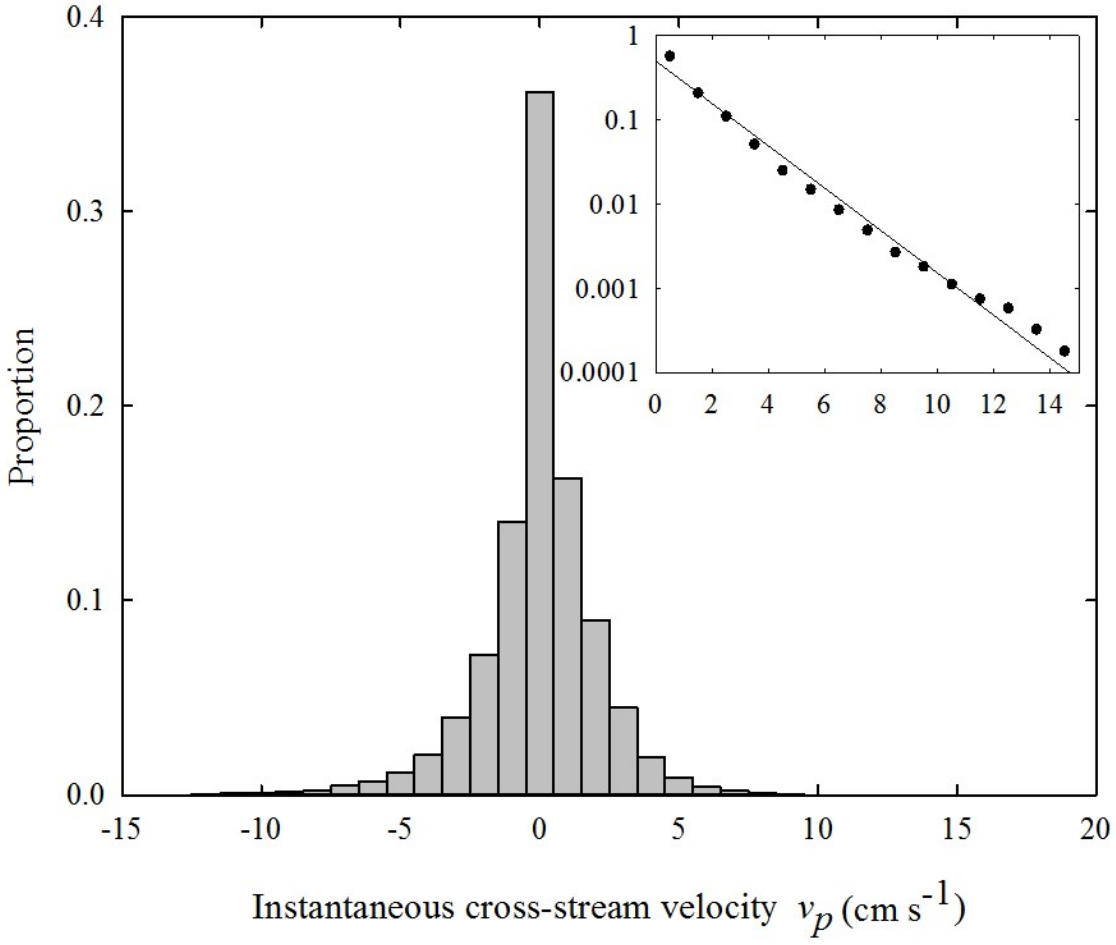

Figure 2.4: Discrete probability density of cross-stream velocities v_p, and semi-log plot (inset) of probability density versus $|v_p|$, with straight-line fit to data illustrating exponential form of distribution.

which, when expressed as a two-sided exponential distribution, is given by

$$f_{a_x}(|a_x|) = \frac{1}{\overline{|a_x|}} e^{-|a_x|/\overline{|a_x|}}, \tag{2.5}$$

where $\overline{|a_x|}$ is the mean magnitude of the streamwise acceleration. The magnitude of the cross-stream acceleration $|a_y|$ possesses a similar distribution.

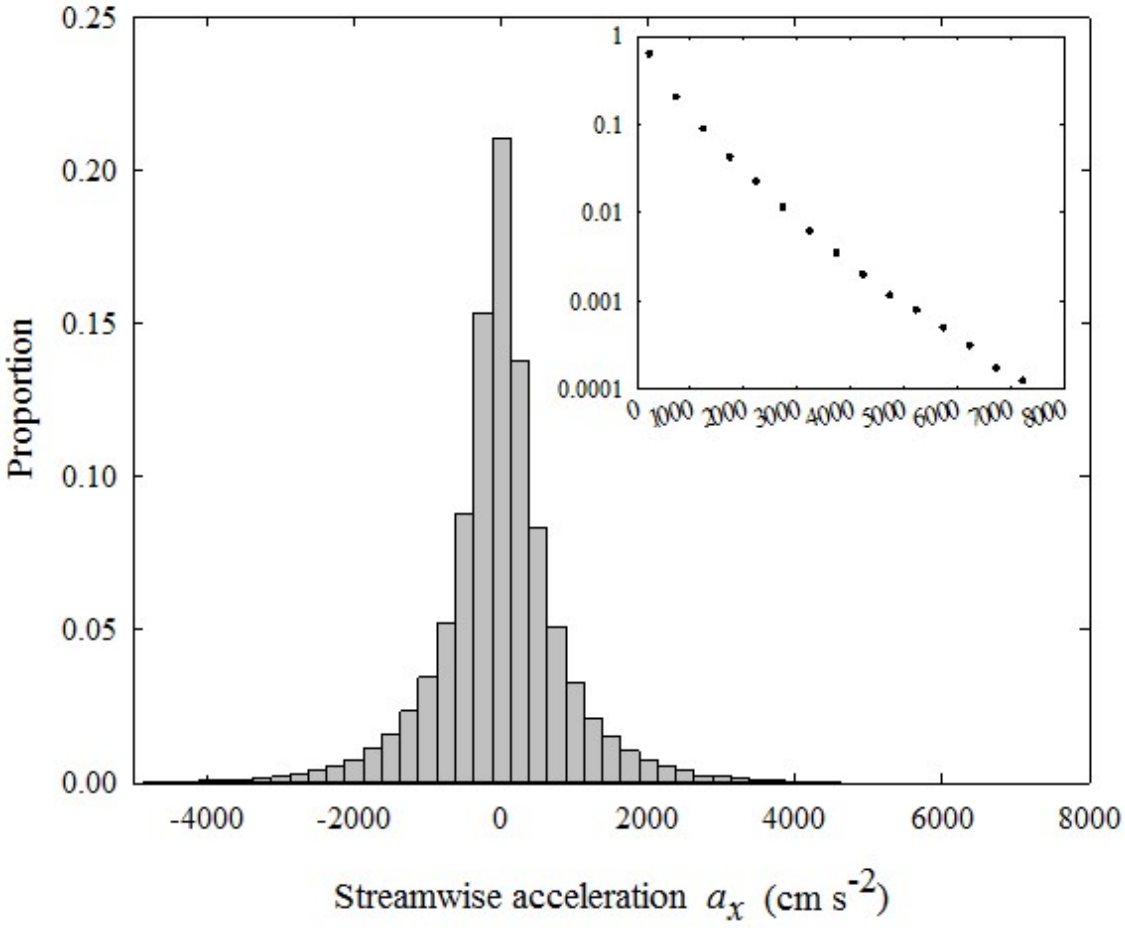

Figure 2.5: Discrete probability density of streamwise accelerations a_x, and semi-log plot (inset) of probability density versus $|a_x|$, with straight-line fit to data illustrating exponential form of distribution.

2.6.3 Particle Hop Distances and Travel Times

We identified approximately 4,000 complete hops (measured start-to-stop) within the field of view during the five seconds of analyzed imagery. Here we present the ensemble distributions of the streamwise hop distances L_x, the cross-stream hop distances L_y and the associated travel times T_p.

Particle travel times T_p are well approximated by an exponential distribution (Figure

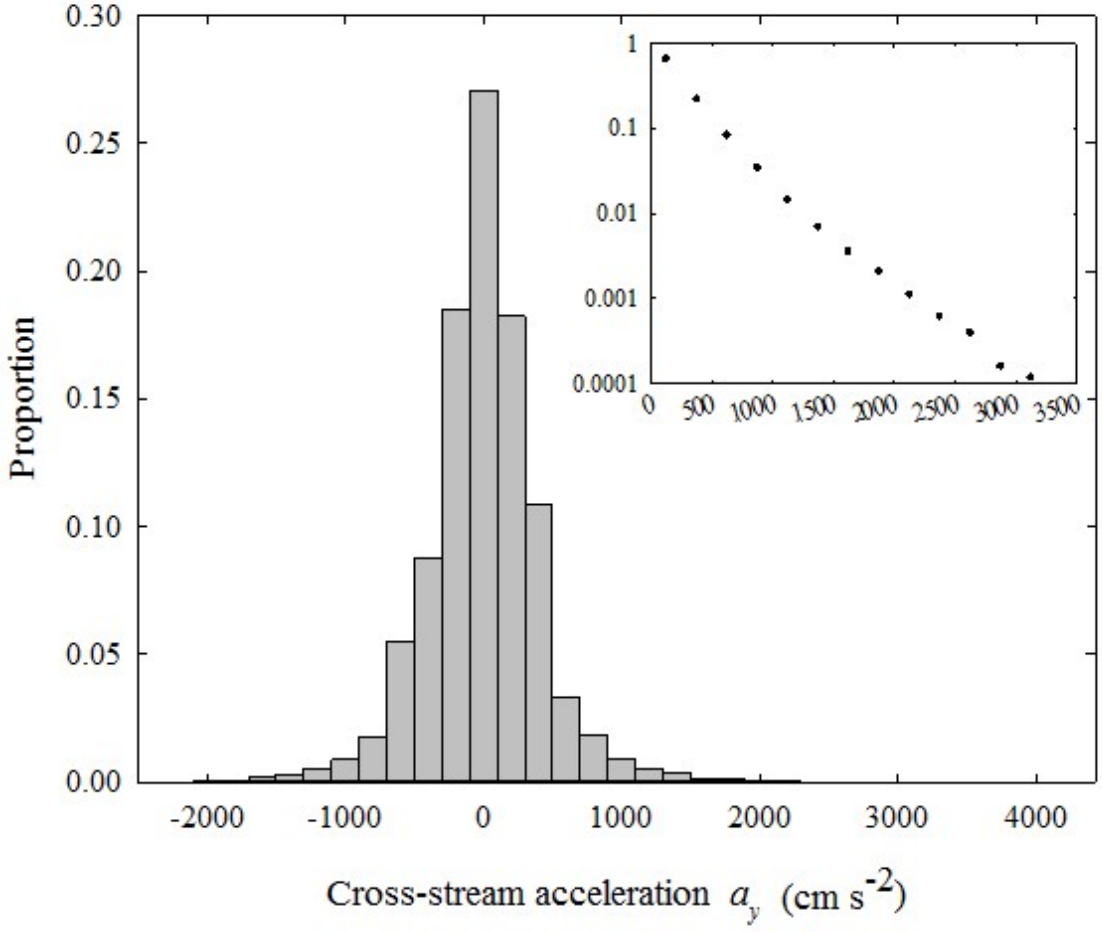

Figure 2.6: Discrete probability density of cross-stream accelerations a_y, and semi-log plot (inset) of probability density versus $|a_y|$, with straight-line fit to data illustrating exponential form of distribution.

2.7), namely,

$$f_{T_p}(T_p) = \frac{1}{\overline{T_p}} e^{-T_p/\overline{T_p}}, \tag{2.6}$$

where $\overline{T_p}$ is the mean travel time, estimated from the data to be $\overline{T_p} = 0.12$ seconds. The form of this distribution emphasizes that the bulk of the particle motions are short in duration and is consistent with the results of *Martin et al.* [2012] for mobile bed experiments involving steep, shallow flows.

Moreover, this form is consistent with the idea that, with respect to time following en-

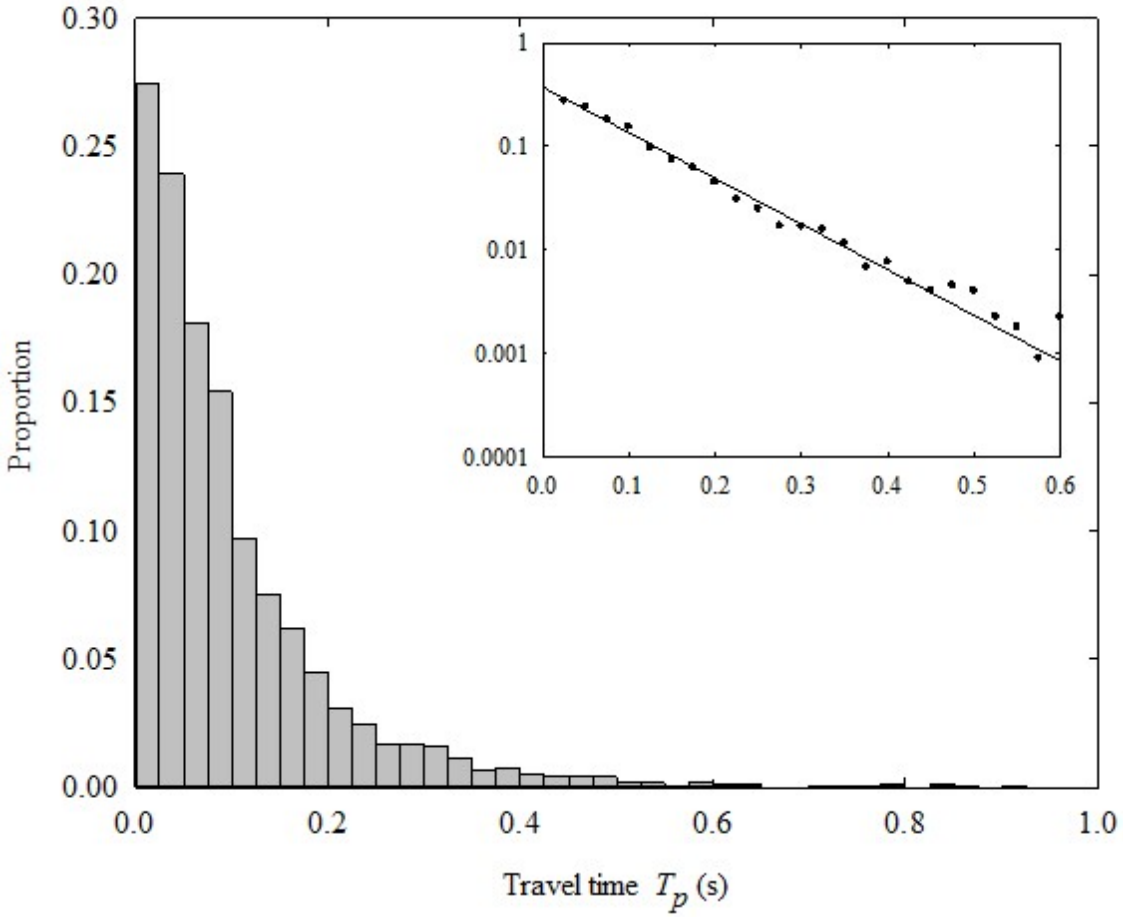

Figure 2.7: Discrete probability density of the hop travel times T_p, and semi-log plot (inset) of probability density versus T_p, with straight-line fit to data illustrating exponential form of distribution.

trainment, particles are likely to be disentrained with equal probability during any small interval of time dt (*Furbish et al.*, 2012a; *Roseberry et al.*, 2012). That is, particles experience a constant temporal disentrainment rate $P_{T_p} = 1/\overline{T_p}$ [T^{-1}] defined by (*Furbish and Haff*, 2010; *Furbish et al.*, 2012a)

$$P_{T_p} = \frac{f_{T_p}(T_p)}{1 - F_{T_p}(T_p)}\,, \tag{2.7}$$

where $F_{T_p}(T_p)$ is the cumulative distribution function of the travel times T_p.

This conclusion, which has a rudimentary theoretical basis (*Furbish et al.*, 2016a), is entirely consistent with the idea that the rate of disentrainment (deposition) is proportional to the number of particles in motion and 'available' to be disentrained (e.g., *Heyman et al.*, 2014; *Ancey and Heyman*, 2014). At any instant the active particles within an area B are in all possible states of entrainment, acceleration, deceleration and disentrainment. Some proportion of this number of particles is in a state of imminent disentrainment (and then does so during any small interval dt). The simplest defensible assumption is that, for steady (equilibrium) transport conditions, this proportion of particles in a state of imminent disentrainment is fixed for all T_p, inasmuch as equilibrium transport involves a time-invariant distribution of all possible particle states.

The distribution of streamwise hop distances L_x (Figure 2.8), ignoring the small number of short upstream hops, has the form of a two parameter Weibull distribution (see (8) below), where hop distances are predominantly small. Similarly, the distribution of the absolute value of the cross-steam hop distances has a Weibull form (Figure 2.9). Estimated values of the mean hop distance in the streamwise and cross-stream directions are $\overline{L_x} = 0.46$ cm and $\overline{|L_y|} = 0.036$ cm.

Focusing on streamwise motions, the Weibull distribution (with shape parameter $k < 1$) is consistent with the idea that, with respect to travel distances following entrainment, particles are likely to be disentrained with decreasing probability within any small interval of distance dx (*Furbish et al.*, 2012a; *Roseberry et al.*, 2012). That is, particles initially have a high likelihood of disentrainment but then experience a decreasing spatial disentrainment rate $P_{L_x}(L_x)$ [L^{-1}] with increasing hop distance L_x. Note that with respect to time, the likelihood of disentrainment is Poissonian (i.e., the probability in a time interval is constant), but in space disentrainment is more likely at the beginning of a hop.

The distribution of streamwise hop distances is closely related to the distribution of travel times as follows. As described in the next section, streamwise hop distances vary with travel times as $L_x = aT_p^2 + \varepsilon$, where a [L T^{-2}] is a characteristic particle acceleration

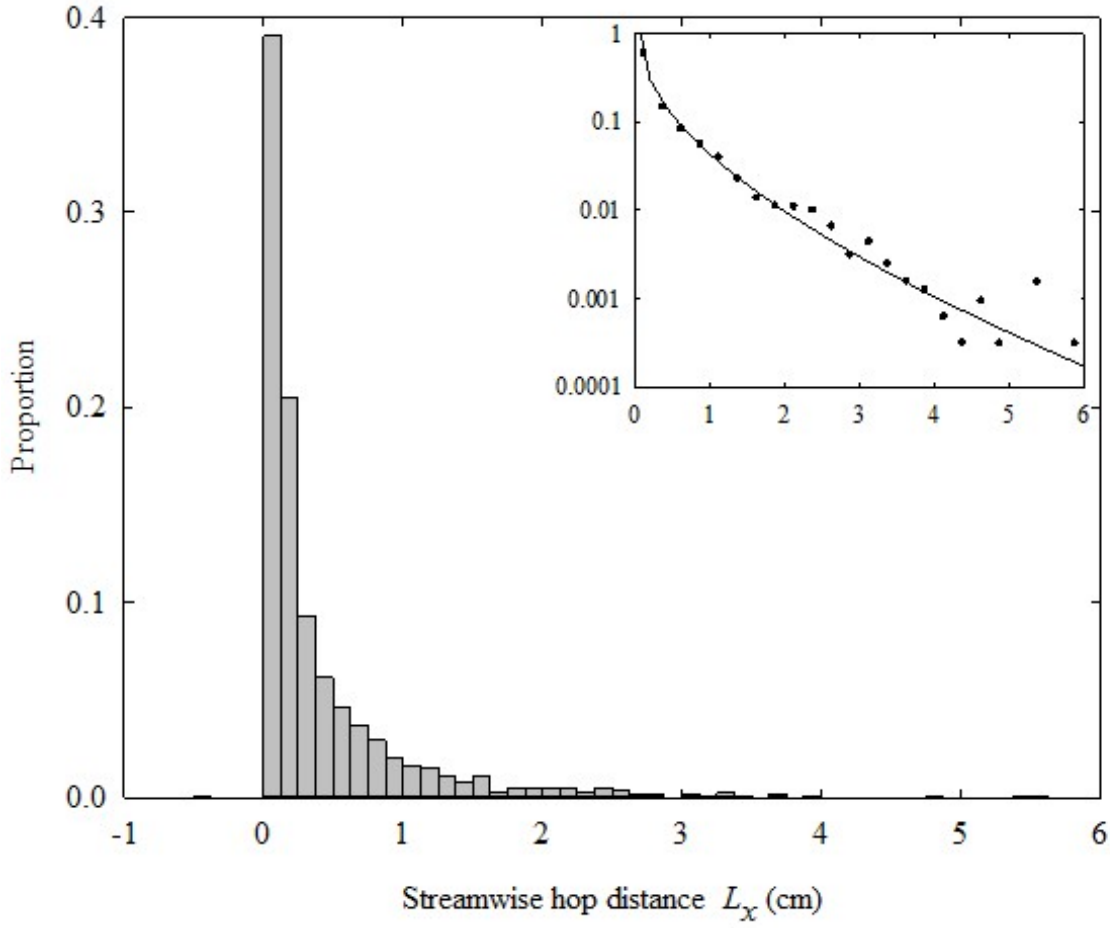

Figure 2.8: Discrete probability density of the streamwise hop distances L_x, and semi-log plot (inset) of probability density versus L_x, where the line represents a Weibull distribution fit to the data.

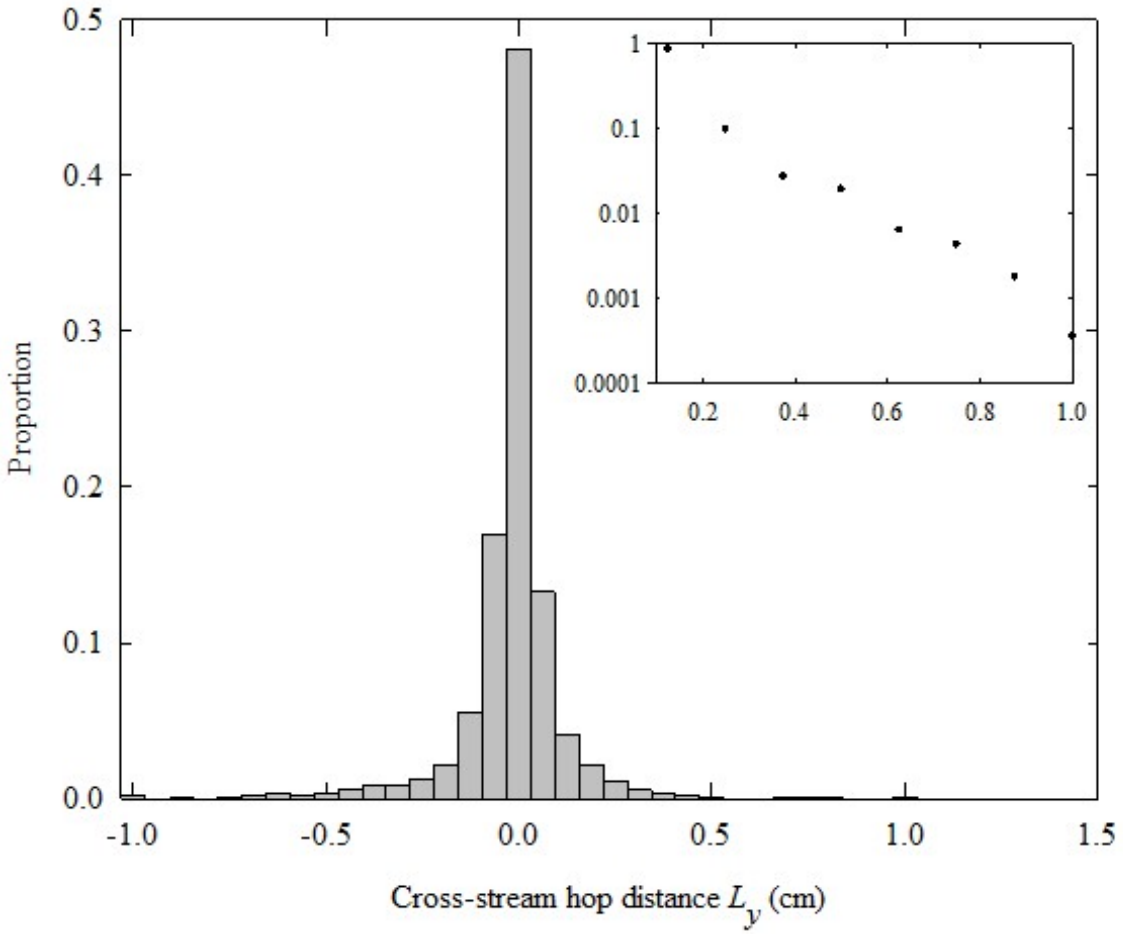

Figure 2.9: Discrete probability density of the cross-stream hop distances L_y, and semi-log plot (inset) of probability density versus $|L_y|$ where the line represents a Weibull distribution fit to the data. The approximate symmetry of the distribution of L_y results from defining the centerline of the flume as zero.

and ε [L] denotes a stochastic deviation about the expected value. If the distribution $f_{T_p}(T_p)$ of travel times T_p indeed is exponential, then it is straightforward to demonstrate (Appendix B) that the expected distribution $f_{L_x}(L_x)$ of hop distances L_x has the form of a Weibull distribution,

$$f_{L_x}(L_x) = \frac{A}{2L_x^{1/2}} e^{-AL_x^{1/2}}, \tag{2.8}$$

where $A = \sqrt{2/\overline{L_x}}$. The shape parameter $k = 1/2$ and the scale parameter $\lambda = \overline{L_x}/2$.

Estimated values of the shape and scale parameters are $k = 0.67$ (rather than 0.5) and $\lambda = 0.33$ (rather than 0.22). This difference of values is partly due to the fact that the transformation leading to (8) (Appendix B) does not account for effects of residual variance associated with ε. Nonetheless, that the data possess a Weibull form with $k < 1$ is consistent with the expected relationship between hop distances and travel times inasmuch as $L_x \sim T_P^2$, as elaborated below.

The data for the hop distances L_x and L_y together with the associated travel times T_p represent a sample drawn from the joint probability density function $f_{L_x,L_y,T_p}(L_x, L_y, T_p)$. To visualize this, plots of streamwise hop distances L_x versus travel times T_p (Figure 2.10) and cross-stream hop distances $|L_y|$ versus travel times T_p (not shown) represent this sample as being drawn from the joint probability density functions $f_{L_x,T_p}(L_x, T_p)$ and $f_{L_y,T_p}(L_y, T_p)$, which are marginal (joint) distributions of $f_{L_x,L_y,T_p}(L_x, L_y, T_p)$.

Both the streamwise and cross-stream hop distances vary nonlinearly with travel time T_p. At first glance, these relationships appear to follow those suggested by *Roseberry et al.* (2012), namely, that $L_x \sim T_p^{5/3}$ (Figure 2.10) and $|L_y| \sim T_p^{4/3}$. As described in the next section, the exponents $5/3$ and $4/3$ likely reflect effects of experimental censorship due to the finite imaging window size, where long hop distances and associated travel times are preferentially censored. Focusing on streamwise motions, more likely $L_x \sim T_p^2$, which has both an empirical basis (next section) and a theoretical basis (*Furbish et al.*, 2016a). This in turn leads to a Weibull distribution of streamwise hop distances L_x with $k < 1$ as described above (Appendix B).

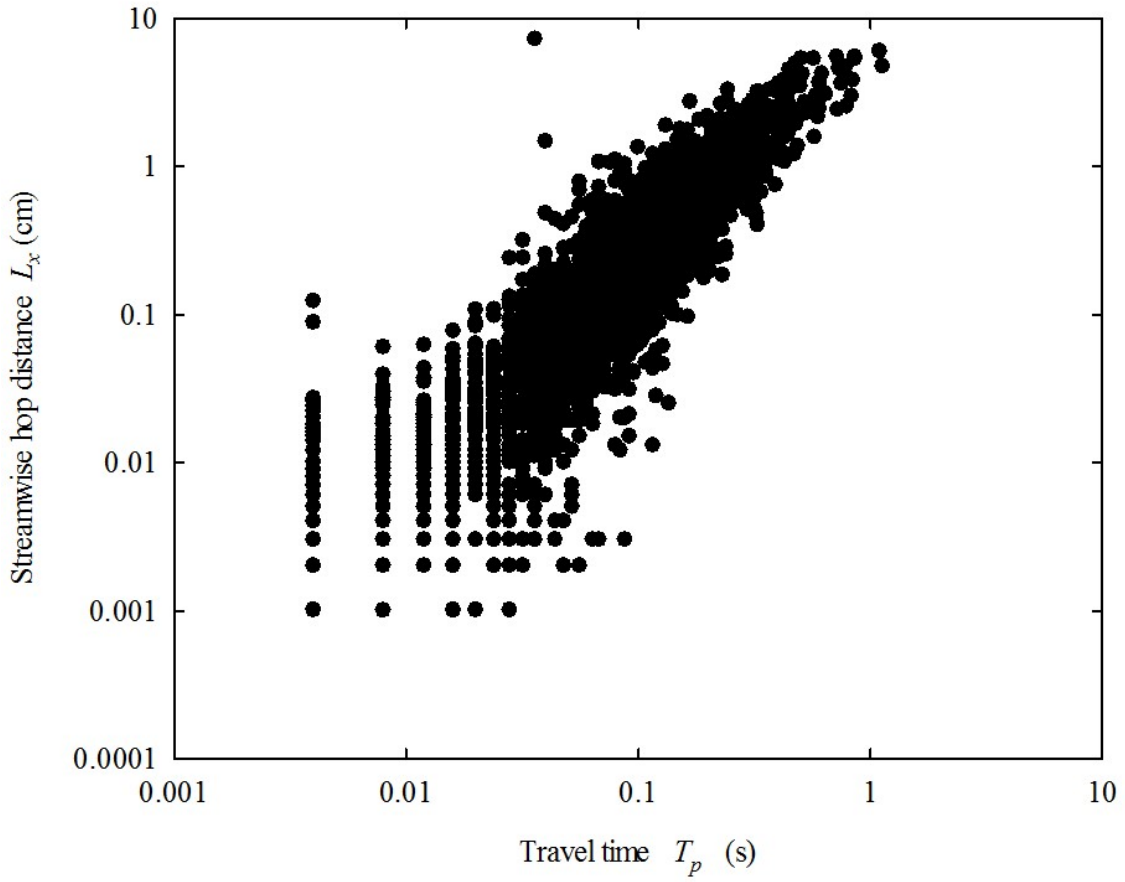

Figure 2.10: Plot of streamwise hop distances L_x versus travel times T_p; note that points significantly below $L_x \sim 0.01$ are effectively zero, representing measurement error.

These nonlinear relationships between hop distances and travel times are indicative of the behavior of the hopping motions. With short travel times, particle velocities on average remain low and the net travel distances therefore are on average short. With longer travel times, the hop distances on average disproportionately increase as the particle velocities increase. That is, particles that gain higher velocities are more likely to travel farther in a shorter amount of time than slower moving particles (*Roseberry et al.*, 2012; *Furbish et al.*, 2012b; *Ball*, 2012). This behavior also is highlighted within the online supplementary video, which shows particles in motion that are colored based on their current velocity. Within this video, it is apparent that particles must achieve a minimum velocity in order to travel a 'long' hop distance.

2.7 Effects of Experimental Censorship of Hop Distances and Travel Times

2.7.1 Bias due to Censorship

Video imaging of particle motions (e.g., *Drake et al.*, 1988; *Lajeunesse et al.*, 2010; *Roseberry et al.*, 2012; *Campagnol et al.*, 2013; *Seizilles et al.*, 2014) provides particularly valuable data to infer the forms of the distributions $f_{L_x}(L_x)$ and $f_{T_p}(T_p)$ as well as to estimate the moments of these distributions. These techniques likely will become increasingly popular, so there is value in paying attention to the details of what is actually being estimated. In particular, the motions of particles that enter or leave the video sampling area are spatially censored, and particles that are in motion when the video starts or stops are temporally censored. This means that estimates of $f_{L_x}(L_x)$ and $f_{T_p}(T_p)$ and their moments based only on hops of length L_x and duration T_p completed within the sampling area are biased.

Consider a sampling area B with streamwise length X. We set $x = 0$ at the upstream boundary of B and $x = X$ at its downstream boundary. Suppose that during a sampling interval T_s a large number of particle motions occur within B. Many represent full hops, but

some particles enter B then stop during T_s, and some particles start within B then exit during T_s. These are spatially censored motions. We momentarily exclude from consideration those particle motions censored in time, that is, particles that are in motion within B at times $t = 0$ and $t = T_s$. For simplicity we also exclude particles that enter or leave B across its transverse boundaries during T_s. An image of such motions is provided by *Roseberry et al.* (2012).

Following the formulation of *Furbish et al.* (1990), let $P_u(x; L_x, X)$ denote the probability that a particle motion with hop distance L_x starts within between the upstream boundary and the downstream boundary, specifically between the interval $0 < x < X - L_x$. This defines the case in which a motion is uncensored. The notation $P_u(x; L_x, X)$ indicates that this probability may be a function of position x, where L_x and X are treated as parameters. The probability that a motion occurs within the small interval L_x to $L_x + \mathrm{d}L_x$ and starts within the interval $0 < x < X - L_x$ is $P_u(x; L_x, X) f_{L_x}(L_x) dL_x$, and the censored, cumulative distribution function is

$$G_{L_x}(L_x) = \frac{\int_0^{L_x} P_u(x; L_x, X) f_{L_x}(w)\, \mathrm{d}w}{\int_0^{X} P_u(x; L_x, X) f_{L_x}(w)\, \mathrm{d}w}, \tag{2.9}$$

where w is a variable of integration.

We now assume that a sufficient number of motions occurs such that any initial patchiness in starting positions during T_s vanishes and $P_u(x; L_x, X)$ is independent of position x, that is, $P_u(x; L_x, X) = P_u(L_x, X)$. In this case $P_u(L_x, X) = (X - L_x)/X$, and (2.9) becomes

$$G_{L_x}(L_x) = \frac{\int_0^{L_x} (X - w) f_{L_x}(w)\, \mathrm{d}w}{\int_0^{X} (X - w) f_{L_x}(w)\, \mathrm{d}w}. \tag{2.10}$$

We now rewrite this as

$$G_{L_x}(L_x) = \frac{X F_{L_x}(L_x) - \int_0^{L_x} w f_{L_x}(w)\, \mathrm{d}w}{X F_{L_x}(L_x) - \int_0^{X} w f_{L_x}(w)\, \mathrm{d}w}, \tag{2.11}$$

where $F_{L_x}(L_x)$ is the cumulative distribution of $f_{L_x}(L_x)$. Taking the derivative of (2.11)

with respect to L_x and factoring X then yields the probability distribution of censored hop distances, namely,

$$g_{L_x}(L_x) = \frac{f_{L_x}(L_x) - (1/X)L_x f_{L_x}(L_x)}{F_{L_x}(X) - (1/X)\int_0^X w f_{L_x}(w)\,\mathrm{d}w}. \tag{2.12}$$

Notice that in the limit of $X \to \infty$, the second term in both the numerator and denominator of (2.12) goes to zero while the first term in the denominator goes to unity, so the distribution $g_{L_x}(L_x)$ approaches the underlying distribution of hop distances, $f_{L_x}(L_x)$.

To gain a clearer sense of the bias introduced by the finite widow size X let us factor $f_{L_x}(L_x)$ and $F_{L_x}(L_x)$ from (2.12) to give

$$g_{L_x}(L_x) = \frac{f_{L_x}(L_x)}{F_{L_x}(X)}\left(\frac{1 - L_x/X}{1 - [1/XF_{L_x}(X)]\int_0^X w f_{L_x}(w)\,\mathrm{d}w}\right). \tag{2.13}$$

We now observe that

$$\overline{L_x^*} = \frac{1}{F_{L_x}(X)}\int_0^X w f_{L_x}(w)\,\mathrm{d}w \tag{2.14}$$

is a biased mean hop distance, that is, the mean based on values $L_x < X$. Substituting this into (2.13) and expanding the result as a binomial series then gives

$$g_{L_x}(L_x) = \frac{f_{L_x}(L_x)}{F_{L_x}(X)}\left(1 - \frac{L_x}{X} + \frac{\overline{L_x^*}}{X} - \ldots\right). \tag{2.15}$$

At lowest order $g_{L_x}(L_x)$ differs from $f_{L_x}(L_x)$ by the factor $1/F_{L_x}(X)$. That is, $g_{L_x}(L_x)$ is a truncated version of $f_{L_x}(L_x)$. The term L_x/X indicates that small values of L_x ($L_x \ll X$) are well represented in $g_{L_x}(L_x)$, but that values of L_x as L_x increases and approaches X are increasingly underrepresented. The contribution of the term involving $\overline{L_x^*}$ to the bias of $g_{L_x}(L_x)$ is negligible if $\overline{L_x^*} \ll X$. As a practical guide, therefore, the censored distribution $g_{L_x}(L_x)$ based on completed hops is likely to be a good approximation of the underlying distribution $f_{L_x}(L_x)$ if $\overline{L_x^*} \ll X$ and if the fraction of the longest measured hop distances $L_x \gg \overline{L_x^*}$ is small.

In our experiments the sampling interval T_s is sufficiently long that travel times T_p are

negligibly censored with the start and stop of the video. Nonetheless, values of the travel time T_p associated with censored values of L_x are, by definition, also censored. Because L_x and T_p are in general correlated, this means that estimates of the distribution $f_{T_p}(T_p)$ and its moments based only on completed motions also are biased.

2.7.2 A Demonstration of Censorship, and the Relation between Hop Distances and Travel Times

To explore the effects of censorship, particularly spatial censorship, we examine various window sizes and compare differences in the measured quantities. Within this experiment, we have recorded complete particle hops within the entire window length X, where $X =$ 7.57 cm, such that all hops that start and stop between $x = 0$ and $x = X$ are measured. We then compare this to complete hops within $x = 0$ to $x = X/2$ and within $x = 0$ to $x = X/4$. If x' denotes the starting position of a hop, then these three sets of measurements involve censorship of hop distances $L_x > X - x'$, $L_x > X/2 - x'$ and $L_x > X/4 - x'$. By nature, the associated values of the travel time T_p also are censored.

Consider a plot of L_x versus T_p (Figure 2.11), with data for each window size denoted by a different shading. The largest window size contains all hops recorded in Figure 2.11, and the color-coding highlights the hops that occur just within the two smaller windows. On average L_x varies with T_p as $L_x \sim T_p^{\alpha}$. As seen in this plot, whereas some proportion of all hop distances and associated travel times is censored, the visual effect of censorship is a preferential reduction in the largest hop distances and travel times, which gives the appearance of a less steep overall relationship between these quantities. This provides the empirical basis for suggesting that, in the relation $L_x \sim T_p^{\alpha}$, the value $\alpha \sim 2$ rather than 5/3 as suggested by *Roseberry et al.* (2012) (a value which was supported by *Fan et al.* (2014)). In addition, on dimensional grounds we may assume that $L_x = aT_p^2 + \varepsilon$ if a is interpreted as a characteristic particle acceleration. In physical terms this relationship represents a particle-averaged impulse over the period T_p (*Furbish et al.*, 2016a).

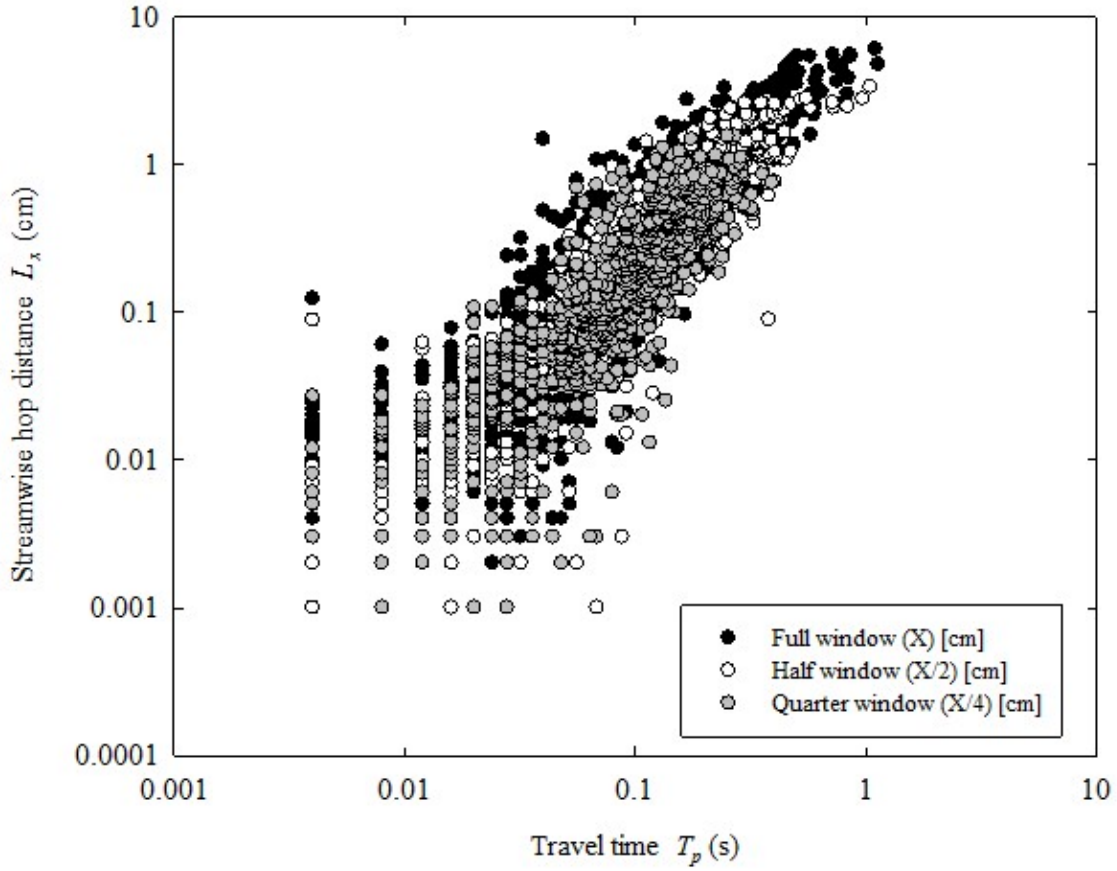

Figure 2.11: Plot of streamwise hop distances L_x versus travel times T_p, where the points are color-coded according to the window size; black points are censored by the half window, and black and white points are censored by the quarter window.

This relationship and the specific value of α merit further attention. Inasmuch as $\alpha > 1$, then an exponential distribution of travel times T_p necessarily leads to a Weibull distribution for the hop distances L_x with scale parameter $k < 1$ (Appendix B). We therefore suggest that the experimental results presented here — an exponential distribution of travel times T_p, a Weibull distribution of hop distances L_x with $k < 1$, and a nonlinear relationship between L_x and T_p with $\alpha > 1$ — reflect a clear internal consistency concerning expected particle behavior.

2.8 Significance of Measurements

The measurements presented above bear on several topics pertaining to the details of bed load sediment transport, and also point to key ideas that merit further attention. Here we highlight several of these topics and ideas.

Foremost, our measurements provide clear empirical results that can be viewed as a target for testing and constraining theories of particle behavior during transport, including numerical treatments of this behavior. Demonstrating ensemble particle behavior is key, inasmuch as we may then appeal to the idea that this behavior, as reflected by time-invariant distributions of quantities describing particle motions, is a signature of the transport process for specified sediment and macroscopic flow conditions. For example, whereas there is a theoretical basis, grounded in statistical mechanics, for expecting an exponential distribution of particle velocities (*Furbish and Schmeeckle*, 2013), there is not yet a clear theoretical basis for predicting the moments of this distribution in a way that connects particle motions with fluid motions. Making this connection requires a clear empirical target which can only be achieved through precise measurements to first define the distributions of sediment motions. In this vein, we note that the distributions of particle hop distances and associated travel times reported above may actually represent special cases (consistent with the experimental conditions) of a more general family of distributions. For example, the exponential distribution used here to describe travel times is a special case of both the

gamma and the Weibull distributions.

Furthermore, to produce a clear theoretical basis for sediment motions in bed load transport, it is key to produce formulations based on the physics of the particle motions for varying sediment and flow conditions, beyond the conditions reported here. For example, our results suggest that the disentrainment rate with respect to time is fixed, but we still need an underlying theory to set this rate. Understanding the controls on particle disentrainment is particularly important. Namely, whereas our understanding of the physics of particle entrainment is reasonably well developed in certain areas of sediment transport, our understanding of the physics of disentraiment is rudimentary at best. But it is this process of disentrainment that determines key features of particle motions, notably the distances over which particles are dispersed following the initiation of motion, that is, the distribution of hop distances. We also emphasize that our results specifically pertain to a uniform grain size, and that work ultimately is needed to understand the behavior of mixed-grain sizes.

Second, recent work (*Furbish et al.*, 2012a; *Ancey and Heyman*, 2014) indicates that the 'activity' form of the bed load flux generally consists of advective and diffusive terms, for example,

$$q_x(x,t) = \overline{u_p}\gamma - \frac{1}{2}\frac{\partial}{\partial x}(\kappa_x \gamma), \tag{2.16}$$

where $q_x(x,t)$ [L^2 T^{-1}] is the streamwise flux, γ [L] is the volumetric particle activity (the volume of particles in motion per unit streambed area), and κ_x [L^2 T^{-1}] is the particle diffusivity. Here, the first two moments of the particle velocity distribution $f_{u_p}(u_p)$ are key. Namely, the average particle velocity $\overline{u_p}$ is an element of the advective term in (2.16), and the diffusivity κ_x in the diffusive term is related to the variance $\sigma^2_{u_p}$ [L^2 T^{-2}] of the velocities as $\kappa_x = \sigma^2_{u_p}\tau_L$, where τ_L [T] is the Lagrangian integral timescale of the particle velocities. Inasmuch as the velocity distribution is exponential, then $\sigma^2_{u_p} = \overline{u_p}^2$ so that $\kappa_x \sim \overline{u_p}\delta$, where $\delta \sim \overline{u_p}\tau_L$ [L] is a characteristic distance of motion that is similar in magnitude to the average hop distance $\overline{L_x}$ (*Furbish et al.*, 2012b). These points reinforce the significance of establishing the form of the ensemble distribution of particle velocities.

In turn, the probabilistic properties of particle hop distances and travel times are central in 'entrainment' forms of the particle flux and the Exner equation. For example, focusing on one-dimensional transport parallel to x involving only downstream motions,

$$c_b \frac{\partial \eta(x,t)}{\partial t} = -E(x,t)$$

$$+ \int_{-\infty}^{t} \int_{-\infty}^{x} E(x',t') f_{L_x,T_p}(x-x',t-t')\,\mathrm{d}x'\mathrm{d}t' . \tag{2.17}$$

Here, $c_b = 1-\phi$ is the volumetric particle concentration of the sediment surface where ϕ is the porosity, η [L] denotes the local elevation of the sediment surface, E [L T^{-1}] denotes the volumetric rate of sediment entrainment, $x' = x - L_x$, and $t' = t - T_p$. This 'nonlocal' formulation emphasizes that particles arriving at x at time t started their motions at many preceding times t' at many positions x' far upstream (*Furbish et al.*, 2012a, 2016a). Simplifications of (2.17) (e.g., *Parker et al.*, 2000b; *Pelosi et al.*, 2014) assume negligible travel times T_p or involve temporal averaging such that the integral with respect to time is neglected and the joint probability distribution $f_{L_x,T_p}(L_x,T_p)$ is replaced with the distribution of hop distances, $f_{L_x}(L_x)$. In either case, it is important to note that this formulation involves the distribution of hop distances measured start-to-stop, not a distribution of travel distances involving multiple hops and intervening rest periods. We also note that the related, entrainment form of the flux for equilibrium transport conditions reduces to the result originally provided by *Einstein* (1950), that $q_x = E\overline{L_x}$. These points reinforce the significance of establishing the forms of the ensemble distributions of particle hop distances and associated travel times, and the relationship between these.

2.9 Conclusions

The size and resolution of the data set presented in this paper allow us to confidently describe the forms and qualities of the ensemble distributions of particle velocities, accelerations, hop distances and travel times for the experimental conditions. Convergence

statistics support the idea that the forms of these distributions are time-invariant. These ensemble distributions best represent the probabilitistically expected behavior of particle motions consistent with the macroscopic sediment and flow conditions, and thus provide a clear target for further analyses of transport, including statistical mechanics theory and numerical simulations. Our principal conclusions are:

1) Our data show exponential distributions for the streamwise and cross-stream particle velocities, consistent with previous experiments and theory. Importantly, we can confirm the presence of a "light" tail in the streamwise velocities, where the largest particle velocities are limited by near-bed fluid velocities. Distributions of streamwise and cross-stream particle accelerations are Laplace in form and centered on zero means, consistent with equilibrium transport conditions.

2) The majority of sediment 'hops' involve short positive displacements, and the streamwise and cross-stream components of the hop distances possess Weibull distributions. In contrast to previous work involving a smaller data set, the distribution of travel times of individual hops is exponential, consistent with a fixed temporal disentrainment rate. The Weibull distribution of hop distances is consistent with a decreasing spatial disentrainment rate, and is physically related to the exponential distribution of travel times.

3) Streamwise and cross-stream components of the hop distances vary nonlinearly with travel times. If particles gain a sufficiently high velocity, they tend to travel farther in a shorter amount of time than similar slower moving particles. Thus, with increasing travel times, hop distances on average disproportionately increase as particle velocities increase.

4) By taking into account the effects of experimental censorship, the relationship between streamwise hop distances and travel times, $L_x \sim T_p^{\alpha}$, likely involves an exponent of $\alpha \sim 2$. This differs from previous measurements, and is dimensionally consistent with an averaged impulse integrated over the period T_p.

5) The experimental results presented here — an exponential distribution of travel times T_p, a Weibull distribution of hop distances L_x with shape parameter $k < 1$, and a nonlinear

relationship between L_x and T_p with $\alpha > 1$ — reflect a clear internal consistency concerning expected particle behavior.

6) There is a pressing need for improving automated particle tracking methods that can provide high fidelity measurements of the small particle displacements and velocities that dominate bed load particle motions.

2.10 APPENDIX: Advection of Probability with Particle Aging

The advection equation (1) can be obtained several ways. To illustrate its probabilistic basis in a simple manner, let $n(t_p,t)$ [T^{-1}] denote the number density of particles with age t_p at time t. That is, $n(t_p,t)\mathrm{d}t_p$ is the expected number of particles whose ages are within the interval t_p to $t_p + \mathrm{d}t_p$. If N denotes the total number of particles, then $f_{t_p}(t_p,t)\mathrm{d}t_p = n(t_p,t)\mathrm{d}t_p/N$ is the expected proportion of the particles within the interval t_p to $t_p + \mathrm{d}t_p$. That is, $f_{t_p}(t_p,t)$ [T^{-1}] is the probability density of particle ages t_p.

In the absence of a source (entrainment) or sink (deposition), the substantive derivative of $n(x,t)$ yields $[\partial n(x,t)/\partial t_p](\mathrm{d}t_p/\mathrm{d}t) + \partial n(t_p,t)/\partial t = 0$. Dividing this by N and adding the failure rate D_f gives (1) in the text, where $\mathrm{d}t_p/\mathrm{d}t = 1$ is the aging rate of the particles. One may think of each particle as possessing a probability equal to $1/N$ that is 'advected' to larger values with aging.

Alternatively, we note that (1) is a Fokker-Planck equation (an approximation of the Master equation) with a sink term, absent the usual diffusive term, as aging at a rate $\mathrm{d}t_p/\mathrm{d}t = 1$ is a fixed quantity without variations that are required for diffusion of probability. Thus, (1) also can be obtained following the developments of the Master equation presented in *Furbish et al.* [2012b].

2.11 APPENDIX: Distribution of Hop Distances

At the outset we assume from the results of section 2.7.2 that hop distances vary with travel times as $L_x = aT_p^2 + \varepsilon$, where ε denotes a stochastic deviation about the expected

value. Taking averages, $\overline{L_x} = a\overline{T_p^2}$. Further assuming that T_p indeed is exponentially distributed, then $\overline{T_p^2} = 2\overline{T_p}^2$, or $\overline{L_x} = 2a\overline{T_p}^2$. The distribution $f_{L_x}(L_x)$ of hop distances L_x is then given by

$$f_{L_x}(L_x) = \left| \frac{\mathrm{d}}{\mathrm{d}L_x}[g^{-1}(L_x)] \right| f_{T_p}[g^{-1}(L_x)]\,, \tag{2.18}$$

where, neglecting the random deviation ε, the function $L_x = g(T_p) = aT_p^2$ so that the inverse function $g^{-1}(L_x)$ is $T_p = \sqrt{L_x/a}$. These relations then yield

$$f_{L_x}(L_x) = \frac{A}{2L_x^{1/2}} e^{-AL_x^{1/2}}\,, \tag{2.19}$$

where $A = \sqrt{2/\overline{L_x}}$. This has the form of a Weibull distribution with shape parameter equal to $1/2$ and scale parameter equal to $\overline{L_x}/2$.

CHAPTER 3

The Source of Anomalous Versus Normal Spreading of Bed Load Sediment Particles

3.1 Abstract

Bed load sediment transport is the basic physical ingredient of river evolution. Formulae exist for estimating transport rates, but the diffusive contribution to the sediment flux, and the associated spreading rate of tracer particles, are not clearly understood. The start-and-stop motions of sediment particles transported as bed load on a streambed mimic aspects of the Einstein-Smoluchowski description of the random-walk motions of Brownian particles. Using this touchstone description, recent work suggests the presence of anomalous diffusion, where the particle spreading rate differs from the linear dependence with time of Brownian behavior. We demonstrate that conventional measures of particle spreading reveal different attributes of bed load particle behavior depending on details of the calculation. When we view particle motions over start-and-stop timescales obtained from high-speed (250 Hz) imaging of coarse-sand particles, high-resolution measurements reveal ballistic-like behavior at the shortest (10^{-2} s) timescale, followed by apparent anomalous behavior due to correlated random walks in transition to normal diffusion ($>10^{-1}$ s) — similar to Brownian particle behavior but involving distinctly different physics. However, when treated as a 'virtual plume' over this timescale range, particles exhibit inhomogeneous diffusive behavior because both the mean and the variance of particle travel distances increase nonlinearly with increasing travel times, a behavior that is unrelated to anomalous diffusion or to Brownian-like behavior. Our results indicate that care is needed in suggesting anomalous behavior when appealing to conventional measures of diffusion formulated for ideal particle systems.

3.2 Introduction

Bed load sediment particles entrained by a turbulent shear flow undergo a series of start-and-stop motions involving a combination of rolling, sliding and small saltations between successive states of rest. Because of the significance of bed load particle transport in river science and engineering (*Church and Ferguson*, 2015), including aquatic ecology (*Hassan et al.*, 2008), numerous studies over the past century have focused on calculating bed load transport rates (e.g., *Shields*, 1936; *Einstein*, 1950; *Wilcock*, 2001; *Ancey et al.*, 2006). As part of this continuing effort, the idea of diffusion of bed load particles has emerged as a key element of their behavior during transport. Indeed, diffusion of bed load particles is central in two compelling problems within sediment transport research, namely, characterizing the spreading behavior of tracer particles in flume experiments and natural channels (*Sayre and Hubbell*, 1965; *Hassan et al.*, 1991; *Nikora et al.*, 2002; *Ganti et al.*, 2010; *Martin et al.*, 2012, 2014; *Pelosi et al.*, 2014), and determining the contribution of bed load particle diffusion to the sediment flux under nonuniform transport conditions (*Schmeeckle and Furbish*, 2007; *Furbish et al.*, 2012a,c; *Seizilles et al.*, 2014).

Recent studies of the downstream spreading of bed load tracer particles (*Nikora et al.*, 2002; *Bradley and Tucker*, 2010; *Ganti et al.*, 2010; *Hill et al.*, 2010; *Martin et al.*, 2012, 2014) indicate the possibility of anomalous diffusion, where the rate of particle spreading may be slower (subdiffusion) or faster (superdiffusion) than the Gaussian spreading associated with normal (or Brownian, or Fickian) diffusion — the touchstone description of the behavior of Brownian particles undergoing quasi-random walk motions within a fluid (*Einstein*, 1905; *von Smoluchowski*, 1906). The presence of anomalous versus normal diffusion bears on formulations of transport rates and particle dispersion (e.g., *Schumer et al.*, 2009; *Furbish et al.*, 2012b), which raises a key question: What is the physical basis for the appearance of anomalous diffusion in bed load particle motions?

Bed load particle motions involve frequent collisions with the bed (*Drake et al.*, 1988; *Lajeunesse et al.*, 2010; *Roseberry et al.*, 2012; *Fathel et al.*, 2015), which, together with

effects of near-bed turbulence, produce stochastic variations in particle displacements and velocities (*Einstein*, 1937, 1950; *Roseberry et al.*, 2012; *Furbish et al.*, 2012c; *Fathel et al.*, 2015). These motions mimic random-walk behavior of particles (e.g., Brownian particles) in fluid systems. But individual bed load particle motions are brief, and involve far fewer collisions (*Roseberry et al.*, 2012; *Fathel et al.*, 2015) than particles in fluid systems over geometrically scaled timescales and distances. As a point of reference, *Nikora et al.* (2002) defined three characteristic spatial and temporal scales of particle motions. A "local" scale is defined by motions between successive particle-bed collisions and is analogous to the ballistic regime of Brownian particles. An intermediate scale is associated with the durations and distances of particle motions between successive states of rest, herein referred to as particle 'hops.' A "global" scale involves multiple particle hops and intervening rest times.

We focus here on particle behavior associated with the local and intermediate scales, deferring consideration of the effects of rest times that dominate particle spreading behavior at long times (*Martin et al.*, 2012; *Hassan et al.*, 2013), and which are not reflected within the data presented here. Our analysis involves a comparison of conventional measures of particle spreading that are based on the mean squared displacement of particles (*Einstein*, 1905) and the particle velocity autocovariance (*Taylor*, 1922). Specifically, we demonstrate that these measures of particle diffusion, developed for particle motions that continue indefinitely under statistically homogeneous conditions, reveal different attributes of bed load particle behavior depending on details of the calculation. We start by outlining key elements of these conventional calculations of particle diffusion. We then provide an analysis of these measures of diffusion using an unusually large, high-resolution data set obtained from high-speed imaging of the motions of coarse sand transported as bed load in two flume experiments (*Fathel et al.*, 2015). We demonstrate that the start-and-stop motions of bed load particles yield apparent signatures of anomalous as well as normal diffusion. We suggest that the anomalous behavior may be attributed in part to the intrinsic

periodicities of motion (*Furbish et al.*, 2012b), and in part to the effects of a nonlinearly increasing variance in hop distances with increasing travel times. Namely, the mean squared displacement "sees" a small variance for many particles at small times and an increasing variance about the expected travel distances for fewer particles with increasing transport times, resulting in a behavior that appears to be anomalous. These effects are transient and dominate spreading behavior at small times.

3.3 Three Measures of Particle Diffusion

Studies of bed load particle diffusion have appealed to three key measures, each involving a Lagrangian perspective of particle displacements. Specifically, if $x_p(t)$ denotes the position of a particle at time t so that $r(\tau) = x_p(t+\tau) - x_p(t)$ denotes the particle displacement during an interval τ, then the Einstein-Smoluchowski equation as originally applied to Brownian particle motion in one dimension is

$$2\kappa_x \tau = \langle [r(\tau) - \langle r(\tau) \rangle]^2 \rangle = R_x(\tau)\,, \tag{3.1}$$

where κ_x is the particle diffusivity and the angle brackets denote averaging over all displacements during τ calculated for an individual particle or for a group of particles. This indicates that the mean squared displacement $R_x(\tau)$ increases linearly with the time interval τ for sufficiently large τ (*Einstein*, 1905). More generally we may write $R_x(\tau) \sim \tau^a$, where $0 < a < 1$ indicates subdiffusion, $1 < a < 2$ indicates superdiffusion, and the special case of $a = 2$ coincides with ballistic behavior at small τ (*Huang et al.*, 2011). For reference below we refer to (1) as an ensemble calculation of $R_x(\tau)$.

A second measure treats the sediment motions as a virtual plume of tracer particles starting from the same position $x_p(0) = 0$ at time $t = 0$, namely,

$$R_x(t) = \langle [x_p(t) - \langle x_p(t) \rangle]^2 \rangle. \tag{3.2}$$

where now the angle brackets denote averaging over the group of particles (*Nikora et al.*, 2002; *Bialik et al.*, 2012, 2015). To be clear, whereas the mean squared displacement using (1) involves averaging over all paired coordinate positions separated by the interval τ without regard to starting time, the mean squared displacement using (2) involves averaging over a group of particles at time t rather than over paired coordinate positions. We refer to (2) as a tracer calculation of $R_x(t)$.

A third measure is provided by G. I. Taylor's description of the behavior of continuous particle motions in a homogeneous turbulent flow (*Taylor*, 1922), although it is entirely relevant to Brownian-like particle motions, and is based on the autocovariance of particle velocities. Imagine a tracer particle with small Stokes number moving with the fluid. Letting $u'_p(t) = u_p(t) - \overline{u_p}$ denote a deviation about the average streamwise particle velocity $\overline{u_p}$, then for a sampling interval T_s the velocity autocovariance is

$$C(\tau) = \frac{1}{T_s - \tau} \int_0^{T_s - \tau} u'_p(t) u'_p(t+\tau)\, \mathrm{d}t\,. \tag{3.3}$$

When $\tau = 0$, the autocovariance equals the variance of the streamwise velocity u_p, that is, $C(0) = \sigma^2_{u_p}$. The autocorrelation is $A_x(\tau) = C(\tau)/C(0) = C(\tau)/\sigma^2_{u_p}$. In turn, the Lagrangian integral timescale is $\tau_L = \int_0^\infty A_x(\tau)\mathrm{d}t$, which is a measure of persistence within the velocity signal. If the integral converges such that τ_L is finite, then particle spreading becomes Fickian at $t \geq \tau_L$ with diffusivity $\kappa_x = 2\sigma^2_{u_p}\tau_L$. The absence of convergence indicates superdiffusive behavior. The autocovariance (3) can be generalized for many particle motions (*Furbish et al.*, 2012a), and represents an ensemble calculation for all paired observations separated by τ, regardless of starting times. This calculation is consistent with the description of the mean squared displacement $R_x(\tau)$ embodied in (3.1).

Einstein, von Smoluchowski and Taylor were quite clear that their measures of particle diffusion describe the statistically expected spreading of an individual particle whose motion continues indefinitely, and whose behavior is fully representative of ensemble be-

havior, including the associated property of time invariance. By this we mean the following. The mean squared displacement $R_x(\tau)$ and the velocity autocorrelation function $A_x(\tau)$ calculated for an individual particle are the same as those calculated for any other identical particle and surrounding fluid. Moreover, if we imagine setting $t = 0$ at any instant in the random-walk lifetime of a particle, its statistically expected spreading behavior measured from any such instant is the same. For these reasons the measures (1) and (2) yield identical results for particles subjected to statically homogeneous, time invariant conditions. Formally, the joint probability density function $f_{x_p(t),x_p(t+\tau)}[x_p(t),x_p(t+\tau)]$ is invariant with respect to an arbitrary translation in time t for all intervals τ. Moreover, the joint probability density function $f_{u'_p(t),u'_p(t+\tau)}[u'_p(t),u'_p(t+\tau)]$ also is invariant with respect to a translation in time t for all τ.

This behavior of a Brownian-like particle is quite different from the expected behavior of bed load sediment particles that start and stop during transport. The expected spreading behavior of an individual bed load particle varies during its random-walk lifetime, and this behavior also varies from one particle to the next. That is, the statistically expected behavior of an individual bed load particle is rarely the same as that of any other particle nor that of the ensemble, and it is not time invariant. As a consequence, the previous measures of spreading, (1) and (2), reveal different elements of diffusive particle behavior; and (1) and (3) reveal key differences between individual and collective particle behavior. We elaborate these points after describing our experimental measurements.

3.4 Methods and Measurements

Advances in measurement techniques centered on imaging are providing increased resolution of sediment particle motions in flume studies (*Lajeunesse et al.*, 2010; *Roseberry et al.*, 2012; *Martin et al.*, 2012; *Radice et al.*, 2013; *Campagnol et al.*, 2013; *Heyman*, 2014; *Ancey and Heyman*, 2014). Here we describe measurements from high-speed (250 Hz) imaging of coarse sand (D_{50} = 0.05 cm) transported as bed load under equilibrium

conditions in two flume experiments conducted in a 8.5 m $\times$ 0.3 m recirculating flume in the River Dynamics Laboratory at Arizona State University. The high-speed imagery captures an area of the sediment bed that is 7.57 cm long (streamwise) and 6.05 cm wide (cross-stream), with a corresponding resolution of 1280 $\times$ 1024 pixels (see *Supplementary Material*, Movie S1 and S2 to view imagery). Flow conditions in both experiments were fully turbulent with Reynolds numbers of approximately 9.3×10^4 (Run 1) and 1.2×10^5 (Run 2), and Froude numbers of 0.30 and 0.37 (Table 1). The experimental conditions in

	Run 1	**Run 2**
Run Time (s)	5.0	2.0
Flow Depth (cm)	12.5	10.3
Velocity at 1 cm (cm/s)	31.0	36.7
Reynolds Number	9.3×10^4	1.2×10^5
Froude Number	0.30	0.37
Shear Velocity (cm/s)	2.0	2.4
Mean Particle Velocity (cm/s)	4.4	5.6
Mean 'Hop' Length $\overline{L_x}$(cm)	0.79	0.37
Max 'Hop' Length (cm)	7.1	6.0
Mean Travel Time $\overline{T_p}$ (s)	0.12	0.16
Max Travel Time (cm)	1.3	1.1

Table 3.1: Summary of experimental conditions and particle measurements in Run 1 and Run 2. Note that the mean fluid velocity is recorded 1 cm above the bed using an acoustic Doppler velocimeter.

these two runs are similar, although the particle activity (the number of particles in motion per unit streambed area) in Run 2 is on average approximately 250% higher than in Run 1.

Particle tracking was performed using the open-source software ImageJ. This involved marking the centroid of each particle as it moves through successive frames. We manually tracked particle motions, frame-by-frame, in each experiment. Approximately 95% of the particles in motion were tracked; the 5% of particles that were not tracked either left the field early or proved too difficult to follow through the course of the video. For Run 1 we measured more than 150,000 particle coordinate positions involving more than 10,000 active particles during 5 seconds, and nearly 170,000 positions in Run 2 involving more than 11,000 active particles during 2 seconds. We also identified approximately 4,000 complete

hops (measured start-to-stop) in Run 1 and approximately 3,500 hops in Run 2. Particles were tracked only after they began to move. We did not track the motions of particles that "wiggled" back and forth within their pockets but otherwise did not move or hop. Individual hops were measured from incipient motion to a stopped position such that both the streamwise and cross-stream velocities are zero. All particles were manually tracked by one individual to maintain consistency. This manual, time-intensive measurement technique yields sub-pixel resolution measurements and provides high fidelity characterization of particle motions, notably including measurements of small motions which dominate the probability distributions of particle velocities, hop distances and associated travel times (*Fathel et al.*, 2015).

3.5 Diffusive Nature of Individual Particles

With reference to our high-resolution measurements of particle motions, the behavior of an individual particle as measured by its mean squared displacement $R_x(\tau)$ using (1) (Fig. 3.1) and its velocity autocorrelation function $A_x(\tau)$ (see *Supplementary Material* for examples) is distinct, unlike any other particle or the ensemble behavior (described below). The basic source of this result resides in the fact that particle travel times are too short for the stochastic signature of individual particle-fluid and particle-bed interactions to become statistically similar to those of other particles. These calculations moreover reveal the inherent periodicities of start-and-stop motions (*Furbish et al.*, 2012b).

Specifically, $R_x(\tau)$ for an individual particle reflects the effect of the dominant harmonic in its motion. By definition these hops start from rest, then stop, with a peak velocity in between. So regardless of how the velocity varies during the hop, at a basic level the hop possesses a fundamental harmonic, often the dominant harmonic. Indeed, *Furbish et al.* (*Furbish et al.*, 2012b) show that the shape of the function $R_x(\tau)$ is well described by the mean squared displacement calculated for a single sinusoid having period T and amplitude A coinciding with the dominant harmonic. The mean squared displacement for an individ-

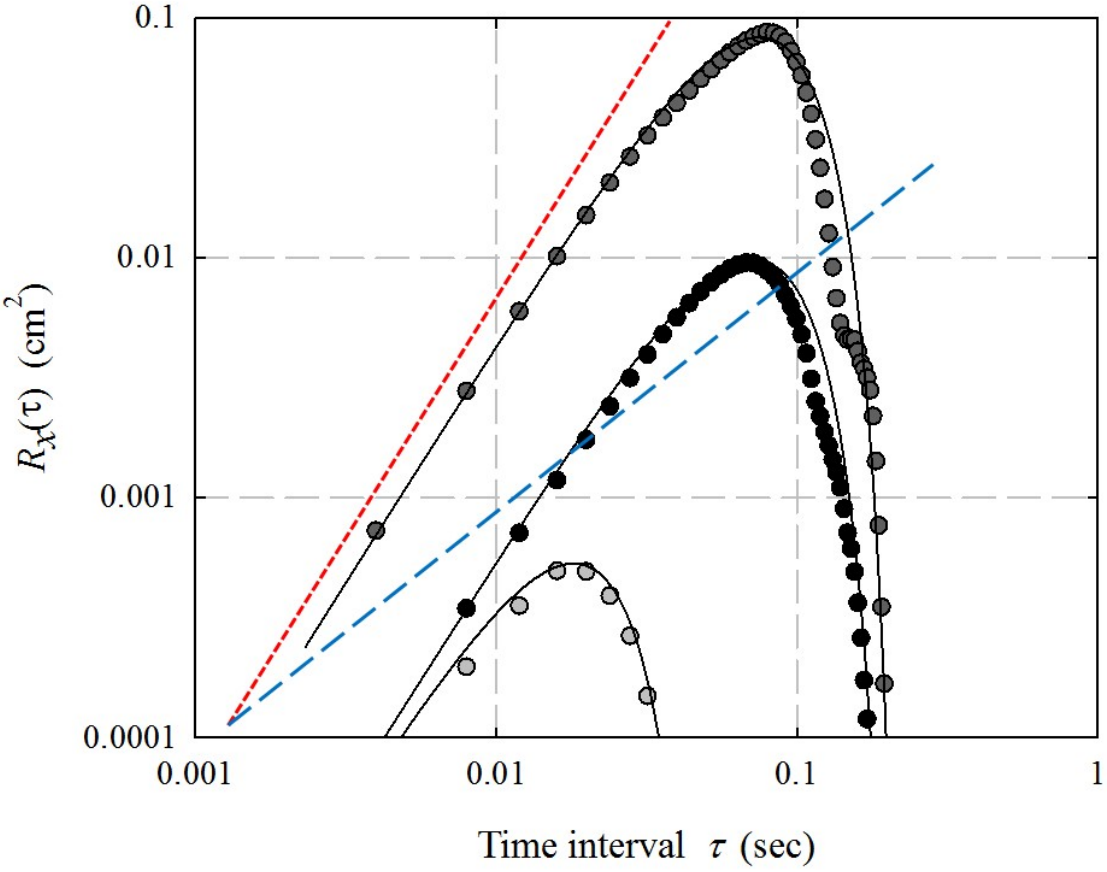

Figure 3.1: Plot of calculated (filled circles) and theoretical (solid lines) values of the mean squared displacement $R_x(\tau)$ versus time interval τ for individual particle motions in Run 1 whose dominant harmonics have periods $T = T_p$ and amplitudes A, where ballistic-like regime is given by $(2\pi^2 A^2/T^2)\tau^2$. The short-dashed red line possesses a log-log slope of 2, whereas the long-dashed blue line has a log-log slope equal to 1. Figure modified from (*Furbish et al.*, 2012b). Copyright ©2012. American Geophysical Union.

ual particle thus characteristically shows ballistic-like behavior ($a = 2$) at small τ given by $(2\pi^2 A^2/T^2)\tau^2$, followed by a declining slope ($1 \leq a \leq 2$) with increasing τ (Fig. 3.1). The value of $R_x(\tau)$ in (1) peaks and thereafter declines toward zero as a consequence of the finite travel time T_p, that is, as the interval $\tau \to T_p$, where (1) must equal zero when $\tau = T_p$. The ballistic-like behavior reflects that particle velocities are approximately constant over small τ, likely representing a characteristic interval between particle-bed collisions (*Nikora et al.*, 2002). But with strong particle-fluid coupling with small Stokes number, this is not true ballistic behavior in the sense of a Brownian particle moving through a vacuum between successive collisions. It is for this reason that we refer to the behavior $R_x \sim \tau^2$ associated with a bed load particle as being "ballistic-like" rather than ballistic (*Furbish et al.*, 2012b). Moreover, the declining slope over the range $2 < a < 1$ then over $1 < a < 0$ before the peak value of $R_x(\tau)$ reflects that particle motion is essentially a correlated random walk. Like a Brownian particle this is a transitional behavior; it does not represent anomalous diffusion, as it is not an emergent, time-invariant behavior. But unlike a Brownian particle, it is not attributable to inertial effects.

In comparison, experiments (*Li et al.*, 2010; *Huang et al.*, 2011) reveal that the form of $R_x(\tau)$ for a Brownian particle is similar to that above, including the ballistic regime ($a = 2$) described by $(k_B T/m^*)\tau^2$, where k_B is Boltzmann's constant, T is temperature and m^* is the effective particle mass, followed by an inertially influenced transition ($1 < a < 2$) to the normal regime ($a \to 1$). In these experiments the peak and the decline to zero as $\tau \to T_s$ observed with sediment particles is replaced with a plateau in $R_x(\tau)$ due to effects of the optical trap used to contain the Brownian particle (*Huang et al.*, 2011).

3.6 Calculations for Groups of Particles Reveal both Normal and Inhomogeneous Diffusion

We use both (1) and (2) to calculate the mean squared displacement for groups of particles. In the first case, because the ensemble calculation (1) averages over all paired co-

ordinate positions (for all particle motions) associated with the interval τ (*Furbish et al.*, 2012b; *Martin et al.*, 2012), we are not concerned with when particles start and stop. We thus include all tracked particle motions, rather than just completed hops. In the second case, because the tracer calculation (2) treats the particles as a virtual plume, averaging over all particles (rather than all paired coordinate positions), the starting position $x_p(0)$ and time $t = 0$ matter. We thus include only completed hops, treating these particles as tracers.

The ensemble calculation of $R_x(\tau)$ involving all motions reveals ballistic-like behavior at small τ, similar to the plots of $R_x(\tau)$ for individual particles (Fig. 3.2). Then, over small to intermediate τ, the exponent $a > 1$ suggests an apparent superdiffusive behavior. The slope of $R_x(\tau)$ then declines and approaches $a = 1$ with increasing τ, indicating normal diffusive behavior. Finally, similar to the plot of $R_x(\tau)$ for individual particles, $R_x(\tau)$ reaches a peak then declines towards zero with increasing τ, as the sample size of paired observations also decreases with increasing τ.

The apparent superdiffusive behavior ($a >1$) represents the collective effect of correlated (sinusoidal) random walks of the many particles included in the calculation of $R_x(\tau)$, which then become increasingly randomized by brief, rapid accelerations due to particle-fluid and particle-bed interactions (*Furbish et al.*, 2012b). As the motions become increasingly randomized through longer travel times, they tend towards normal diffusion ($a = 1$). The slope of $R_x(\tau)$ from Run 2 approaches Fickian diffusion more quickly than Run 1, highlighted by the fitted lines in Figure 3.2. This is likely due to the higher activity in Run 2, wherein moving particles have increased interactions with the bed and other active particles. Importantly, for comparison the ensemble calculation of $R_x(\tau)$ using only those particles completing full hops (start-to-stop) yields virtually identical results (Fig. 3.2). This is expected, as these hops represent a sample of all possible motions.

In contrast, by treating these full hops as tracer particles, the tracer calculation (2) of $R_x(t)$ yields both apparent superdiffusive (Run 1) and apparent super-ballistic (Run 2) be-

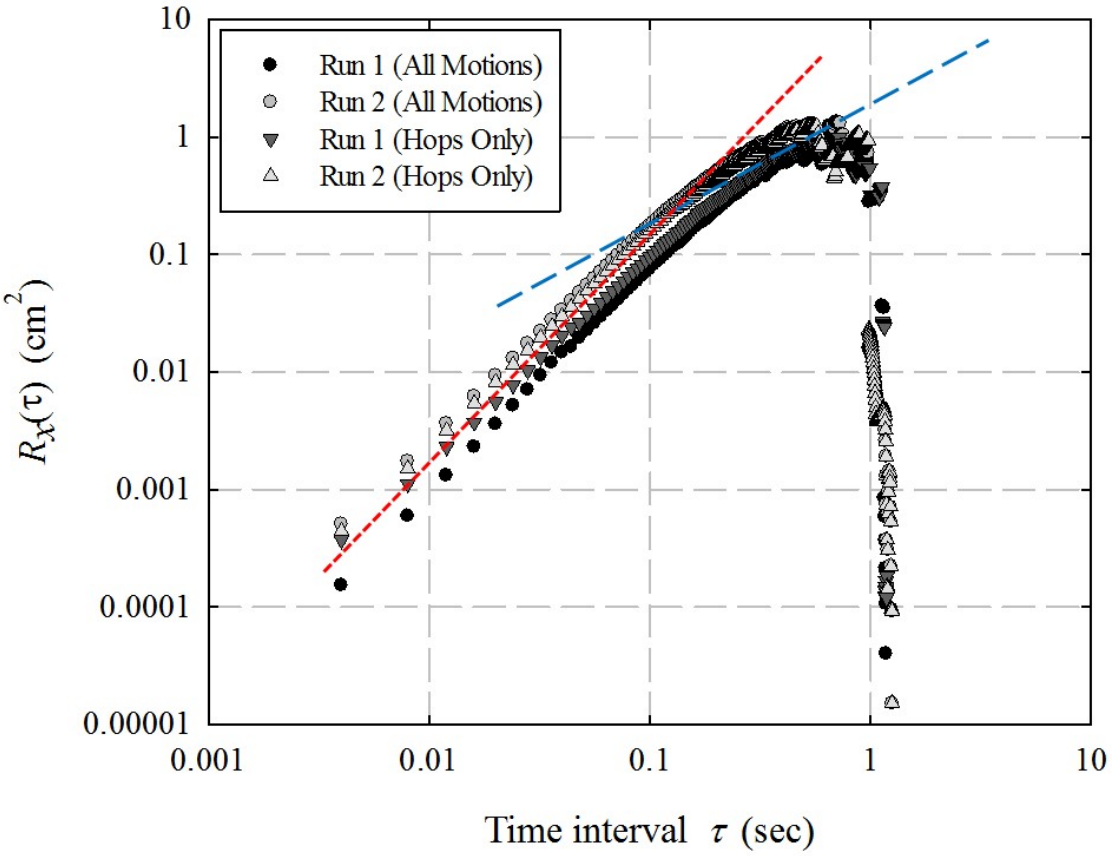

Figure 3.2: Plot of the mean squared displacement $R_x(\tau)$ versus the time interval τ for all particles motions within Run 1 (black circles) and Run 2 (light gray circles), and for all complete hops within Run 1 (dark gray triangles) and Run 2 (white triangles). The short-dashed red line possesses a log-log slope of 2, whereas the long-dashed blue line has a log-log slope equal to 1.

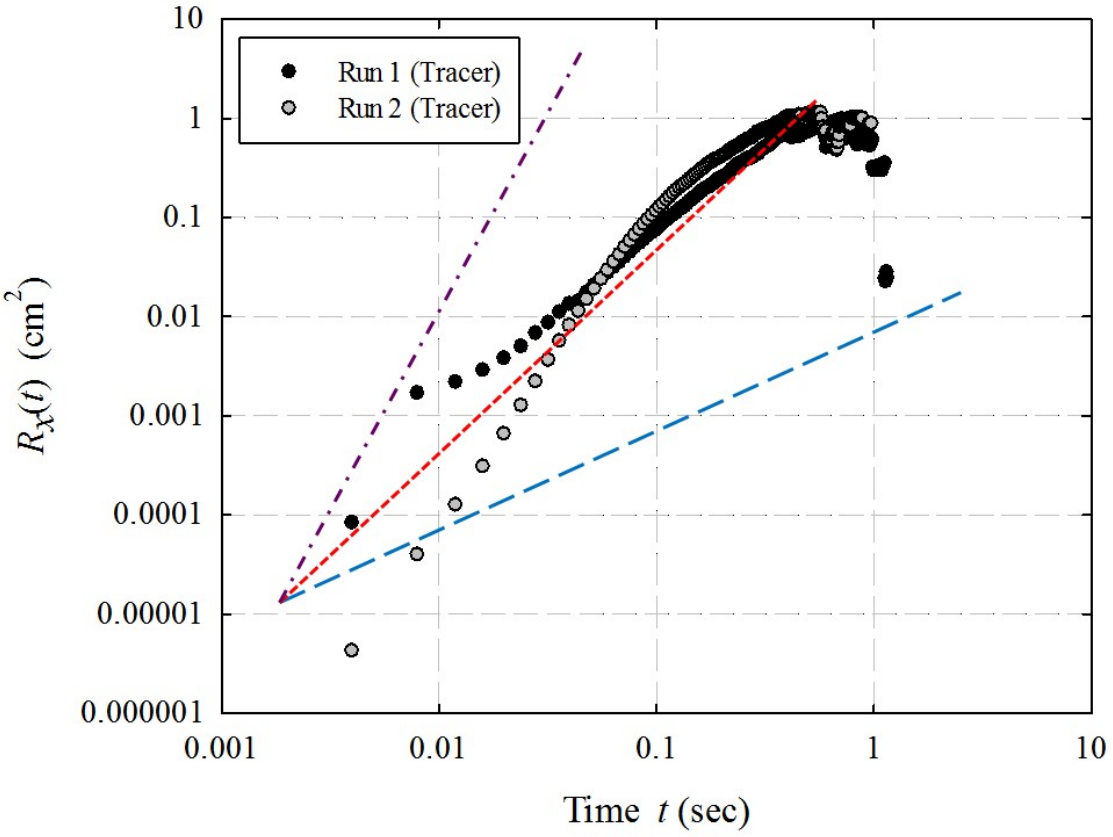

Figure 3.3: Plot of the mean squared displacement $R_x(t)$ versus time t for all complete hops within Run 1 (black circles) and Run 2 (gray circles). Here, the dotted-dashed purple line has a log-log slope equal to 4, the short-dashed red line possesses a log-log slope of 2, and the long-dashed blue line has a log-log slope equal to 1.

haviors (Fig. 3.3). The essential reason for this apparent anomalous behavior resides in the joint probability distribution of hop distances L_x and associated travel times T_p (*Supplementary Material*, Figures S2-S3). Specifically, experimental data and dimensional analysis (*Fathel et al.*, 2015; *Furbish et al.*, 2016a) suggest that

$$L_x = a_x T_p^2 + \varepsilon, \tag{3.4}$$

where a_x [L T^{-}2] is a characteristic acceleration and ε denotes a stochastic deviation about the expected hop distance. Importantly, the deviation ε is heteroscedastic in arithmetic space involving an increase in the variance about the expected hop distance with increasing travel times (*Supplementary Material*, Figure S2), whereas it is approximately homoscedastic in log-log space such that the variance about the expected hop distance is uniform with increasing travel times (*Supplementary Material,* Figure S3). This means that the local variance in hop distance for a given travel time, denoted as V_ε, increases with T_p as

$$V_\varepsilon(T_p) \sim T_p^b, \tag{3.5}$$

with exponent $b > 1$ (*Supplementary Material*). Indeed, $b \approx 3$ (Fig. 3.4), which is consistent with values reported by *Campagnol et al.* (2015). This result influences the mean squared displacement $R_x(t)$ as follows.

Particle hops in both experiments are distributed as a Weibull distribution with shape parameter $k < 1$, such that the majority of hops involve short displacements (*Fathel et al.*, 2015). Whereas there is not a direct correspondence between $R_x(t)$ and $V_\varepsilon(T_p)$ for $t = T_p$, this correspondence is exact for the subset of particles that come to rest within an interval T_p to $T_p + \mathrm{d}T_p$. Moreover, particles that move beyond this interval (eventually stopping at longer total travel times) are likely distributed in a manner at $t = T_p$ that is similar to those particles stopping within this interval. We may thus assume that $R_x(t) \sim V_\varepsilon(T_p)$ for $t = T_p$. This means that at small times the tracer calculation of $R_x(t)$ on average "sees"

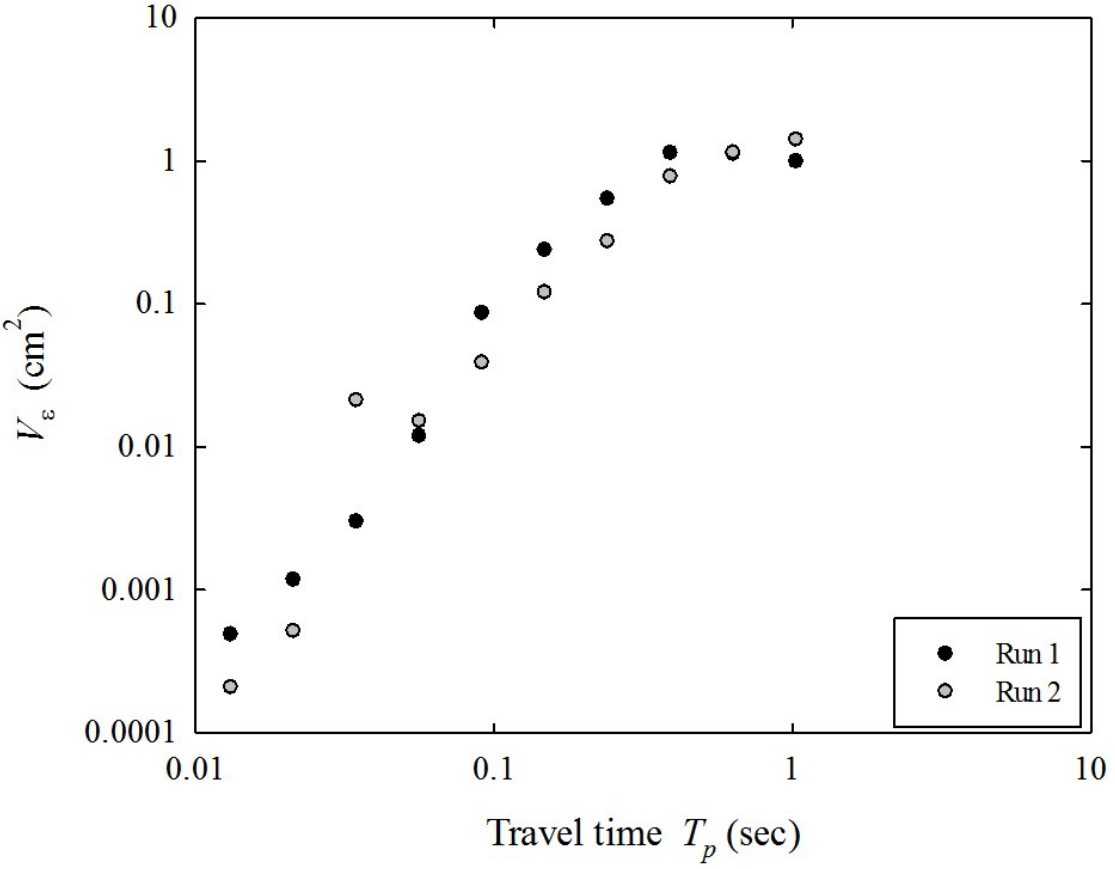

Figure 3.4: Plot of the local variance in hop distances V_ε versus travel time T_p for Run 1 (black circles) and Run 2 (gray circles). The variance V_ε is calculated for arithmetic values of hop distances within equally spaced bins (log values) of travel times T_p.

a small variance about the expected travel distance from many particles. With increasing time this calculation sees an increasing variance about the expected distance dominated by fewer particles with larger travel times. The tracer calculation therefore reflects the behavior of mostly short hops (and the early stages of longer hops) at small times, and the behavior of increasingly longer hops with increasingly larger times. This behavior is statistically inhomogeneous and time dependent. Moreover, the calculated average displacement, which increases nonlinearly with time, is associated with an expected time-average velocity $\langle L_x/T_p \rangle$ that also increases with time. This is not an average velocity in the sense of a uniform mean motion with superimposed, homogeneous diffusion. For these reasons the behavior represented in Figure 3.3 represents inhomogeneous diffusion, not anomalous diffusion.

3.7 Velocity Autocorrelations Show Normal Diffusion

The ensemble calculation of the autocorrelation function $A(\tau)$ involves all paired velocity values (for all particle motions) separated by the interval τ, and therefore is the same for pooled motions and for particles completing full hops (Fig. 3.5). Numerical integration of the functions $A_x(\tau)$ reveals rapid convergence to fixed timescales for these experiments. However, contrary to previous assertions (*Furbish et al.*, 2012b; *Fathel et al.*, 2015), we cannot use these integrations to provide a Lagrangian timescale as Taylor intended. In both runs the lag-one value of $A_x(\tau)$ is substantially less than one, and the second and higher lags then decay exponentially more slowly than what would be anticipated based on the lag-one value. This behavior also appears in similar data (*Martin et al.*, 2012) and in calculations of $A_x(\tau)$ for individual particles. It represents an unstructured noise in the velocity signals of individual particles, which may in part be associated with the limits of image resolution. It also is the signature of a mixture of velocity signals with different covariance structures (and degrees of persistence), reflecting the point made above, that particle travel times are too short for the stochastic structure associated with individual particles to be-

come statistically similar to those of others. Moreover, values of $A_x(\tau)$ with increasing lag τ are increasingly represented by fewer particles with travel times $T_p \geq \tau$. The significance of these functions therefore is that their convergence is consistent with a normal diffusive behavior, that is, lacking any long-term memory in collective velocity behavior — a result that cannot be readily inferred from the autocorrelation functions of individual particles.

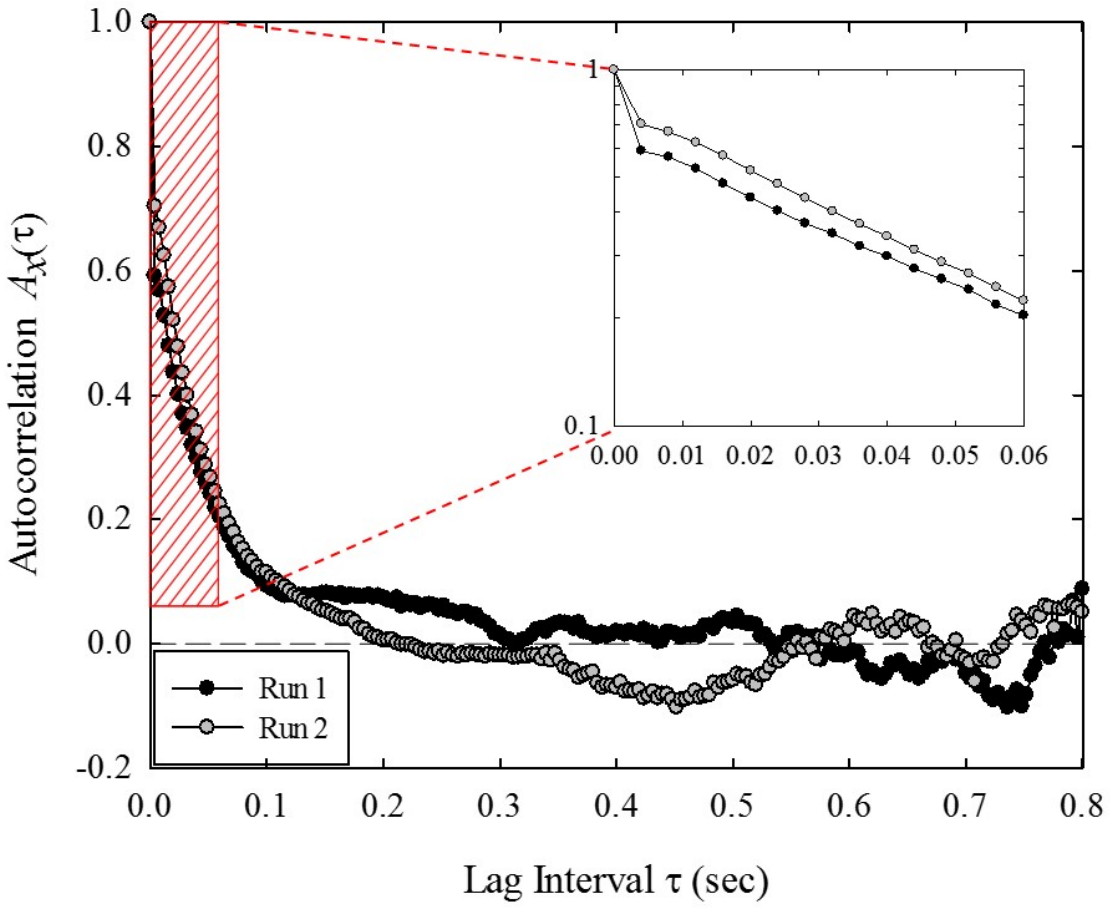

Figure 3.5: Plot of the particle velocity autocorrelation function $A_x(\tau)$ for Run 1 (black circles) and Run 2 (gray circles), with inset showing exponential decay after first lag.

3.8 Conclusions: Parsing the Different Diffusive Behaviors

In the context of the tracer calculation of $R_x(t)$, the longest travel times are approximately 1.2 s, and the mean travel times are 0.12 s (Run 1) and 0.16 s (Run 2). Therefore,

we suspect that apparent anomalous behavior represents a small proportion of the total duration of particle spreading that occurs within a flume experiment or natural system. In our experiments, apparent anomalous diffusion at the intermediate timescale of particle hops is a brief transition behavior preceding the onset of effects of rest times on the spreading of a plume of particles, for which there is reason and experimental evidence to expect emergent anomalous behavior (*Martin et al.*, 2012).

Because the ensemble calculation of $R_x(\tau)$ is based on all paired coordinate positions associated with intervals τ without reference to when the motions started, this calculation is appropriate for describing particle diffusion in relation to the particle flux. Envision a cloud of particles which are moving with varying velocities through a surface A normal to the x axis under conditions of steady transport. For sufficiently large A, the particles intersecting this surface at time t represent a sample of all velocity states in proportion to all stages of motion during hops, whether these involve (mostly) short or long travel times. That is, these particles at any instant represent the ensemble distribution of particle velocities for given sediment and macroscopic flow conditions. The ensemble calculation of R_x thus provides a measure of the rate of particle spreading within the vicinity of A. From Figure 3.2 where the slope $a = 1$, the pooled data give κ_x equal to 0.71 $\text{cm}^2\ \text{s}^{-1}$ (Run 1) and 1.37 $\text{cm}^2\ \text{s}^{-1}$ (Run 2).

Inhomogeneous diffusion indeed represents the spreading of tracer particles, and whereas the mean squared displacement has the signature of anomalous diffusion, this behavior is not anomalous diffusion as normally envisioned. It is a consequence of the tracer calculation of R_x, which start all full hops at the same time and averages over particle displacements rather than all paired observations separated by the interval τ as is done in the ensemble calculation. The behavior of particle spreading differs in these calculations, such that the apparent superdiffusive (Run 1) and apparent super-ballistic behaviors (Run 2) reveal the nonlinear rate of increase in the local variance of particles displacements as reflected in the 'static' distribution of hop distances L_x versus travel times T_p.

The data presented here are specific to our experimental conditions. Details of the statistical behavior of bed load particles will change with different sediment and flow conditions. Thus, there is a pressing need to improve automated particle tracking techniques that provide high fidelity measurements of the small particle displacements and velocities that dominate bed load particle motions (*Fathel et al.*, 2015) in order to explore a wider range of sediment and flow conditions. Meanwhile, the key ideas presented here are transferable to other conditions, as bed load particle motions share common attributes that are strongly manifest in the calculations of particle spreading, most notably their start-and-stop behavior in response to particle-fluid and particle-bed interactions, and the statistical inhomogeneity amongst particle motions over start-and-stop timescales. Moreover, particles in other complex natural systems may similarly exhibit start-and-stop motions that are statistically inhomogeneous, likely including biotic 'particles' (*Viswanathan et al.*, 2005; *de Jager et al.*, 2014). Our analysis indicates that care is needed in suggesting anomalous behavior when appealing to conventional measures of diffusion formulated for ideal particle systems. Despite the similarity between the behavior of sediment and Brownian particles as measured by the ensemble calculation of the mean squared displacement $R_x(\tau)$, the ballistic-like behavior, followed by apparent anomalous behavior due to correlated random walks in transition to normal diffusion, involves distinctly different physics between these systems.

CHAPTER 4

Experimental Exploration of Elements of Sediment Entrainment and Disentrainment

4.1 Abstract

Detailed measurements of individual sand grains moving on a streambed allow us to obtain a deeper understanding of the characteristics of incipient motion and evaluate spatial and temporal patterns of particle entrainment. We use bed load particle motions measured from high-speed imaging (250 Hz) of uniform, coarse grained sand from two flume experiments, which have different mean fluid velocities near the bed. Particle tracking reveals more than 6,000 entrainment events in 5 seconds (Run 1) and over 5,000 events in 2 seconds (Run 2). We manually track particles from entrainment to either disentrainment or until the particle leaves the frame. Within these experiments we find that over 90% of all initial motions contain a cross-stream component of motion where approximately a third of the motions may be cross-stream dominated, and furthermore, up to 7% of the motions may be negative (i.e., move backwards). We propose that the variability in the direction of initial motion is, in part, a product of the bed microtopography, where we find that with increasing mean fluid velocity, the initial motion of the sand particles are less sensitive to bed topography, and are more likely to be dominated by fluid forces. The high resolution of this data set, containing positions of particles measured start-to-stop, allows us to examine the distributions of particle rest times (the duration of time between the disentrainment of a particle and the reentrainment of that particle) and particle wait times (the duration of time between successive particle motions in an area). Our examination of particle rest times reveals a distribution that is distinctly not exponential and provides a clear example of experimental censorship. The distribution of wait times indicates an intermittency in sediment transport. Analysis of simultaneous measurements of near-bed fluid velocities and particle motions

in Run 2 indicate that fluid velocities are not necessarily higher near entrainment events. These results suggest the connection between the fluid and particle entrainment is complex and will require a clearer understanding of the factors that jointly influence entrainment at the particle scale. Our work suggests that the probability of entrainment likely depends on physical factors such as bed microtopography and the magnitude of the fluid velocity, in addition to varying with space and time scales.

4.2 Introduction

4.2.1 Key Elements of Bed Load Transport

Recent probabilistic formulations of bed load sediment transport and the spreading behavior of tracer particles in flumes and natural channels have focused on the entrainment form of the Exner equation (*Parker et al.*, 2000b; *Ganti et al.*, 2010; *Furbish et al.*, 2012a, 2016b; *Pelosi et al.*, 2014) in which the local rate of change in streambed elevation or tracer concentration is expressed as the difference between the rate of particle entrainment and the rate of deposition (*Tsujimoto*, 1978). The rate of deposition, in turn, may be expressed as a convolution of the upstream entrainment rate, modulated by the distribution of particle hop distances (*Furbish et al.*, 2012a; *Parker et al.*, 2000b). As a general probabilistic description of conservation, this form of the Exner equation explicitly accounts for the motions of all particles (including tracer particles), and its use therefore is particularly appealing in studies of both streambed morphodynamics and the spreading behavior of tracer particles (*Furbish et al.*, 2016a, b; *Pelosi et al.*, 2013), notably involving coarse-sediment rivers in which sediment transport predominantly occurs as bed load close to threshold (e.g., *Pitlick and Cross*, 2002; *Mueller et al.*, 2005; *Phillips and Jerolmack*, 2016), where rarefied conditions likely are the norm.

The central elements of the entrainment form of the Exner equation include the volumetric entrainment rate and the distribution of particle hop distances measured start-to-stop.

When formulated specifically to describe the motions of tracer particles, key elements also include particle rest times between successive motions. Until recently, these elements of particle motions have been described based on experimental measurements of transport involving limited resolution, or their properties (e.g., the forms and moments of the distributions of hop distances and rest times) have been based on limited data, or assumed (*Furbish et al.*, 2016a). This has had the effect of limiting efforts to more fully develop and constrain theoretical treatments of transport. For example, starting with the early work of *Einstein* (1937), researchers have examined the consequences of various forms of the distributions of hop distances on morphodynamic behavior and tracer particle spreading (*Hubble and Sayre*, 1964; *Sayre and Hubble*, 1965; *Yang and Sayre*, 1971; *Bradley et al.*, 2010; *Bradley and Tucker*, 2012), but this is limited to comparing the spreading behavior of tracer particles with predicted behavior predicated on the assumed distribution. Recently, however, experimental methods, centered on high-speed imaging of both particles and fluid motions (e.g. *Martin et al.*, 2012; *Radice et al.*, 2013; *Houssais et al.*, 2015; *Fathel et al.*, 2015, 2016), are providing the opportunity describe details of the motions of particles transported as bed load. For example, these methods have led to recent advances in clarifying the distributions of hop distances and associated travel times (*Martin et al.*, 2012; *Ancey and Heyman*, 2014; *Heyman et al.*, 2013; *Fathel et al.*, 2015; *Furbish et al.*, 2016a), although little work has been focused on direct measurements of rest times and wait times. In addition, these methods are capable of revealing details that suggest elements of the physics of entrainment and disentrainment in relation to fluid motions, thereby providing the opportunity to gain a deeper mechanical understanding of these quantities, and move beyond semi-empirical formulations of entrainment and disentrainment, and other features of particle motions that influence particle spreading.

With respect to particle entrainment, the "initial motion problem" centered on sediment particles has been a focus of study for many years (e.g., *DuBoys*, 1879; *Komar and Li*, 1986; *Bridge and Bennett*, 1992; *Buffington and Montgomery*, 1997; *Papanicolaou et al.*,

2001). At a macroscopic scale larger than the particle scale, the volumetric entrainment rate E typically has been expressed as a semi-empirical function of the shear velocity u_* or the bed stress $\tau_b = \rho u_*^2$, where ρ is the fluid density. Early formulations are represented by those of *Einstein* (1950), *Fernandez Luque* (1974), *Fernandez Luque and van Beek* (1976), *Yalin* (1977) and *Nakagawa and Tsujimoto* (1976, 1980), and have been elaborated more recently by, for example, *Seminara et al.* (2002) and *Parker et al.* (2000a). These formulations mostly suggest that $E \sim (\tau_b - \tau_c)^{3/2}$, where τ_c is a critical stress required for initiation of particle motion. Furthermore, studies have also shown that a variety of factors may influence initial motion, such as grain protrusion and exposure (*Fenton and Abbott*, 1977; *Raudkivi and Ettema*, 1982), friction angle (*Buffington and Dietrich*, 1992), bed packing (*Church*, 1977), and bed relief (*Laronne and Carson*, 1976) among others. Although we recognize the influence of these factors on incipient motion and understand the general stress conditions required to mobilize sediment (*Shields*, 1936), predicting initial sediment motions often proves to be more difficult (*Buffington and Montgomery*, 1997). In general, bed load transport equations tend to perform well only under specific conditions (*Gomez and Church*, 1989), and often errors are substantial such that transport rates are overestimated by several orders of magnitude (e.g *Yager et al.*, 2007; *Rickenmann*, 2001; *Recking*, 2012).

In addition to the factors influencing the incipient motion of particles, predicting bed load sediment entrainment likely will require a better understanding of near-bed fluid turbulence. Studies have shown that turbulence is related to bed load sediment transport (e.g., *Sumer et al.*, 2003) and now researchers often include turbulence within models of incipient particle motions (e.g., *Zanke*, 2003; *Vollmer and Kleinhans*, 2007). Researchers have also demonstrated the existence of coherent turbulence structures which span scales from small near-bed eddies to structures occupying the entire flow depth (e.g., *Grass*, 1971; *Nezu et al.*, 1994; *Dwivedi et al.*, 2010). It has been suggested that these structures play a key role in sediment entrainment and transport (e.g., *Grass*, 1970; *Jackson*, 1976; *Drake et al.*,

1988; *Mazumder*, 2000). The coupling between turbulent structures and bed load sediment motions is frequently mentioned in research on this topic, and is thought to be important to bedform initiation (e.g., *Nelson et al.*, 1995; *Nikora et al.*, 2002; *Lajeunesse et al.*, 2010; *Singh et al.*, 2012; *Bialik*, 2013). Yet, despite the suggested importance of turbulence structures, direct observations of coupled fluid and sediment motions are sparse.

With respect to the spreading behavior of tracer particles, early work envisioned this problem as involving motions of particles only over the bed surface or confined within a thin "active layer" (*Hirano*, 1971; *Parker*, 1991), where particle hops are separated by rest times with a well-defined probability distribution. Like treatments of the hop distances, this early work was largely limited to exploring the consequences of assumed forms of the distribution of rest times for comparison with experiments (e.g. *Bialik et al.*, 2015). In addition, recent theoretical and experimental evidence has emerged suggesting that the idea of a thin active layer is an over-simplification (*Parker et al.*, 2000b; *Furbish et al.*, 2012a, 2016b), and that lengthened rest times associated with particle exchanges with the streambed can have a strong influence on the downstream spreading of tracer particles as well as overall particle residence times (*Hassan et al.*, 2013; *Voepel et al.*, 2013).

Within this context, achieving a clearer understanding of the transport and spreading behavior of bed load particles and tracers requires a more detailed description of key features associated with the processes of particle entrainment and disentrainment. Particle entrainment, together with wait times between successive entrainment events, determines the intensity of transport. Particle disentrainment determines the distance that particles move following entrainment, that is, the distribution of hop distances, and together with intervening rest times, influences the virtual velocity and spreading of tracer particles. The processes of entrainment and disentraiment, however, involve more than 'starting' and 'stopping.' As outlined next, we are aimed at describing details of particle behavior that may reveal important aspects of the mechanical behavior of particles during entrainment and disentrainment, as well as provide guidance concerning limitations of experimental

measurements of particle rest times.

4.2.2 Objectives

The purpose of this paper is to provide details of particle behaviors pertinent to the processes of bed load sediment entrainment and disentrainment. We begin by addressing factors that specifically concern particle entrainment: a description of the initial direction of particle motions, the spatial distribution of entrainment, and connections between the near-bed fluid and sediment entrainment. We then turn to the distribution of wait times between entrainment events, which informs the transport intensity. Finally we address the problem of particle rest times, or the durations of time between entrainment events for a single particle, which, although a consequence of disentrainment rather than being a part of disentrainment, bears importantly on the spreading behavior of tracer particles. To investigate each of these factors, we utilize precise measurements of particle motions and fluid velocities obtained from two different flume experiments: Run 1 and Run 2. The details of these experiments can be found in the following section. In the remainder of this section, we provide information concerning each of our objectives and place them within the context of the larger problem of sediment entrainment and disentrainment.

In Section 4.4, we use detailed measurements of particle motions to evaluate the distribution of angles and magnitudes of the first motion of a particle. Microtopography in stream beds has been analyzed in various studies, wherein researchers have shown that cluster microforms, which stand above an otherwise planar bed, effectively shield particles and lower the probability of entrainment (*Laronne and Carson*, 1976; *Brayshaw*, 1985). While this process has been noted in both natural systems (*Dunkerley*, 1990) and experimental work (*Church et al.*, 1998), generally microtopography is not considered to have a substantial consequence on particle entrainment on the grain-size scale. Yet, our measurements of initial particle motions from Run 1 and 2 suggest that microtopography influences the direction and magnitude of initial sediment motions and therefore may also provide a

certain amount of shielding to particle motions.

Section 4.5 provides an analysis of the spatial distribution of entrainment using a nearest neighbor analysis to determine if entrained particles are clustered, uniformly distributed, or dispersed. Previous studies have indicated a patchiness in spatial entrainment associated with selective entrainment and deposition controlled by the mean diameter of local sediment (e.g., *Paola and Seal*, 1995). Furthermore, *Powell and Ashworth* (1995) show that variations in bed structure and stability can lead to spatial variability in entrainment. In addition, micro-bedforms (as described above) can create areas of preferential entrainment. While this has been a topic of study, the majority of data available analyzes the distribution of entrainment on the reach scale, and often involves a heterogeneous mixture of grain-sizes and persistent bedforms. The scale and nature of these studies differ from this study. Here, we find that entrainment positions are highly clustered, especially when considering particle positions from large groups of frames. We suspect that the clustered nature of entrainment may be a product of microtopography and collective entrainment, where resting particles may be activated by moving particles which can interact directly (collision) or indirectly (wake effect, advection of turbulent structure) to entrain particles (*Ancey et al.*, 2008; *Ancey*, 2010).

Within Section 4.6, we begin to analyze the complex relationship between the near-bed fluid velocities and newly activated particles. Here we use a combination of particle tracking measurements taken from Run 2 along with near-bed fluid velocity measurements obtained from particle image velocimetry, which allows us to gain a better understanding of fluid controls on incipient motion. These simultaneous measurements provide an initial step towards describing the dynamic relationship between the fluid and particle entrainment. Correlating the fluid velocities and the initiation of sediment transport may seem simple, but properly delineating this relationship is likely more complex. Section 4.6 is separated into two subsections which analyze correlations between near-bed fluid velocities and entrained particles by utilizing two different methods. First we apply an Eulerian *a*

priori method, where we grid the analyzed area and compare the fluid velocity time series to the time series of entrainment events within each grid. We progressively increase the size of the grids and monitor the correlation between the time series. In the second subsection, we take an *a posteriori* method, such that we focus on the fluid velocities in the vicinity of entrained particles, both at the moment of entrainment and prior to the initiation of motion. Each of these methods provides us with a direct look at interactions between the fluid and particle motions. The results of both methods, perhaps surprisingly, do not indicate a strong correlation between the nearby fluid velocities and locations of entrainment.

In Section 4.7, we consider particle wait times T_w. The distinction here between a wait time and rest time is that a wait time is defined as the time elapsed between successive particle motions in an area, rather than looking at an individual particle. Importantly, the distribution of wait times informs the intensity of transport, as it measures the frequency of entrainment events over a given area. Furthermore, if sediment entrainment is a Poisson process, wherein particles are entrained only when the fluid-derived forces acting on a stationary particle exceed the resisting force and there is no collective entrainment, the distribution of wait times should be exponentially distributed (e.g. *Ancey et al.*, 2008; *Bradley and Tucker*, 2012). *Ancey et al.* (2008) proposed a "birth-death" Markov model, where the number of particles in motion can be entrained due to water effects *and* interaction with moving particles (i.e. collective entrainment). Within this model, an estimate of the wait time between entrainment events is required, but often these values are estimated from hop distances and travel times or are assumed, rather than being obtained from direct measurements (*Ancey et al.*, 2008; *Ancey*, 2010; *Turowski*, 2010). Our work provides a direct, albeit limited, measurement of the wait time distribution, which provides a step towards understanding the nature of the bed load transport.

Section 4.8 illustrates and examines the distribution of particle rest time T_r measured in Run 1 and Run 2. Here, we define a rest time as the duration of time elapsed between the disentrainment of a particle and the rentrainment of that particle. Bed load sediment trans-

port involves the movements of individual grains. These particle motions are discrete and are comprised of a series of particle 'hops' consisting of brief active periods separated by periods of rest (e.g., *Einstein*, 1937; *Hassan et al.*, 1991; *Lajeunesse et al.*, 2010; *Roseberry et al.*, 2012; *Fathel et al.*, 2015). Therefore, to properly define entrainment and, more generally, bed load transport, we must also gain an understanding of these rest periods. Many probabilistic models of bed load transport consider particle velocities, hop times (continuous periods of motion), rest times (continuous periods of inactivity), and rates of entrainment and disentrainment (e.g., *Nikora et al.*, 2002; *Lajeunesse et al.*, 2010; *Furbish et al.*, 2012a; *Furbish and Schmeeckle*, 2013). While new measurement techniques, including high speed imaging, are providing an unprecedented opportunity to observe and measure particle motions, information on the nature of rest times is limited. As summarized by *Bialik et al.* (2015), available data indicate that this distribution is either exponential (*Einstein*, 1937, 1950; *Habersack*, 2001) or may take the form of a power law if deposited particles are buried by other particles (*Martin et al.*, 2012, 2014; *Voepel et al.*, 2013). Here lies a distinct problem: Governing partial differential equations for sediment transport are highly responsive to heavy-versus light-tailed rest times distributions. For example, the commonly used advection-diffusion equation, which describes a diffusive change in particle concentration with time as a function of average velocity and spread around that average, is only valid for light-tailed particle rest times (*Ganti et al.*, 2010; *Hassan et al.*, 2013). Additionally, *Nikora et al.* (2002) suggest that anomalous diffusion on intermediate to global timescales may arise from rest periods with a heavy tail. The tail (either light or heavy) of the rest time distribution acts as a control over diffusion, such that if particle rest times are heavy tailed, then the dynamics of rest times should dominate the dispersive behavior of particles (*Martin et al.*, 2012; *Hassan et al.*, 2013; *Voepel et al.*, 2013).

Another clear implication of the form of the rest time distribution deals with inconsistencies in the conceptualization of bed load discharge. More specifically, *Einstein* (1937) considered bed load transport as a compound Poisson process which is comprised of short

periods of motion of random distances with intervening rest periods of random length. Consistent with this, Einstein and others have assumed that both the hop distances and rest times are exponentially distributed, but recent work has shown the distribution of rest times may not follow an exponential distribution (*Martin et al.*, 2012, 2014; *Heyman et al.*, 2013; *Voepel et al.*, 2013). These examples all highlight the importance of obtaining more empirical evidence of the distribution of rest times. Data from Run 1 and 2 indicate that the rest time distributions are distinctly non-exponential and take a form similar to a power-law distribution. We fundamentally recognize that our measurements of rest times are limited by our sampling times (0.4 seconds) and window size (~ 45 cm^2). Therefore in the latter part of Section 7, we examine whether the form of this distribution is a product of the system, or rather a result from the spatial and temporal censorship of these data.

4.3 Methods and Measurements

The experimental data presented here were collected in the River Dynamics Laboratory at Arizona State University using an 8.5 $\times$ 0.3 m recirculating flume. Measurements were taken from high-speed (250 Hz) imaging of coarse sand (D_{50} = 0.05 cm) transported as bed load under equilibrium conditions in two flume experiments. The sediment bed is photographed through a plexiglass "sled" window placed on the surface of the water. This provides a clear view of the bed, preventing distortion of the images caused by light refraction from fluctuations in the water surface. The flow is sufficiently deep that the plexiglass window does not interfere with the flow at the bed surface. The high-speed imagery captures an area of the sediment bed that is 7.57 cm long (streamwise) and 6.05 cm wide (cross-stream), with a corresponding resolution of 1280 $\times$ 1024 pixels. Flow conditions in both experiments were fully turbulent with Reynolds numbers of approximately 9.3×10^4 (Run 1) and 1.2×10^5 (Run 2), and Froude numbers of 0.30 and 0.37.

In Run 2, our experimental set-up differs in order to capture simultaneous measurements of sediment transport and near-bed fluid velocities. Here, we use two high speed

cameras positioned above the bed, which focus on the same area, and are operated in synchronization. An 808 nm laser diode light sheet illuminated a plane as close as possible to the bed (within 1-3 mm). Then neutrally buoyant, tracer particles are added to the flume to illuminate the flow field, allowing us to use particle image velocimetry to evaluate the near-bed fluid velocity. The frames are split into interrogation areas. Within each region a displacement vector is calculated, which can then be converted into a cross-stream and streamwise velocity measurement.

The experimental conditions in these two runs are similar, although the particle activity (the number of particles in motion per unit streambed area) in Run 2 is on average approximately 250% higher than in Run 1. We manually tracked particle motions, frame-by-frame, in each experiment, using the open-source software ImageJ. This involved marking the centroid of each particle as it moved through successive frames. ImageJ provides sub-pixel resolution of the centroid coordinates. The software records the pixel coordinates for each particle throughout the set of consecutive images as individual particle "tracks." The pixel coordinates from each particle track were then converted into streamwise x_p [L] and cross-stream y_p [L] coordinate positions. Approximately 95% of the particles in motion were tracked; the 5% of particles that were not tracked either left the field early or proved too difficult to follow through the course of the video. We measured more than 150,000 particle coordinate positions involving more than 10,000 active particles during 5 seconds in Run 1, and nearly 170,000 positions involving more than 11,000 active particles during 2 seconds in Run 2 . We also identified approximately 6,000 individual entrainment events in Run 1 and more than 5,000 events in Run 2. These large data sets are based on sub-pixel resolution measurements and provide high fidelity characterization of particle motions, including measurements of small motions which dominate the probability distributions of particle velocities, hop distances and associated travel times (*Fathel et al.*, 2015).

Particles were tracked only after they began to move. We did not track the motions of particles that "wiggled" back and forth within their pockets, but otherwise did not move or

hop. All particle motions were manually tracked by one individual to maintain consistency. This manual method provides accurate measurements of all motions without a bias towards short or long displacements. Individual hops were measured from incipient motion to a stopped position such that both streamwise and cross-stream velocities are zero.

4.4 Magnitude and Direction of Motion

Here, detailed measurements of particle motions are used to develop distributions of initial particle trajectories, providing a description of the direction and magnitude of initial particle motions. The distribution of these motions bears on the relationship between the local flow conditions and the microtopography of the bed. Ultimately, these measurements provide information concerning particle motions at the moment of entrainment which may be used to better model and understand this process.

The data presented here represent a large sample of initial particle motions which occur under the flow conditions in Run 1 ($\sim$ 6000) and Run 2 ($>$ 5000). The direction of initial motion is calculated (in degrees) for all active particles within Run 1 and 2 following the first time step (0.004 s) of motion. The angle associated with these motions is measured as the deviation from the downstream direction, such that particles may move from 0°, purely streamwise, to 180°, purely backward, or any combination in between. More specifically, for each active particle we calculate the angle associated with the vector of motion as a particle moves from its initial position to a position a single time step (or frame) later.

Within these experiments we find that over 90% of all initial motions contain a measurable cross-stream component of motion, where approximately a third of the motions may be cross-stream dominated, and furthermore, up to 7% of the motions may be negative (i.e. move backwards) (Figure 4.1). With increasing time, the vector of these motions becomes streamwise-dominated and increasingly controlled by the fluid as the particles are accelerated and interact with the bed with decreasing frequency, whereas, at small times the variability in the direction of motions may be a product of the microtopography of the bed.

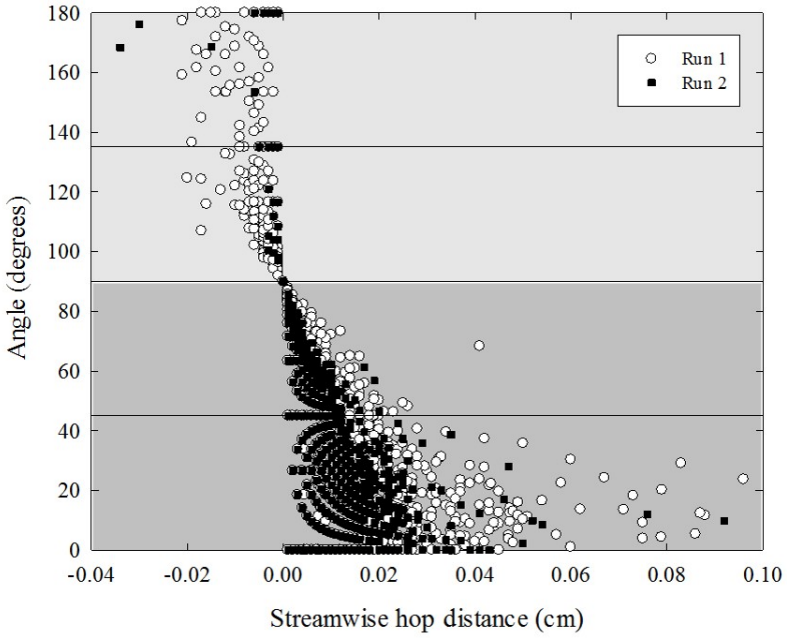

Figure 4.1: Plot of streamwise hop distance L_x and the associated first direction of motion A_p. The white circles represent data from Run 1 and the black squares represent the data from Run 2.

Additionally, it appears that with a higher mean fluid velocity (Run 2), the initial motions of the particles are less sensitive to bed topography and are more likely to be dominated by the fluid.

The initiation of bed load transport is typically described as the moment when the fluid force on the particle exceed the resisting force of the particle which results from the weight of the particle and the friction coefficient. Research has also shown that the degree of exposure and shielding due to clustering may inhibit entrainment. Yet, both of these factors are typically associated with a mixed-alluvial system where there is a wide range of sediment sizes, such that the larger grains act to shield nearby (smaller) particles (e.g., *Laronne and Carson*, 1976; *Brayshaw*, 1985). However, little research regarding the potential impacts of microtopography in single grain-size systems has been performed.

Within these experiments, we start with a smooth bed surface and do not allow bed forms to initiate, such that large clusters of grains are not evident. Nevertheless, we see

a wide range of angles associated with the initial motion of a particle, especially within lower velocity flows. We suspect that this range of motions is related to the particle-scale microtopography of the streambed, where particles must roll out of their resting position to be entrained by the flow. Yet, in higher flow velocities the fluid overcomes resistance created by the microtopography, and there are fewer particles that initially move in the cross-stream direction. This behavior is consistent with work performed by *Seizilles et al.* (2014), in that particle tracking reveals cross-stream motions as a result of the bed roughness or with associated variations in the fluid.

We must also consider the persistence that may be inherent within the initial direction of motion for a particle. For example, if a particle starts its motion in a cross-stream or upstream dominant dominant direction (which accounts for approximately 29% and 21% of the motions within Run 1 and Run 2, respectively), then it likely takes a longer period of time for the particle to become fully streamwise dominated in comparison to particles that begin their motions in the streamwise direction. The characteristic timescale for all particles to be streamwise-dominated, such that the vector of motion is less than 45 degrees, are similar in each experiment. Within Run 1, 99% of all particles are streamwise-dominated within 0.104 seconds, whereas the characteristic timescale for 99% of the particles is slightly shorter in Run 2 at 0.100 seconds. There are a few particles which are not streamwise-dominated past this threshold, and do not become streamwise-dominated until 0.584 seconds (Run 1) and 0.184 seconds (Run 2) into their continuous motions.

Now, let us put this idea of persistence into the context of travel times associated with sediment particle 'hops'. Figure 4.2 presents the distribution of travel times T_p for Run 1 (left) and Run 2 (right). The highlighted region indicates the complete particle hops which occur within the characteristic timescale for particle motions to be streamwise-dominated. Approximately 63% (Run 1) and 43% (Run 2) of particle hops are completed in the time it could potentially take a particle to become streamwise-dominated. This observation may suggest that short motions contribute early cross-stream spreading, while longer motions

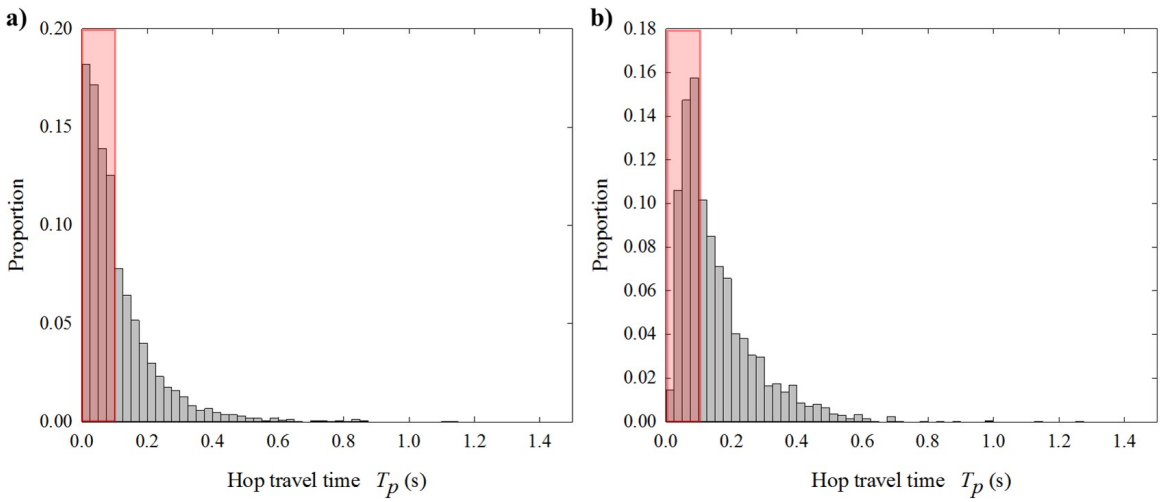

Figure 4.2: The discrete probability distribution of particle travel times T_p from Run 1 (a) and Run 2 (b). The highlighted regions in red indicate the portion of complete particle motions which occur within the timescale in which it may take a particle to become streamwise-dominated.

are more clearly related to streamwise spreading and contribute less to cross-stream spreading. Regardless, the persistence of these cross-stream motions may be particularly relevant to describing cross-stream diffusion, such that to correctly measure the diffusive flux, one needs to understand the cross-stream gradient of bed load transport (e.g. *Seizilles et al.*, 2014), ultimately providing a clearer understanding of particle motions.

4.5 Spatial Distribution of Entrained Particles

In our analysis of entrainment we turn to the spatial distribution of entrainment. Studies have considered preferential entrainment patches (*Paola and Seal*, 1995; *Powell and Ashworth*, 1995), yet little work has been performed on the particle-scale. Our analysis of the spatial distributions of entrained particles acts as a step closer to understanding potential controls on entrainment and prediction of entrainment locations.

To describe the spatial distribution of entrained particle positions we perform a nearest neighbor analysis for individual frames and for increasingly large groups of frames. This method measures the amount of spatial clustering in a set of points. More specifically, we

measure the distances between each location of entrainment in the data set and its nearest neighbors, then calculate the average of all these nearest neighbor distances. We then calculate the nearest neighbor index r, which is a ratio of the observed average nearest neighbor distance to the expected average distance from a hypothetical, spatially-random distribution. If the observed average distance is less than the average expected distance, we consider the distribution to be clustered. Conversely, if the observed distance is greater than the expected distance, the distribution is dispersed.

Figures 4.3 and 4.4 present the distribution of nearest neighbor ratios for individual frames for Run 1 and Run 2, respectively. These distributions are strongly skewed towards clustered values ($r < 1$), with mean values of 0.50 (Run 1) and 0.23 (Run 2). Although the majority of nearest neighbor ratios r in Figures 4.3 and 4.4 indicate that the locations of entrainment are clustered, the spatial distribution of entrainment locations in a single frame may be random ($r \sim 1$) or dispersed ($r > 1$). In particular, Run 1 displays a wider distribution of r values. This indicates that there is more variability in the distribution of entrained particles, which is likely a product of the lower mean fluid velocity, such that a small number of particles are entrained at many time steps and therefore may appear to be more dispersed or randomly distributed.

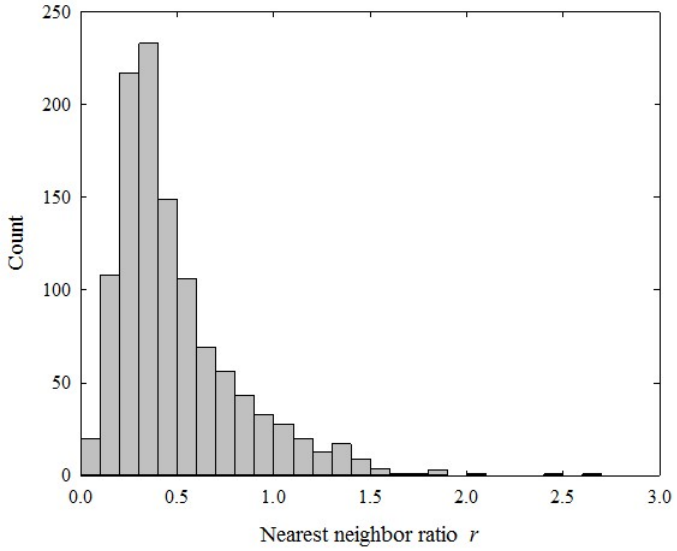

Figure 4.3: Histogram of the nearest neighbor ratio r for individual frames in Run 1.

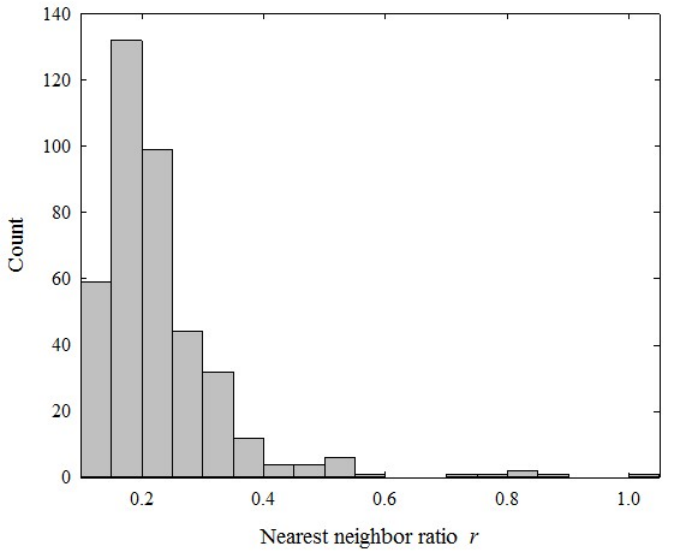

Figure 4.4: Histogram of the nearest neighbor ratios r for individual frames in Run 2.

Let us expand this type of analysis from examining the spatial distribution of entrainment in individual frames to the distribution of locations in increasingly large groups of frames. A good visualization to understand our methodology is to imagine a sliding window of a predetermined number of frames, n. We calculate the nearest neighbor ratio in this subset of n frames, which considers all the locations within the subset. This subset is

modified by 'shifting forward', where the first frame of the series is excluded and the frame following the original subset is included. We continue to shift this sliding window forward until the end of the subset falls on the last frame analyzed. So, for example, if we choose a sliding window size of 10 frames (n =10) and apply it to Run 1, we shift the window forward —one frame at a time— until the end of the subset falls on the final frame (Frame 1250), which is the last frame we analyzed. Within this example, we have $N-(n-1)$ subsets or 1241, where N is equal to the total number of frames analyzed, and we therefore calculate the nearest neighbor index r 1241 times, once for each subset. Using this method, we systematically increase the size of the temporal sliding window from $n = 1$ (each frame individually) to $n = N$ for Run 1 and Run 2.

For a sliding window size n of 1 to 20 twenty frames in Run 1 and Run 2, we plot r values in box plots to depict spread of values (Figures 4.5 and 4.6).

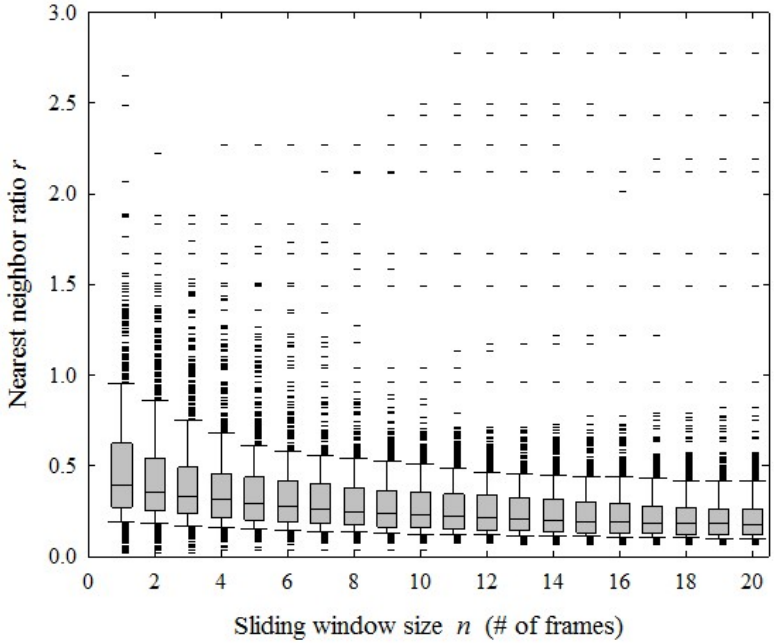

Figure 4.5: Boxplot of nearest neighbor ratio r values in Run 1, where each box represents a sliding window size. The body of the box extends from the first quartile to the third quartile. Within the box, the horizontal line is drawn at the second quartile which is the median of the data sets. The lower whisker marks the 5th percentile while the upper whisker 95th percentile of the data. The small dashes above and below the whiskers represent outliers in the data set.

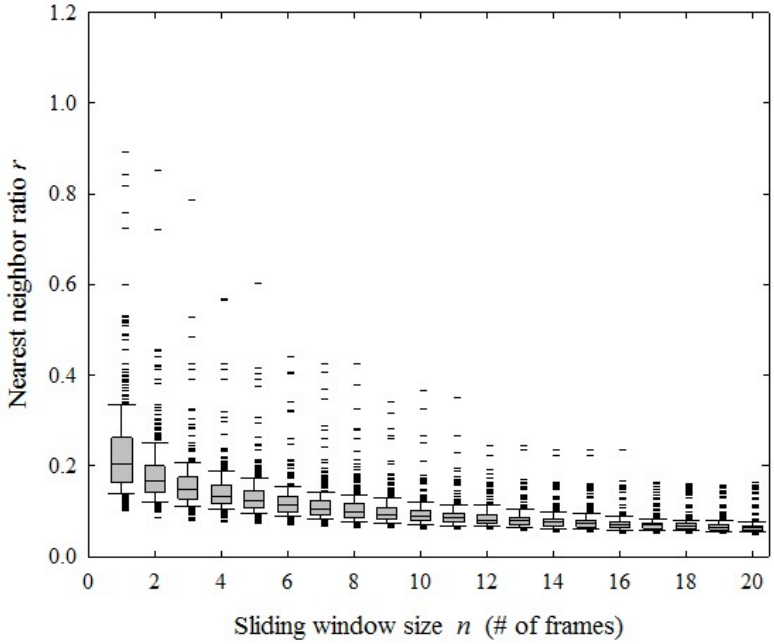

Figure 4.6: Boxplot of nearest neighbor ratio r values in Run 2, where each box represents a sliding window size. The body of the box extends from the first quartile to the third quartile. Within the box, the horizontal line is drawn at the second quartile which is the median of the data sets. The lower whisker marks the 5th percentile while the upper whisker 95th percentile of the data. The small dashes above and below the whiskers represent outliers in the data set.

First, notice that the first box in Figure 4.5 represents the same data presented in the histogram in Figure 4.3, and similarly the first box in Figure 4.6 represents the data found in Figure 4.4. Within both boxplots we see that the range of data quickly condenses toward clustered r values, with this trend more apparent in Run 2. In Run 1, outliers continue to show random and dispersed spatial patterns of entrainment for a window size of n = 20 frames, but the vast majority of r values show clustering. The higher range of r values in Run 1 is likely a product of the flow conditions in the experiment. On average, there are fewer particles entrained in Run 1 than Run 2 at any given time. Therefore, this lowered activity may be a factor in the wider range of r values in Run 1, where, for example, if only 2 or 3 particles are activated over the entire window area, the sparse amount of particles activated are random or dispersed. For example, if only two or three particles are activated

at any given time, in comparison to tens of particles, entrained sediment may appear to be dispersed, random, or clustered with too few points to accurately represent the spatial distribution.

A simplification of these data can be found in Figure 4.7, where we plot the mean nearest neighbor ratio for each sliding window. Notice that in both runs, the mean nearest ratio quickly approaches zero which indicates highly clustered distributions. Interestingly, we do not see complete spatial randomeness within either experiment. This result suggests that the fluid and bed microtopography both act together to control the activation of particles, which creates spatial clustering over these relatively short timescales. Additionally, this may be a result of collective entrainment, where particles may be activated by moving particles which can interact directly (collision) or indirectly (wake effect, advection of turbulent structure) to entrain particles (*Ancey et al.*, 2008; *Ancey*, 2010).

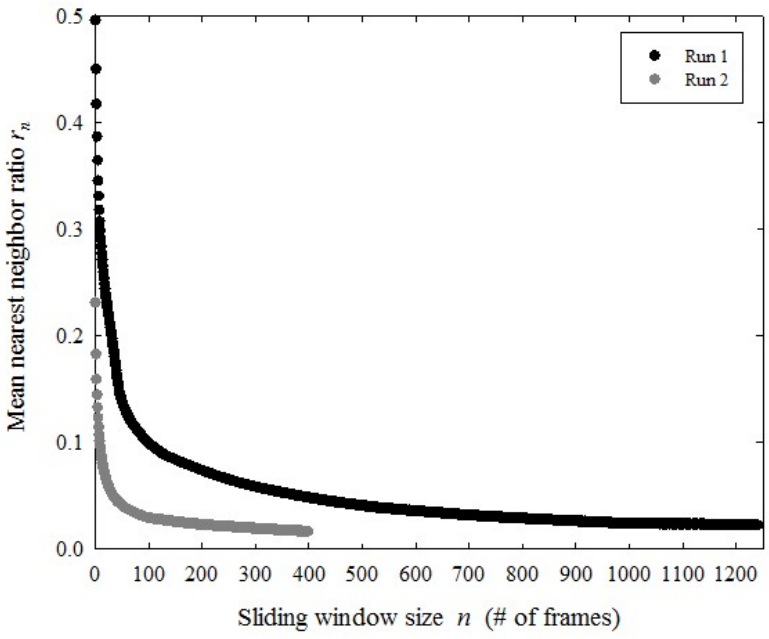

Figure 4.7: Plot of the mean nearest neighbor index ratio, where the black circles represent Run 1 and the gray circles represent Run 2.

4.6 Connections Between Near-bed Fluid Velocities and the Entrainment Particles

Research suggests that an increase in the turbulence, or fluctuations in the fluid velocity, correlates to increased particle activity (e.g., *Sumer et al.*, 2003). Furthermore, there is a suggested coupling between turbulent structures and bed load motions (e.g., *Nelson et al.*, 1995; *Nikora et al.*, 2002; *Lajeunesse et al.*, 2010; *Singh et al.*, 2012; *Bialik*, 2013). Our work provides novel and direct observations of coupled fluid and entrainment locations, which acts to better define the relationship between near-bed fluid velocities and particle entrainment.

To analyze the relationship between fluid velocities and points of entrainment we apply two different methods which utilize the simultaneous measurements taken in Run 2. The first method is purely Eulerian in nature, in which we choose locations *a priori* and then compare the time series of streamwise fluid velocities to the time series of entrainment. We then turn to an *a posteriori* method, wherein we examine the streamwise velocities in the vicinity of each entrained particle. Ultimately, these methods are sampling different relationships between the fluid and entrained particles. The following subsections explore the results of these methods.

4.6.1 Eulerian Analysis of Velocity and Entrainment Time Series

We split each frame into equally spaced, gridded boxes. Within these boxes we compare the time series of near-bed streamwise velocities to the time series of particle entrainment. We start at the small scale of the particle image velocimetry interrogation region, of which there are 4292 in each frame. Figure 4.8 shows an example of one such region, where the upper plot is the time series of fluid velocities and the lower plot contains the time series of entrainment events. Given the size of the interrogation regions, entrainment events on this scale are infrequent and many regions do not experience a single event for the duration of our measurements. For visualization purposes, the interrogation region in Figure 4.8 was

chosen as it contains the highest number of entrainment events measured within a single region.

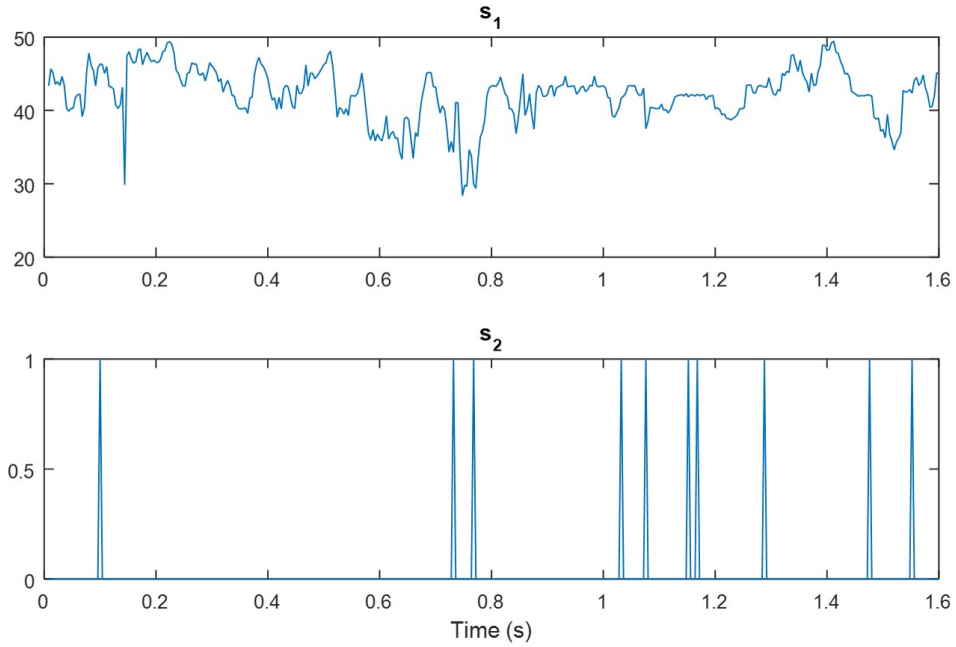

Figure 4.8: This figure plots the time series of streamwise fluid velocities (upper) and entrainment events (lower) in Run 2 for the duration of the particle tracking measurements.

Let us summarize this data in a different way. At each time step, for each interrogation region, we have an associated velocity and entrainment event (or lack thereof). Figure 4.9 is a plot where each box represents the distribution of velocities for each number of entrainment events. Note that there are many moments where there are no entrainment events in an interrogation area. Also the maximum number of entrained particles at a given time is two for this size region. There are close to 2 million data points contained within the zero entrainment event bar, 4344 points in the one event bar, and only 18 events within the two event bar (Figure 4.9). We somewhat surprisingly do not see a difference in the velocities associated with entrained particles compared to moments when particles are not activated.

We now expand the area from individual interrogation regions to areas double, triple, etc. in size. Within increasing grid size, there are more entrainment events occurring within

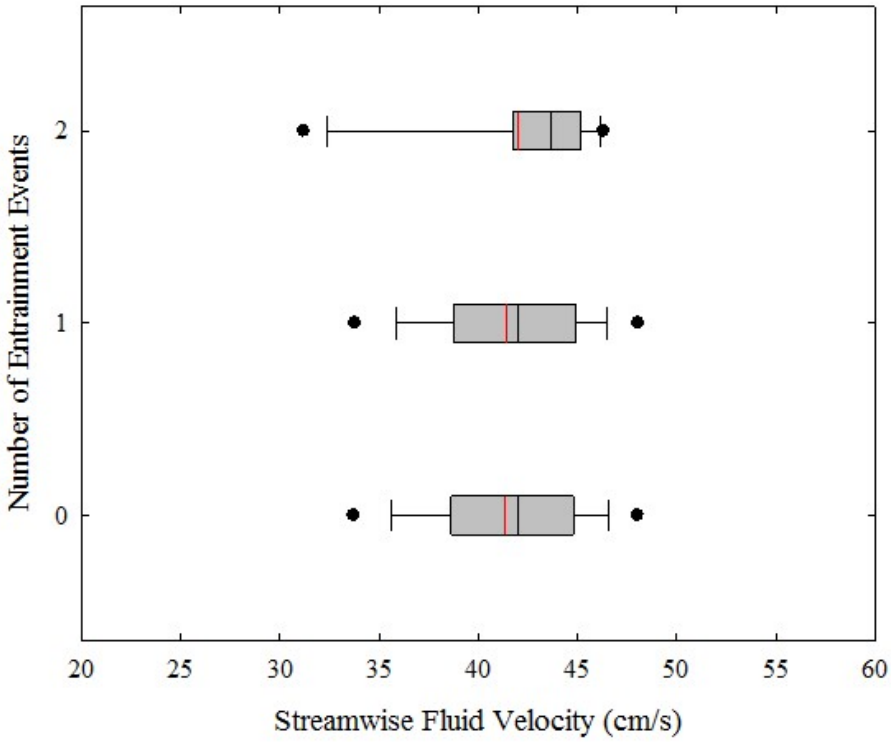

Figure 4.9: Each box represents the distribution of velocities associated with the number of entrainment events for a given frame. The body of the box extends from the first quartile to the third quartile. Within the box, the vertical black line is drawn at the second quartile which is the median of the data, and the red line is drawn at the mean of the data.. The lower whisker marks the 5th percentile while the upper whisker 95th percentile of the data. The black circles indicate the 1st and 99th percentile outliers in the data.

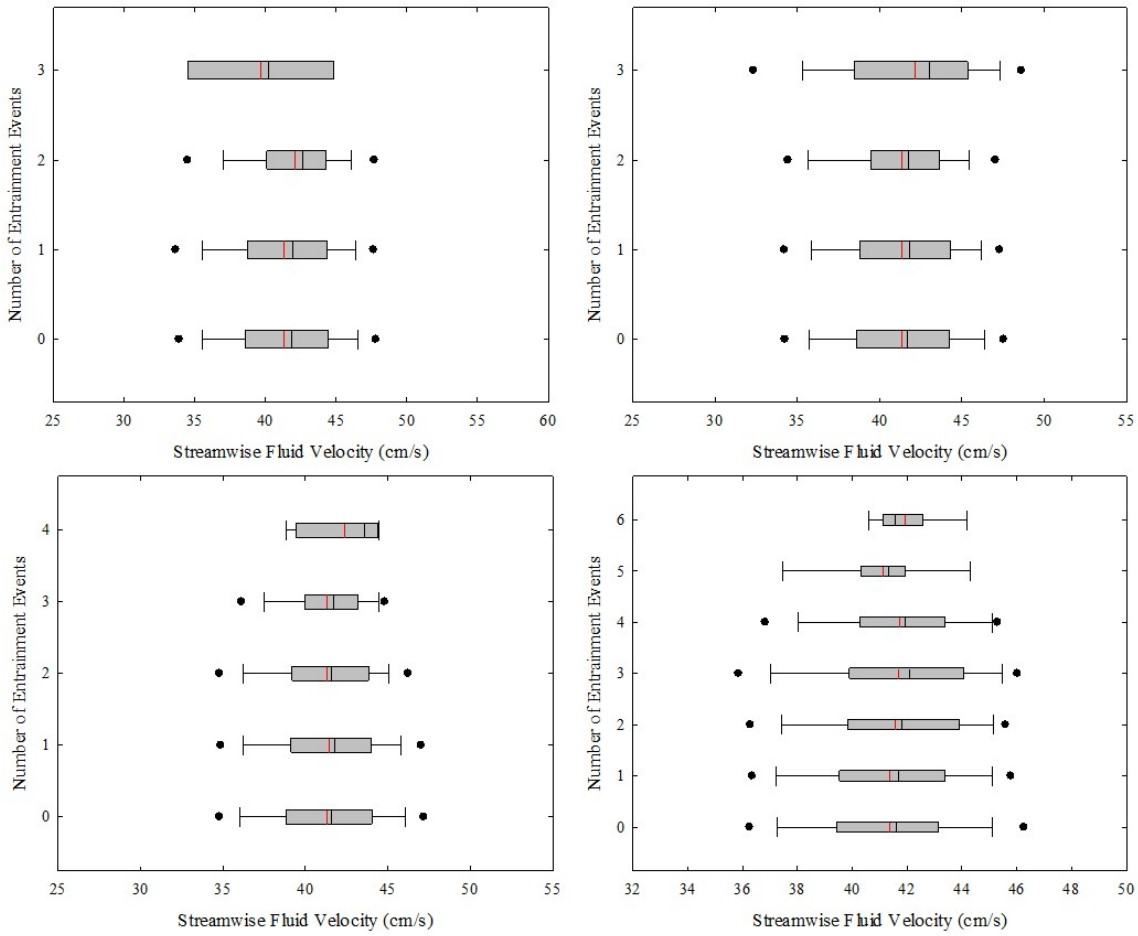

Figure 4.10: Each box represents the distribution of velocities associated with the number of entrainment events for a given frame. From left to right and top to bottom the size of each gridded area is defined in terms of an interrogation region: double, triple, four and five times the size. The body of the box extends from the first quartile to the third quartile. Within the box, the vertical black line is drawn at the second quartile which is the median of the data, and the red line is drawn at the mean of the data.. The lower whisker marks the 5th percentile while the upper whisker 95th percentile of the data. The black circles indicate the 1st and 99th percentile outliers in the data.

a single grid, from a maximum of 2 events per grid in the smallest box size (Figure 4.9) to a maximum of 6 events per grid in boxes five times the size of an interregation region (lower left, Figure 4.10). Spatially, the largest grid spacing splits the area into 2 individual boxes, which each are approximately 3.8 cm by 3 cm in size. Given these dimensions, it is perhaps surprising that there is only a maximum of 6 entrainment events per frame. This

highlights the patchiness of entrainment, in that even over relatively large areas there are few particles activated at any given time. Importantly, we also note that even in larger grid spacing, there does not appear to be a strong connection between the entrainment events and the average fluid velocity in the area. This further suggests that there is a patchiness in the entrainment that is not related in a simple way to the near-bed fluid velocities.

4.6.2 Fluid Velocities in Vicinity of Entrainment Particles

Here we apply the *a posteriori* method, in which we analyze the relationship between nearby fluid velocities to entrainment locations. We start by examining the nearest fluid velocity measurement at the time and location of entrainment events to the average streamwise fluid velocity for the entire frame. We suspect that this ratio, of nearby fluid velocity to average fluid velocity, should be indicative of a relationship between local streamwise velocities and bed load sediment entrainment. We normalize this ratio in Figure 4.11, where positive values indicate the nearby fluid velocity is greater than the average velocity of the frame and, conversely, negative values indicate the velocity near the entrained particle is less than the average frame velocity.

Somewhat surprisingly, Figure 4.11 does not reveal any correlation between local velocities at the time and location of entrainment. Of the over 5000 entrainment events, approximately 30% of the nearby velocities are $\geq$ 2 cm/s above than the average velocity, 38% are $\leq$ 2 cm/s below the average velocity, and 32% of the nearby velocities are similar to the average velocity and fall in the remaining range ($>$ 2 cm/s and $<$ -2 cm/s).

We further examine the relationship between fluid velocities and entrainment by expanding our analyses to include an area within a radius of the entrained particle in an effort to capture the larger flow structure. We suspect that the lack of correlation seen in Figure 4.11 may be a result of focusing only on the closest velocity, rather than a range of nearby velocities. We therefore compare the mean velocity of the fluid in a radius of 1, 3, 5, 7, and 10 mm around an entrained particle to the average streamwise fluid velocity of the entire

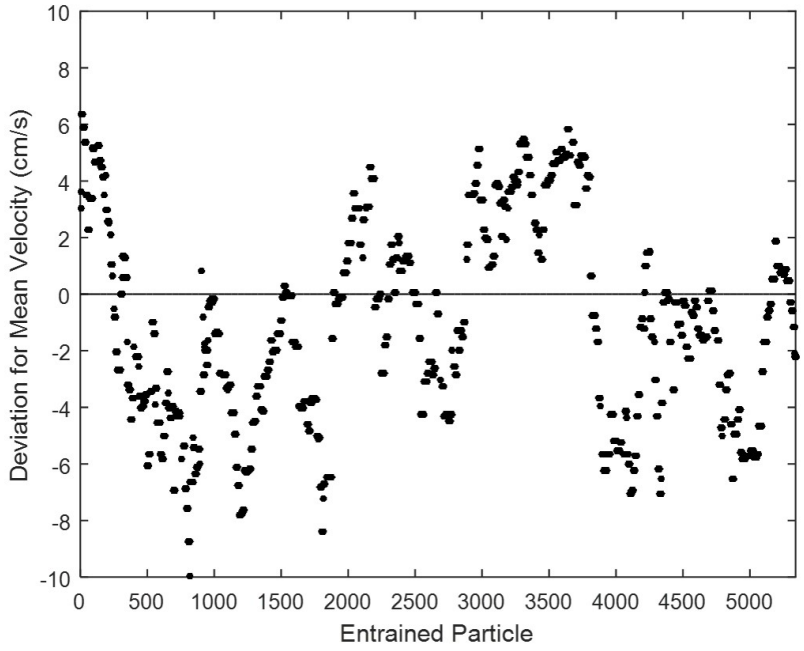

Figure 4.11: Plot of the normalized ratio of the fluid velocities nearest to an entrainment location to the mean fluid velocity of the frame. Each point in the graph represents an individual particle entrained within Run 2.

frame (Figure 4.12). Each box in Figure 4.12 summarizes the normalized velocity values for each radius. Figure 4.12 shows that with a larger radius, values tend to be positive with the highest mean value found within a 3 mm radius, perhaps suggesting the scale of turbulence required to initiate sediment motions. While this trend is evident, values in a wider radius do not tend to be significantly higher than the average fluid velocity for the entire frame. So, while this suggests that there may be a minimum distance we must consider when analyzing fluid velocities in the vicinity of entrainment events, there is not a significant correlation that suggests higher velocities are needed to activate particles into motion.

4.6.3 Investigating a Lagged Relationship Between Entrainment and Fluid Velocities

We hypothesized that the streamwise velocity near the particle should be higher than the average streamwise velocity, yet the data in Figure 4.12 are not indicative of this idea.

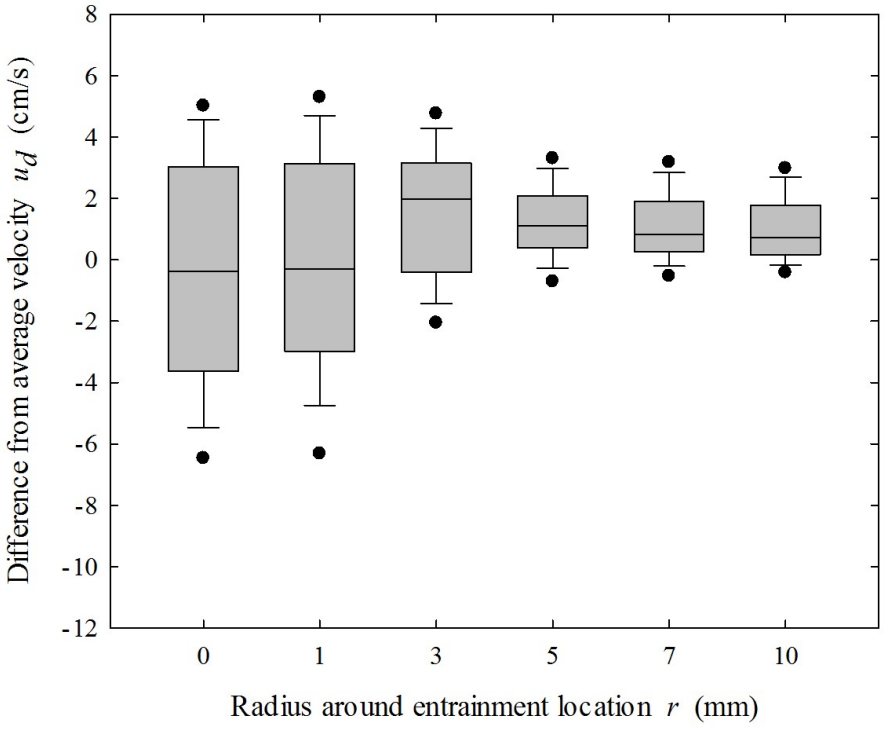

Figure 4.12: Each box represents the distribution of normalized ratio of nearby velocities to the mean fluid velocity of the frame for entrained particles in Run 2. Within increasing radius (from left to right) we consider the average nearby velocity in the determined radius surrounding each entrained particle. The body of the box extends from the first quartile to the third quartile. Within the box, the horizontal black line is drawn at the second quartile which is the median of the data. The lower whisker marks the 5th percentile while the upper whisker 95th percentile of the data. The black circles indicate the 1st and 99th percentile outliers in the data.

There may be a time lag between an increase in the fluid velocity and the actual activation of the particle (see: Movie 1 in Supplementary). To test this we perform a cross correlation analysis of each particle image velocimetry interrogation region (4292 in total) to determine any lag between entrainment events and fluid velocities. This utilizes the time series developed within the Eulerian methodology as seen in Figure 4.8. Again, here, the upper plot represents the time series of fluid velocities and the lower plot contains the time series of entrainment events. Within the regions which have at least one entrainment event, we performed a cross correlation analysis on the time series pairs, and then calculate the average lag time. The average lag time is approximately 0.236 seconds.

We then return to the analysis described in the previous section to create Figure 4.12, but rather than examine the velocities surrounding points of entrainment at the moment of entrainment, we plot the velocities which occur 0.236 seconds prior to entrainment (Figure 4.13). At this lag time –no matter the radius examined– all mean values are positive, which is evident in the 0 and 1 mm radii boxes. Yet, the distribution of data in the 3 mm to 10 mm radius boxes do not significantly differ from the moment of entrainment (Figure 4.12). While these results may seem compelling, we have to consider that the length of the measured timeseries is only 2 seconds long. So a lag of 0.236 s, excludes $\sim$10% of the particles that occur at the start of the movie. Furthermore, this lag is equal to 59 frames– which is quite long in the context of our measurement. We would not suspect memory within this processes to persist on these time scales. So, while there may be a stronger positive correlation at this lag, we are not confident that the fluid is coupled with sediment motions at these timescales. This examination further reveals that the relationship between the fluid and entrainment of particles is complex and does not appear to follow hypothesized trends. The behavior of the near-bed fluid is fundamentally related to the initiation of particle motions, yet given the analysis presented here, we are not able to reveal a clear relationship.

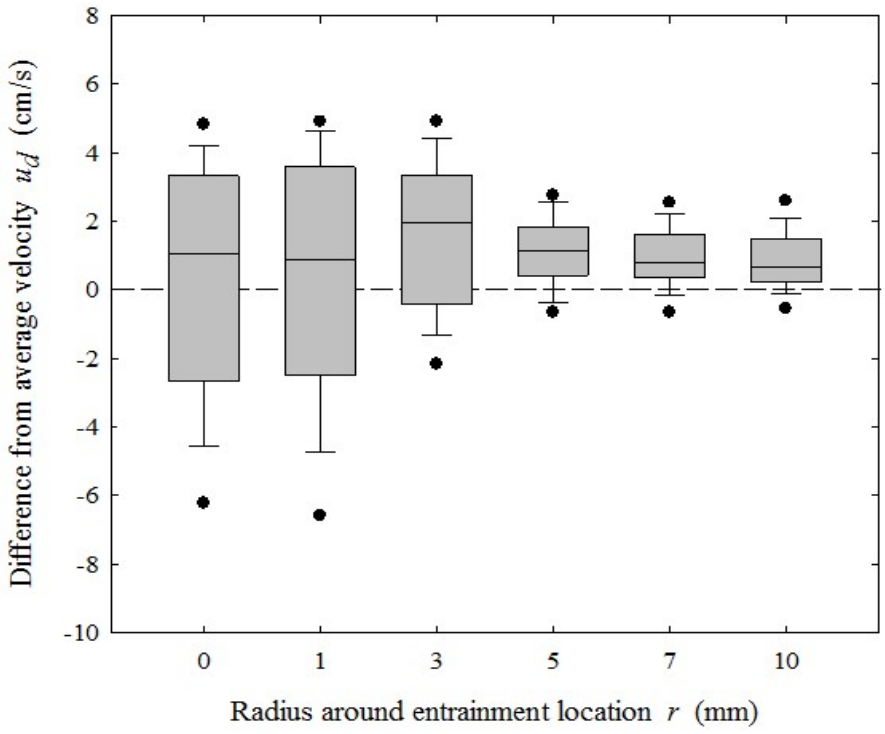

Figure 4.13: Each box represents the distribution of normalized ratio of nearby velocities to the mean fluid velocity of the frame for entrained particles at a lag of 0.236 seconds prior to entrainment locations in Run 2. Within increasing radius (from left to right) we consider the average nearby velocity in the determined radius surrounding each entrained particle. The body of the box extends from the first quartile to the third quartile. Within the box, the horizontal black line is drawn at the second quartile which is the median of the data. The lower whisker marks the 5th percentile while the upper whisker 95th percentile of the data. The black circles indicate the 1st and 99th percentile outliers in the data. Furthermore the dashed line at y = 0 is placed to highlight that each of the mean values is above 0.

4.7 Distribution of Wait Times

Particle wait times T_w are measurements of the duration of time elapsed between successive particle motion in an area. This particularly samples breaks in the sediment load or particle activity over a set area, and is therefore a measure of the intensity of sediment transport. Furthermore, in this section we provide empirical evidence of the form of this distribution, which is essential to the application of the *Ancey et al.* (2008) "birth-death" Markov model of bed load transport.

We measure the particle wait times over the full window and within increasingly smaller windows in both Run 1 and Run 2 (Figure 4.14). Within windows with an area less than the full window, we compute the mean wait times of the subsection windows; these average values are plotted in Figure 4.14.

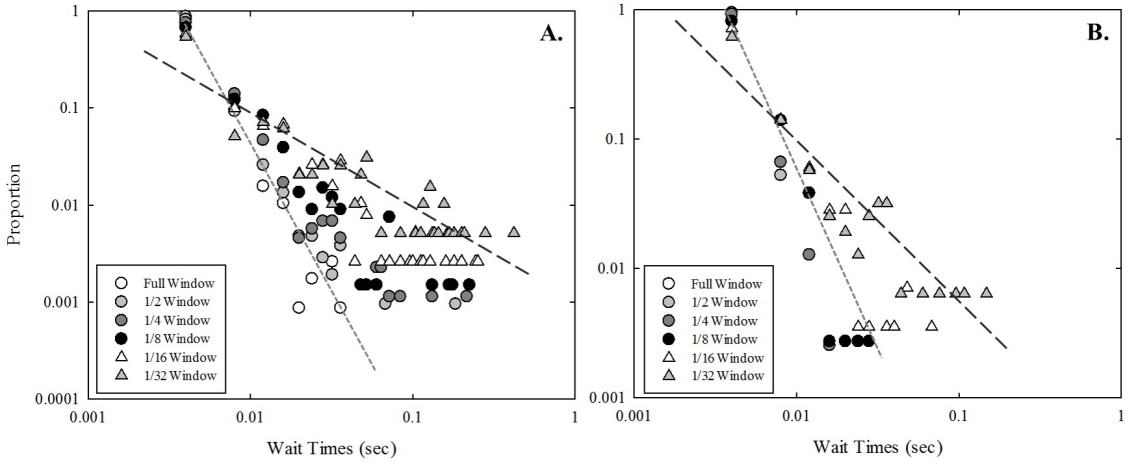

Figure 4.14: Distribution of particle wait times for six different window sizes in Run 1 (A) and Run 2 (B) in log-log space. For windows smaller than the full window, mean values were computed and are plotted here. The short-dashed, light gray line represents the fitted slope for the full window data (white circles) and the long-dashed, dark gray line represents the fitted slope for the 1/32 window data (light gray triangles)

In both runs and for all window sizes, most wait times are equal to the sampling interval (0.004 seconds). This indicates most of the time, there are no breaks in the particle activity. However, in both runs, we find that within increasingly small windows there are longer wait

times, where no particles are active in the area. This trend is highlighted within Figure 4.14 by the dashed lines for both Run 1 and 2. The lighter, short-dashed line is approximately fit to the distribution of wait times in the full window; the darker, long-dashed line is fit to 1/32 sized window. These lines indicate a clear difference in slope, where there are substantially more long wait times in windows with a smaller area than within larger areas. This suggests that the relative transport intensity is dependent on the window.

There are key differences between the wait time distributions in Run 1 and Run 2. We consistently see fewer long wait times in Run 2 than Run 1. This is likely a product of the higher particle activity in Run 2. In Run 1 the average particle activity is $\sim$120 whereas the activity in Run 2 is 250% higher at $\sim$400. Given that there are many more particles in motion in Run 2, it is less likely (no matter the window size) that there are long breaks between active particles. This influences the fitted slopes, such that the fitted lines in Run 2 (Figure 4.14, B) are steeper than those in Run 1 (Figure 4.14, A). In a plot of the mean wait time T_W per window size, Figure 4.15, it is also clearly evident that the average particle wait time in Run 1 is of a longer duration than the average wait time in Run 2, no matter the window size. Importantly, in both Figure 4.14 and Figure 4.15 the disparity between the average wait times in Run 1 and Run 2 increases with increasingly smaller windows.

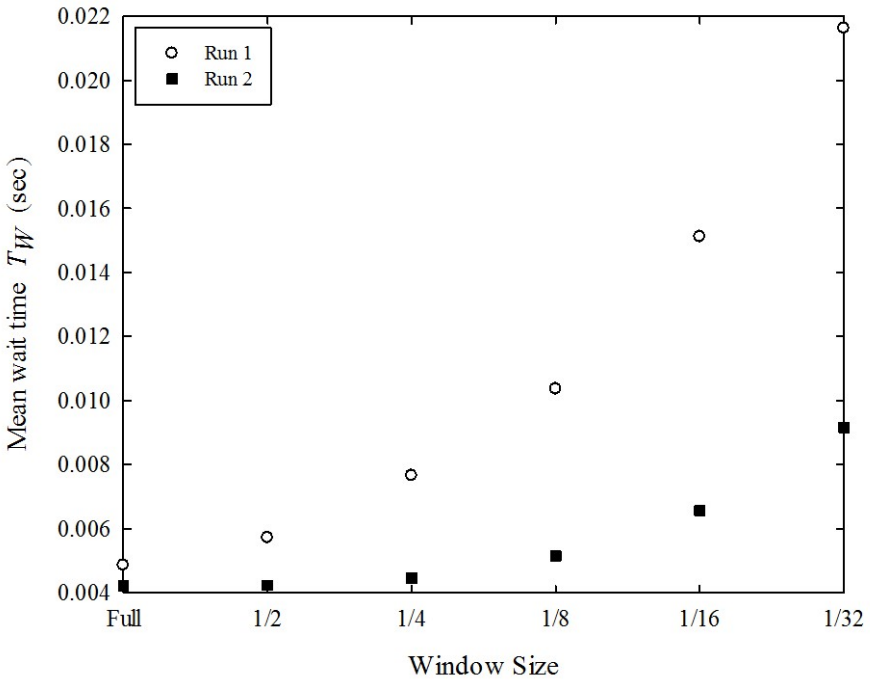

Figure 4.15: Plot of average particle wait times T_W for six different window sizes in Run 1 (white circles) and Run 2 (black squares).

While these data do indeed represent the wait time distributions, we must note that these data are limited, such that there are not many breaks in sediment transport (no matter the size of the window) and that we have analyzed only a limited number of frames in each experiment. Regardless, we do view this as an important step in clarifying the distribution of wait times. In log-log space, wait times plot as approximately straight lines, which is consistent with power law distributions rather than an exponential distribution. This suggests that entrainment within these experiments in *not* a purely Poissonian representation of entrainment (*Papanicolaou et al.*, 2002; *Ancey et al.*, 2006), wherein particles are entrained only when the fluid activates them (*Ancey et al.*, 2008; *Bradley and Tucker*, 2012). Rather, the process appears to be more complicated and may involve collective entrainment *Ancey et al.* (2008). Furthermore, by examining changes in the form on the distribution with decreasing window size, we may better understand intermittence within bed load transport related to the window size, such that wait time may be scaled with window size.

4.8 Distribution of Rest Times

Here we examine the distribution of particle rest times, which are not involved in the process of disentrainment, but rather are a consequence of disentrainment in that rest times are measurements of the time duration a particle is at rest before being reactiveated. The form of this distribution is important to characterizing the diffusive nature of the system (*Martin et al.*, 2012; *Hassan et al.*, 2013) and is key to many formulations of sediment transport. For example the nature of the tail of this distribution (either light or heavy) acts as a control over the diffusion of particles (*Martin et al.*, 2012; *Hassan et al.*, 2013). Furthermore, the form of the distribution is a key component in derivations of the bed load discharge (*Einstein*, 1950). While this work provides an important step towards empirically defining this distribution, we also highlight the experimental limitations of these measurements (4.8.1 and 4.8.2).

Particle rest times T_r are measurements of the duration of time between the disentrainment of a particle and the reentrainment of that particle. Even though we have tracked particle motions in sampling intervals of $T_s = 5$ seconds in Run 1 and $T_s = 2$ seconds in Run 2, the maximum possible rest time is equal to 0.4 seconds or 100 frames of imagery. Due to computer memory constraints, particle tracking was performed in 100 frame increments. The notation for this shorter, 100 frame or 0.4 second, recording interval is T_S. Particles that continued motion at the end of 100 frames were maintained and tracked until the end of the full sampling time T_s or until they left the frame, but particle positions of disentrained particles were not maintained following the 100 frame interval. Indeed, the measurements of rest times will certainly be censored due to these time constraints, which we examine in the following section.

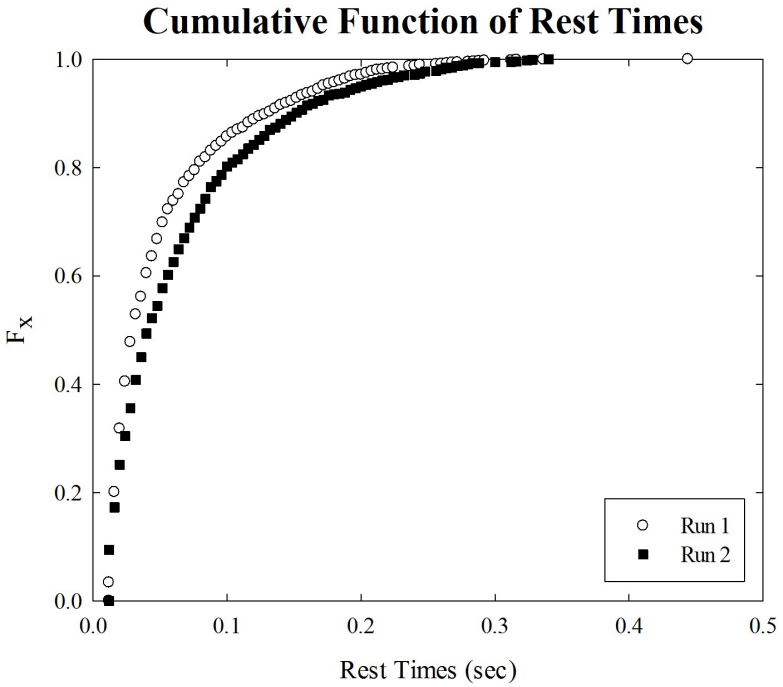

Figure 4.16: Cumulative distribution function F_{T_r} of particle rest time T_r. The white circles represent data from Run 1 and the black squares represent the data from Run 2.

The cumulative distribution F_{T_r} of particle rest times T_r shows that many of the rest times are short where, in both Run 1 and Run 2, 80% of the rest times are less than 0.1 seconds long (Figure 4.16), with noteably more short rest times in Run 1 than in Run 2. This is likely indicative of the transport and experimental conditions. Perhaps the longer rest times in Run 2 result from the higher flow velocity in this experiment, such that particles are more likely to stay in motion when activated, and if they pause they have fallen into a pocket whose geometry prevents easy activation. In Run 1, the slower flow velocity allows for easier deposition of particles without lodging a particle within a pocket.

We can examine the form of the rest time distribution if we plot these data as a survival function S_{T_r}, where $S_{T_r} = 1 - F_{T_r}$ (Figure 4.17). Figure 4.17 is plotted in semi-log space to highlight the distinctly non-linear trend of this distribution. These data do not suggest an exponential distribution, as is commonly assumed following *Einstein's* (1937) work. Rather, at least a portion of these data seems to be more consistent with a power law distribution. Figure 4.18 plots the survival function S_{T_r} in log-log space to more clearly delineate

the slope of this distribution. Here we see a break in slope from less than 1 at small rest times, to a value approximately one at longer rest times.

Heyman et al. (2013)

These data provide an important step in better defining the details of rest times and provides, to our knowledge, the first empirical data of these distributions on the particle-scale. On a preliminary level, the presence of a power-law like distribution indicates that the data may have a heavy-tail. These data are not inconsistent with results from other studies (*Martin et al.*, 2012, 2014; *Voepel et al.*, 2013). Yet, importantly, we note that the tail of this distribution appears patchy, which is consistent with the temporal censorship caused by our shortened recording intervals T_S within the full sampling interval T_s. The next section explores the impacts of experimental censorship due to a finite recording interval T_S, where longer rest times are preferentially censored.

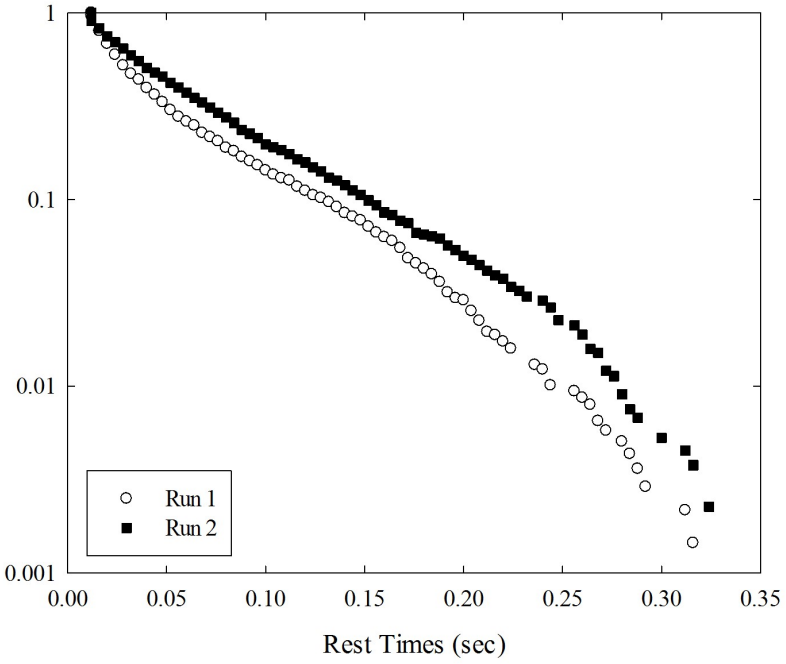

Figure 4.17: Plot of the survival function S_{T_r} of rest times T_r in semi-log space. Here, the white circles represent data from Run 1 and the black squares represent the data from Run 2.

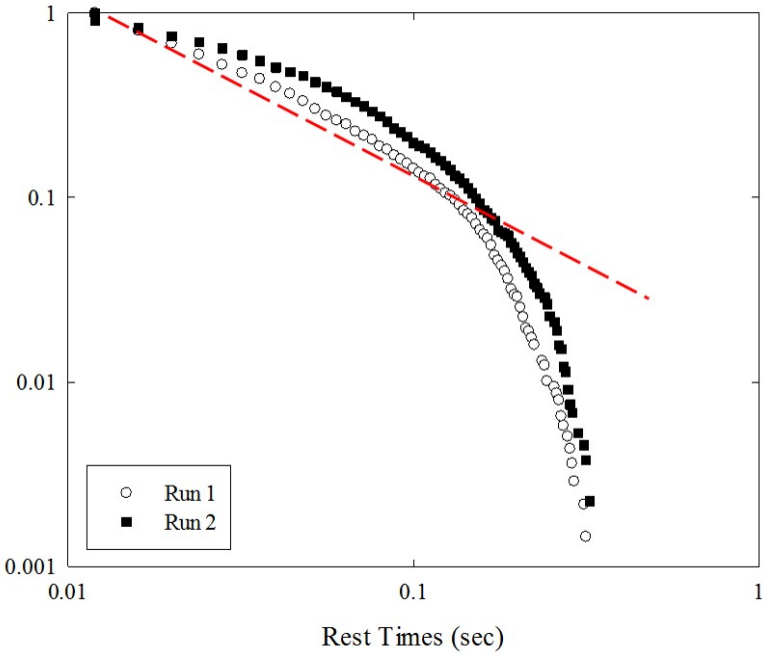

Figure 4.18: Plot of the survival function S_{T_r} of rest times T_r in log-log space. Here, the white circles represent data from Run 1 and the black squares represent the data from Run 2. The red-dashed line is plotted at a slope equal to one.

4.8.1 Censorship of Rest Times

The purpose of this and the following section is to investigate the potential consequences of temporal censorship on rest time distributions. In particular, the motions of particles that enter or leave the video sampling area are spatially censored, and particles that are in motion when the video starts or stops are temporally censored. This means that an estimate of $f_{T_r}(T_r)$, based on rest times T_r, which occur within the sampling area and sampling interval are biased. Our prior work indicates that the form of a measured distribution can be influenced by experimental censorship (*Fathel et al.*, 2015). Specifically, we showed that spatial censorship is evident within measurements of hop distances and their associated travel times, such that there is a visible effect in the preferential reduction of the largest hop distances and travel times. Here, we start with a summary of the derivation provided in *Fathel et al.* (2015), which is modified for rest times (rather than hop distances).

Following *Furbish et al.* (1990) and *Fathel et al.* (2015), let $P_u(t;T_r,T)$ denote the probability that a particle with a rest time T_r starts between the beginning ($t=0$) and end of the sampling time $t=T_S$, specifically between the interval $0<t<T_S-T_r$. This defines the case in which a motion is uncensored. $P_u(t;T_r,T_S)$ indicates that this probability may be a function of time t, where T_r and T are treated as parameters. The probability that a motion occurs within the small interval T_r to $T_r+\mathrm{d}T_r$ and starts within the interval $0<t<T_S-T_r$ is $P_u(t;T_r,T)f_{T_r}(T_r)dT_r$, and the censored, cumulative distribution function is

$$G_{T_r}(T_r)=\frac{\int_0^{T_r}P_u(t;T_r,T_S)f_{T_r}(w)\,\mathrm{d}w}{\int_0^{T_S}P_u(t;T_r,T_S)f_{T_r}(w)\,\mathrm{d}w}, \tag{4.1}$$

where w is a variable of integration.

We now assume that a sufficient number of rest times occur such that any initial patchiness vanishes and $P_u(t;T_r,T_S)$ is independent of time t, that is, $P_u(t;T_r,T_S)=P_u(T_r,T_S)$. In this case $P_u(T_r,T_S)=(T_S-T_r)/T_S$, and (4.1) becomes

$$G_{T_r}(T_r)=\frac{\int_0^{T_r}(T_S-w)f_{T_r}(w)\,\mathrm{d}w}{\int_0^{T_S}(T_S-w)f_{T_r}(w)\,\mathrm{d}w}. \tag{4.2}$$

We now rewrite this as

$$G_{T_r}(T_r)=\frac{T_S F_{T_r}(T_r)-\int_0^{T_r}wf_{T_r}(w)\,\mathrm{d}w}{T_S F_{T_r}(T_r)-\int_0^{T_S}wf_{T_r}(w)\,\mathrm{d}w}, \tag{4.3}$$

where $F_{T_r}(T_r)$ is the cumulative distribution of $f_{T_r}(T_r)$. Taking the derivative of (4.3) with respect to T_r and factoring T_S then yields the probability distribution of censored rest times, namely,

$$g_{T_r}(T_r)=\frac{f_{T_r}(T_r)-(1/T_S)T_r f_{T_r}(T_r)}{F_{T_r}(T_S)-(1/T_S)\int_0^{T_S}wf_{T_r}(w)\,\mathrm{d}w}. \tag{4.4}$$

Notice that in the limit of $T_S\to\infty$, the second term in both the numerator and denominator of (4.4) goes to zero while the first term in the denominator goes to unity, so the distribution $g_{T_r}(T_r)$ approaches the underlying distribution of travel times, $f_{T_r}(T_r)$.

Given the nature of rest times, in that they are more infrequently measured, in comparison to particle travel times or hop distances, these data are fundamentally temporally censored.

4.8.2 Analytical Demonstrations of the Temporal Censorship of Rest Times

This section acts as a guide to identifying the influence of censorship –in this case, temporal censorship– on the form of a measured distribution. Here, we analytically solve the probability distribution of censored rest times (4.4), by making some assumptions about the underlying distribution of rest times. We focus on two known distributions and systematically vary the sampling time T_S to examine any changes within the resulting rest time distribution. The two distributions were chosen based on research suggesting that the rest time distribution is either exponential distributed (*Einstein*, 1937, 1950; *Habersack*, 2001) or may take the form of a heavy-tailed, power law distribution if deposited particles are buried by other particles (*Martin et al.*, 2012, 2014; *Voepel et al.*, 2013). In the latter case, we use a Pareto distribution as a proxy for the heavy-tailed distribution. Prior to varying the sampling time T_S parameter, we start by providing analytical solutions of equation 4.4 for an exponential distribution and Pareto distribution,.

If we follow Einstein's (1950) assertion that the distribution of rest times $f_{T_r}(T_r)$ must be exponential, with a definite mean $\overline{T_r}$ which informed by our experimental measurements, we can determine an analytical solution for different sampling intervals T. Consider an exponential distribution of rest times,

$$f_{T_r}(T_r) = \frac{1}{\overline{T_r}} e^{-T_r/\overline{T_r}}, \tag{4.5}$$

where $\overline{T_r}$ is predefined mean rest time. The censored cumulative distribution $F_{T_r}(T_S)$ of (4.5) is therefore,

$$F_{T_r}(T_S) = 1 - e^{-T_S/\overline{T_r}}. \tag{4.6}$$

We now rewrite (2.12), using (4.5) and (4.6), as

$$g_{T_r}(T_r) = \frac{\left(\frac{1}{\overline{T_r}}\right)e^{-T_r/\overline{T_r}} - (1/T_S)\,T_r\left(\frac{1}{\overline{T_r}}\right)e^{-T_r/\overline{T_r}}}{1 - e^{-T_S/\overline{T_r}} - (1/T_S)\int_0^{T_S} w\left(\frac{1}{\overline{T_r}}\right)e^{w/\overline{T_r}}dw}. \tag{4.7}$$

We can further simplify (4.7) by integrating the third term in the denominator,

$$g_{T_r}(T_r) = \frac{\left(\frac{1}{\overline{T_r}}\right)e^{-T_r/\overline{T_r}} - (1/T_S)\,T_r\left(\frac{1}{\overline{T_r}}\right)e^{-T_r/\overline{T_r}}}{1 - e^{-T_S/\overline{T_r}} - (\overline{T_r}/T_S) - (1+\frac{\overline{T_r}}{T_S})\,e^{-T_s/\overline{T_r}}}. \tag{4.8}$$

This equation can then be applied to a model where we vary the sample time parameter T_S and view changes to the form of the distribution in comparison to its underlying form, which is described in equation (4.5)

Similarly, we can solve equation (2.12) for a Pareto distribution of rest times,

$$f_{T_r}(T_r) = \frac{aT_m^a}{T_r^{a+1}}, \tag{4.9}$$

where T_m is the minimum rest time and a is a positive parameter which determines the concentration of data towards the mode. The censored cumulative distribution $F_{T_r}(T_S)$ of (4.9) is

$$F_{T_r}(T_S) = 1 - \left(\frac{T_m}{T_S}\right)^a. \tag{4.10}$$

We now rewrite (4.4), using (4.9) and (4.10), as

$$g_{T_r}(T_r) = \frac{\frac{aT_m^a}{T_r^{a+1}} - (1/T_s)T_r\left(\frac{aT_m^a}{T_r^{a+1}}\right)}{1 - \left(\frac{T_m}{T_S}\right)^a - (1/T_s)\int_0^{T_S} w\frac{aT_m^a}{T_r^{a+1}}dw}. \tag{4.11}$$

We further simplify (4.11) by integrating the third term in the denominator,

$$g_{T_r}(T_r) = \frac{\frac{aT_m^a}{T_r^{a+1}} - (1/T_s)T_r\left(\frac{aT_m^a}{T_r^{a+1}}\right)}{1 - \left(\frac{T_m}{T_S}\right)^a - (1/T_s)\left(\frac{-aT_m^aT_s^{1-a}}{a-1}\right)}. \tag{4.12}$$

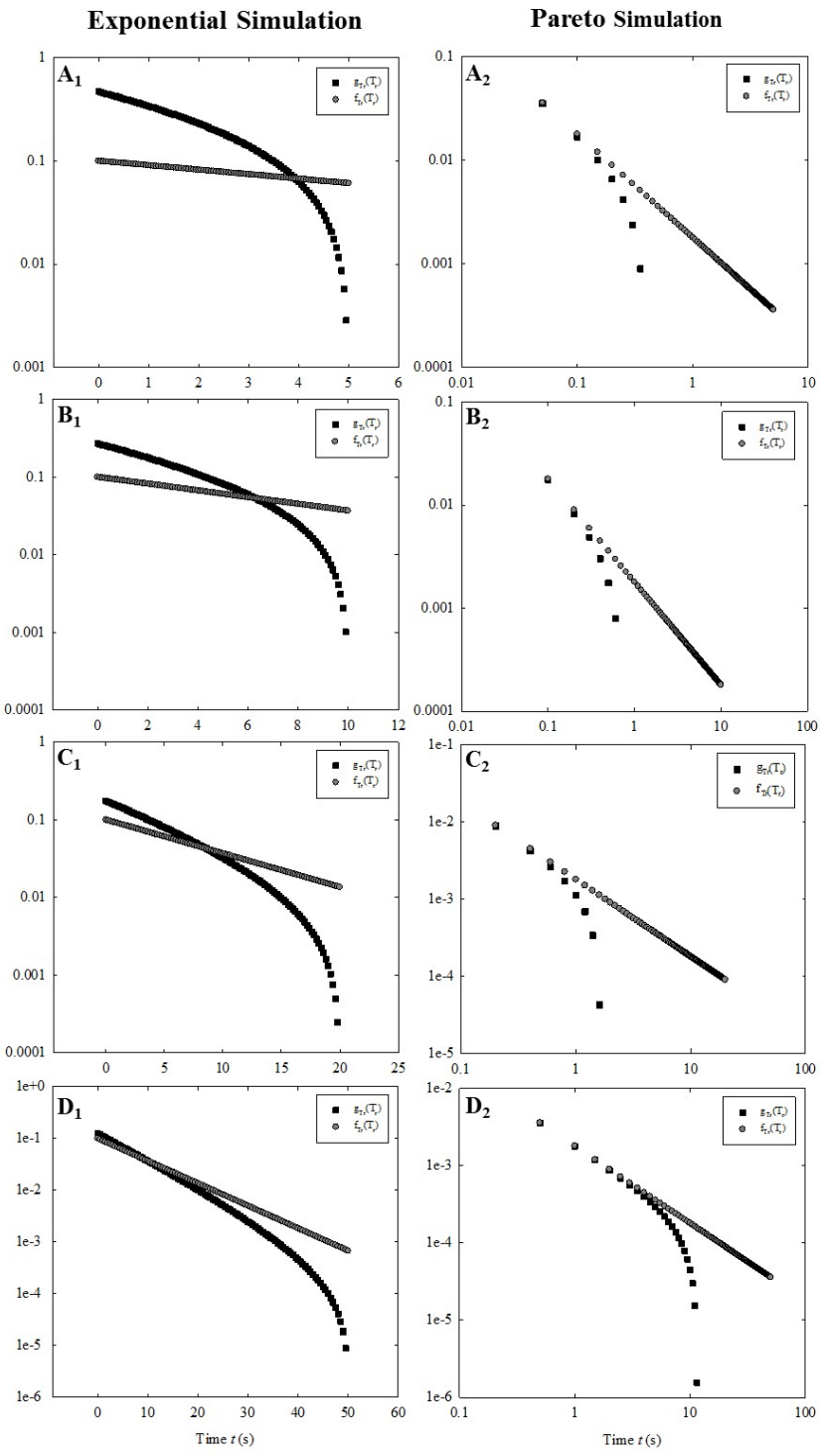

Figure 4.19: Results of analytical solutions for the rest time censorship equation for varying sample times. The sample times for A-D are as follows: 5, 10, 20, and 50 seconds. The left column represents the analytical solutions for a exponential distribution in semi-log space, while the right column shows the solutions for a Pareto distribution in log-log space. Here the gray circles indicate the uncensored distribution $f_{T_r}(T_r)$ and the black squares indicated the censored distribution $g_{T_r}(T_r)$ for increasingly long sampling times, from top to bottom.

It is important to note that we did not fit either distribution to our data, rather we use equations (4.8) and (4.9) to demonstrate the impact of short sampling times T_S. We chose the following parameters two use within these equations: the average rest time for an exponential distribution is $\overline{T_r} = 10$ seconds and the minimum rest time T_m in the Pareto distribution is 0.03 seconds. Figure 4.19 plots the censored and uncensored data for an exponential (left column) and a Pareto (right column) distribution for varying sampling times, where the censored data are plotted as black squares and the uncensored data are plotted as gray circles. The sample times T_S increase from top to bottom. Specifically, the sample time interval corresponds with the letter in the upper left corner of each subplot, such that A = 5 s, B = 10 s, C = 20 s, and D = 50 s. Notice that at increasingly large sample times T_S, the censored data approach the uncensored distribution.

First, we focus on the exponential simulation plots in Figure 4.19. Qualitatively, over much of the domain, the censored data resemble an exponential distribution, and would plot on a straight line in semi-log space. It is evident that the uncensored and censored data do not precisely coincide at short sampling times, yet the form of the censored distribution still appears to be exponentially distributed. These general trends are not evident within the Pareto simulation plots in Figure 4.19. At small rest times, the censored and uncensored distributions coincide, but with increasingly long rest times, there is a break in slope and values quickly become negative as a result of truncation (and therefore do not plot in log-log space). Interestingly, at short sample intervals, the censored Pareto distribution data plot approximately on a straight line, and therefore may appear exponential.

Let us consider these plots as a tool for identifying the form of a distribution. We fundamentally understand that the rest time data measured from Run 1 and 2, or any similar experiment, must be temporally censored. The results of this simulation indicate that if the underlying distribution is exponential, the censored data will still plot as an exponential distribution. However, a censored heavy-tailed, Pareto distribution appears quite different than the underlying uncensored distribution, where the slope changes from approximately

1, to significantly less than 1. This trend was not seen within our data found in Figure 4.17, where the slope changed from approximately 1, to slightly greater than 1.

From this simple test, we can conclude that measurement of rest times in Run 1 and Run 2 are likely not exponentially distributed. Although we suspect they may possess a heavy-tail, our analytical simulation of a Pareto distribution does not support this trend. More generally, this section highlights the need to consider the consequences of experimental censorship and to recognize potential biases inherent within measurements. This style of analysis, wherein we compare a theoretical distribution to a censored distributions, is a helpful starting point to analyzing experimental data.

4.9 Discussion

As summarized in the Introduction, to achieve a clearer understanding of the transport and spreading behavior of bed load sediment particles and tracers, more detailed descriptions of key features associated with the processes of particle entrainment and disentrainment are required. This is a data-rich paper, yet we note that a clearer understanding of these behaviors could be gained with high-fidelity automated particle tracking (*Fathel et al.*, 2015; *Furbish et al.*, 2016a). Our manual method provides accurate particle positions and the timing of entrainment and disentrainment events, but is time-intensive and does not allow for quick analysis of many images or of large areas. However, even with these limitations, our analysis has revealed a few interesting conclusions related to entrainment and disentrainment which merit elaboration.

Importantly, for the given bed stress conditions, there is no simple correlation between near-bed fluid velocities and particle entrainment locations. This result is unanticipated, yet revealing. By searching for a correlation between these two properties we assume that the near-bed fluid velocities are a measure of the drag force on the particle. In absence of this correlation, we find that (1) we must think more deeply about collective entrainment and how it 'works', and (2) we must consider how the microstructure of the particles on the bed

act to set up entrainment. The highly clustered nature of the spatial distributions of entrainment locations (Section 4.5) and the power-law like form of the distribution of particle wait times (Section 4.7) both suggest that collective entrainment may act as a control to activate particles. Although evidence shown here and similar work (e.g., *Ancey et al.*, 2008; *Ancey*, 2010) indicate that collective entrainment occurs is indeed evident, we need to better understand the spatio-temporal timescales and mechanics associated with this process to better understand its influence on bed load entrainment. With regard to the microstructure of the bed, we have found that microtopography likely influences the direction of initial particle motions (Section 4.4) and may also influence the ease at which a particle is activated (Section 4.7). We may therefore consider particle entrainment to ensue when the near-bed fluid velocity has a sufficiently high drag on the particle *and* when the bed surface microtopography is conducive to particle activation. We may imagine this joint occurrence similar to a joint probability distribution of particle entrainment wherein certain, yet unknown, joint conditions are needed from both the fluid and the microstructure of the bed to activate a given particle.

Let us further expand upon the microtopography of the bed as it pertains to the length of particle rest times. Within our analysis, we found that there are more long rest times in the higher activity experiment, Run 2, than within the lower activity experiment, Run 1. We suggest that this counterintuitive result may be caused by the microtopography of the bed, in that particles are more likely to stay in motion in Run 2 given the higher fluid velocity, and if particles pause it is more likely they have been lodged in a pocket that does not allow for easy reactivation. This parsimonious explanation for a phenomenon seen with this and other experiments (*Lamb et al.*, 2008; *Prancevic and Lamb*, 2015). *Prancevic and Lamb* (2015) suggest that models for lowland rivers significantly over-predict sediment transport rates in steep mountain streams due to increased friction angles caused by interlocking grains and particle burial. Perhaps a simplified explanation for this behavior is the trade-off between fluid velocities and pocket angles suggested within this paper.

Our analysis of wait times, while preliminary, suggests that these cannot be simply defined as a exponential distribution. Recent work (e.g., *Ancey et al.*, 2008; *Bradley and Tucker*, 2012) has shown interest in the nature of this distribution, yet empirical evidence of its form is limited. The data presented here indicates an amount of intermittence in sediment transport dependent on the size of the examination area. This highlights that care must be taken when examining these sorts of measurements, as the form of the distribution varies with the window size and therefore we must consider this relationship when setting the transport intensity. We must also be careful when analyzing rest time distributions, as we show that rest time distributions exhibit temporal censorship. Rest times are measured infrequently within our sampling, which fundamentally censors these data. These results point to the importance of addressing censorship, both spatial and temporal, within data sets.

4.10 Conclusions

This paper presents an abundant, myriad of data. In particular this work presents many measurements which have never before been presented with this precision. Although much of this work is preliminary, we are left with several main conclusions.

(1) Microtopographic evidently influences initial motion. We find that the first direction of particle motions is highly varied, and the particle microtopography seems to have a larger consequence on the direction of motion in lower-velocity flows. We also suggest that the spatial clustering of entrained particles may also be a product of microtopography, wherein there are preferentially activated patches on the stream-bed defined by local topography.

(2) Somewhat surprisingly, within both methods for analyzing the relationship between near-bed fluid velocities and entrained particles, we find that there is not a strong correlation between the two measurements. This work is decidedly preliminary, yet it seems to suggest that the relationship between these two measures are more complicated than we first suspected. To further investigate the relationship between particle motions and the

near-bed fluid, in the future we need to examine the influence of collective entrainment and the the microstructure of the bed in terms of particle entrainment.

(3) We provide empirical evidence of the wait time distribution which may be used to understand the transport intensity in varying windows sizes. Furthermore, the form of the distribution appears to follow a power-law distribution and therefore suggests that bed load transport may not be defined in terms of a Poisson process wherein particles are entrained only when the fluid-derived forces acting on a stationary particle exceed the resisting force and there is no collective entrainment.

(4) Measurements of particle rest times are inconsistent with a purely exponential distribution, but also seem to be more complicated than a simple heavy-tailed distribution. We note that this result may be a function of experimental censorship, and provide a guide to analyzing potential consequences of temporal (and spatial) censorship within measurements.

(5) There is a pressing need for improving automated particle tracking methods that can provide high fidelity measurements of the bed load particle motions, which will ultimately allow us to gain a clearer understanding of the properties and controls on particle entrainment.

CHAPTER 5

Conclusions and Looking Forward

We start with a summary of the primary conclusions found within Chapters 2 through 4, then move to reoccurring conclusions found throughout this dissertation, and finally address areas of future work that would nicely follow this dissertation.

Within Chapter 2, we used particle tracking of sediment motions from an experiment to define the forms and qualities of the ensemble distributions of particle velocities, accelerations, hop distances, and travel times. This acts to best represent the probabilistically expected behavior of particle motions consistent with the macroscopic and sediment flow conditions. More specifically, our data show exponential distributions for the streamwise and cross-stream particle velocities. Importantly, we confirm the presence of a "light" tail in the streamwise velocities, such that the largest velocities are limited by the near-bed fluid. We find that both the streamwaise and cross-stream components of hop distances possess Weibull distributions, which is contrary to previous work and supports a decreasing spatial disentrainment rate. Furthermore, streamwise and cross-stream components of the hop distances vary nonlinearly with travel times, which suggests that if particles gain a sufficiently high velocity, they tend to travel farther in a shorter amount of time than similar slower moving particles.

Chapter 3 reveals variations in the apparent type of diffusion based on differences in the calculation of the mean-squared displacement. We find that the ensemble calculation of the mean squared displacement reveals ballistic-like behavior at the shortest (10^{-2} s) timescale, followed by apparent anomalous behaviors. Because the ensemble calculation is based on all paired coordinate positions associated with time intervals without reference to when the motions started, this calculation is appropriate for describing particle diffusion in relation to the particle flux. In the context of the tracer calculation, which treats particles

as a 'virtual plume', particles exhibit inhomogeneous diffusive behavior because both the mean and the variance of the particle travel distances increase nonlinearly with increasing travel times. Inhomogeneous diffusion indeed represents the spreading of tracer particles, and whereas the mean squared displacement has the signature of anomalous diffusion, this behavior is not anomalous diffusion as normally envisioned. It is a consequence of the tracer calculation of mean squared displacement, which start all full hops at the same time and averages over particle displacements rather than all paired observations separated by a time interval as is done in the ensemble calculation. The analysis presented in this chapter indicates that care is needed in suggesting anomalous behavior when appealing to conventional measures of diffusion formulated for ideal (Brownian) particle systems.

In Chapter 4 we focus on key measurements associated with the processes of entrainment and disentrainment. We find that the effects of microtopography on initial motion are evident on the particle-scale and influence the initial directions of motion and may also create preferential entrainment areas. Somewhat surprisingly, our analysis did not reflect a relationship between near-bed fluid velocities and the entrainment of particles. This suggests that the relationship may be more complicated than we anticipated, possibly indicating that we must further examine the influence of collective entrainment and the microstructure of the bed in relation to sediment entrainment. In addition to these findings from each chapter, there is also a certain amount of overlap within these final conclusions. Firstly, the probabilistic methods used within this dissertation have proven to be valuable. In recent years, researchers have built on ideas introduced by (*Einstein*, 1937, 1942, 1950), wherein research has provided probabilistic descriptions of bed load motions and transport which pertain to the particle flux (e.g., *Ancey et al.*, 2006; *Furbish et al.*, 2012a; *Ancey and Heyman*, 2014; *Heyman*, 2014) and to tracer particles (e.g., *Nikora et al.*, 2002; *Schumer et al.*, 2009; *Bradley and Tucker*, 2010; *Hill et al.*, 2010; *Ball*, 2012; *Lajeunesse et al.*, 2013; *Martin et al.*, 2014). While this field is certainly growing, this style of analysis is still in its infancy and current research (including the work presented in this dissertation)

is working to explore the limits of new measurement techniques, including high-speed imagery, to better observe and measure particle motions. The combination of work presented here is aimed at describing the probabilistically expected behavior of particles and we have utilized this methodology with respect to the idea of ensemble behavior, the process of particle diffusion, and to the processes of entrainment and disentrainment. In each of these cases, it is clear that these probabilistic methods provide and reveal additional information concerning the behavior and nature of sediment transport.

To confidently define statistical descriptions of key bed load particle motions and behaviors, large data sets must be obtained. In this dissertation, I manually tracked particle motions from start-to-stop in two different experiments which amounted to over 300,000 individual particle positions. This time-intensive method provides high-fidelity measurements of small particle displacements and velocities which dominate bed load particle motions (*Fathel et al.*, 2015). The data extracted from particle tracking allows for careful characterization sediment motions and behaviors, but has certain limitations. The time-intensive nature of this process makes analysis of many different experimental conditions or of long time periods exceedingly difficult. Thus, there is a pressing need for improving automated particle tracking methods that can provide high fidelity measurements of the bed load particle motions. Furthermore, the manual tracking in this dissertation could act as an ideal set of measurements to test the performance of automated tracking softwares.

Throughout this dissertation, I also consider limitations of the data sets by acknowledging experimental censorship of the measured quantities, both in space and time. Video imaging of particle motions provides valuable data to infer the forms of distributions of key elements of bed load transport. These techniques are becoming increasingly popular, so there is value in paying attention to the details of what is actually being estimated. In particular, the motions of particles that enter or leave the video sampling area are spatially censored, and particles that are in motion when the video starts or stops are temporally censored. For example, in Chapter 2 we show that spatial censorship of streamwise hop

distances and associated travel times has the visual effect of preferentially reducing the largest hop distances and associated travel times, which gives the appearance of a less steep overall relationship between these quantities. Similarly, in Chapter 4, we indicate that the distribution of rest times is fundamentally temporally censored given the relatively small number of frames analyzed.

The rich nature of the data sets obtained from manual particle tracking along with measurements of near-bed fluid velocities provides multiple avenues for future work. Perhaps the most intriguing future work is related to the relationship between the fluid and particle motions. The relationship between sediment entrainment and near-bed fluid velocities is decidedly complex and merits closer analysis. Also, we have yet to address the relationship between moving particles and the near-bed fluid velocities, which may reveal a clearer connection between these properties, especially as a given particle interacts less with the bed and motions become fluid-dominated.

Importantly, the methods used throughout this dissertation are applicable to other experimental conditions and natural systems. The entirety of data presented here is from two controlled, single particle-size experiments. This work focused on a single particle size has proven to be important to understanding fundamental particle motions, yet to properly understand natural systems we must analyze sediment transport in mixed particle systems, like those found in nature. For example, future work should be conducted to determine underlying ensemble distributions of particle motions in mixed-size systems. Also comparisons of the ensemble distributions of individual particle sizes within the mixed system to these data to similar, single-size sediment systems. We expect complexities introduced by interactions between particles of varying sizes, such as shielding from entrainment and particle sorting and burial of smaller particles. By using the same methodology under different experimental conditions, we move a step closer to providing more accurate descriptions of sediment transport that may be used to better understand bed load sediment transport.

BIBLIOGRAPHY

Ancey, C. (2010), Stochastic modeling in sediment dynamics: Exner equation for planar bed incipient bed load transport conditions, *Journal of Geophysical Research*, *115*, doi: 10.1029/2009JF001260.

Ancey, C., and J. Heyman (2014), A microstructural approach to bed load transport: mean behaviour and fluctuations of particle transport rates, *Journal of Fluid Mechanics*, *744*, 129–168, doi:10.1017/jfm.2014.74.

Ancey, C., T. Böhm, M. Jodeau, and P. Frey (2006), Statistical description of sediment transport experiments, *Physical Review E*, *74*(1), 011,302.

Ancey, C., A. C. Davison, T. Böhm, M. Jodeau, and P. Frey (2008), Entrainment and motion of coarse particles in a shallow water stream down a steep slope, *Journal of Fluid Mechanics*, *595*, 83–114, doi:10.1017/S0022112007008774.

Armanini, A., V. Cavedon, and M. Righetti (2014), A probabilistic/deterministic approach for the prediction of the sediment transport rate, *Advances in Water Resources*, doi:10. 1016/j.advwatres.2014.09.008.

Ball, A. E. (2012), Measurements of bed load particle diffusion at low transport rates, Junior thesis, Vanderbilt University, Nashville.

Bialik, R., V. Nikora, and P. Rowiński (2012), 3d Lagrangian modelling of saltating particles diffusion in turbulent water flow, *Acta Geophysica*, *60*(6), 1639–1660, doi: 10.2478/s11600-012-0003-2.

Bialik, R. J. (2013), Numerical study of near-bed turbulence structures influence on the initiation of saltating grains movement, *Journal of Hydrological Hydromechanics*, *61*, 202–207, doi:110.2478/johh-2013-0026.

Bialik, R. J., V. I. Nikora, M. Karpiński, and P. M. Rowiński (2015), Diffusion of bedload particles in open-channel flows: distribution of travel times and second-order statistics of particle trajectories, *Environmental Fluid Mechanics*, *15*(6), 1281–1292, doi:10.1007/s10652-015-9420-5.

Box, G. E. P., and G. M. Jenkins (1976), *Time Series Analysis, Forcasting and Control*, Holden-Day.

Bradley, D., and G. Tucker (2010), Fractional dispersion in a sand bed river, *Journal of Geophysical Research: Earth Surface*, doi:10.1029/2009JF001268.

Bradley, N. a., and G. E. Tucker (2012), Measuring gravel transport and dispersion in a mountain river using passive radio tracers, *Earth Surface Processes and Landforms*, *37*(10), 1034–1045, doi:10.1002/esp.3223.

Brayshaw, A. (1985), Bed microtopography and entrainment thresholds in gravel-bed rivers, *Geological Society of America Bulletin*, *96*(2), 218, doi:10.1130/0016-7606(1985)96⟨218:BMAETI⟩2.0.CO;2.

Bridge, J., and S. Bennett (1992), A model for the entrainment and transport of sediment grains of mixed sizes, shapes, and densities, *Water Resources Research*, doi:10.1029/91WR02570.

Buffington, J., and W. Dietrich (1992), Friction angle measurements on a naturally formed gravel streambed: Implications for critical boundary shear stress, *Water Resources* , doi:10.1029/91WR02529.

Buffington, J., and D. Montgomery (1997), A systematic analysis of eight decades of incipient motion studies, with special reference to gravelbedded rivers, *Water Resources Research*, doi:10.1029/96WR03190.

Campagnol, J., A. Radice, R. Nokes, V. Bulankina, A. Lescova, and F. Ballio (2013), Lagrangian analysis of bed-load sediment motion: Database contribution, *Journal of Hydraulic Research*, *51*, 589–596, doi:10.1080/00221686.2013.812152.

Campagnol, J., A. Radice, F. Ballio, and V. Nikora (2015), Particle motion and diffusion at weak bed load: accounting for unsteadiness effects of entrainment and disentrainment, *Journal of Hydraulic Research*, *53*(5), 633–648, doi:10.1080/00221686.2015.1085920.

Church, M. (1977), Palaeohydrological reconstructions from a holocene valley fill.

Church, M., and R. I. Ferguson (2015), Morphodynamics: Rivers beyond steady state, *Water Resources Research*, *51*(4), 1883–1897, doi:10.1002/2014WR016862.

Church, M., M. A. Hassan, and J. F. Wolcott (1998), Stabilizing self-organized structures in gravel-bed stream channels: Field and experimental observations, *Water Resources Research*, *34*(11), 3169–3179.

de Jager, M., F. Bartumeus, A. Kölzsch, F. J. Weissing, G. M. Hengeveld, B. A. Nolet, P. M. Herman, and J. van de Koppel (2014), How superdiffusion gets arrested: ecological encounters explain shift from Lévy to Brownian movement, *Proceedings of the Royal Society of London B: Biological Sciences*, *281*(1774), 20132,605, doi:10.1098/rspb.2013.2605.

Drake, T. G., R. L. Shreve, W. E. Dietrich, P. J. Whiting, and L. B. Leopold (1988), Bed-load transport of fine gravel observed by motion-picture photography, *Journal of Fluid Mechanics*, *192*, 193–217.

DuBoys, M. (1879), Le rhône et les rivières à lit affouillable, *Ann. Ponts Chaussees*, *18*, 141–148.

Dunkerley (1990), The development of armour in the tambo river, victoria, australia, *Earth Surface Processes and Landforms*, *15*(5), 405412, doi:10.1002/esp.3290150504.

Dwivedi, A., B. Melville, and A. Y. Shamseldin (2010), Hydrodynamic forces generated on a spherical sediment particle during entrainment, *Journal of Hydraulic Engineering*, *136*(10), 756–769, doi:10.1061/(ASCE)HY.1943-7900.0000247.

Einstein, A. (1905), Über die von der molekularkinetischen theorie der wärme geforderte bewegung von in ruhenden flüssigkeiten suspendierten teilchen, *Annalen der physik*, *322*(8), 549–560.

Einstein, H. A. (1937), Bedload transport as a probability problem, Ph.D. thesis, Mitt. Versuchsanst. Wasserbau Eidg. Tech. Hochsch, Zürich, Switzerland.

Einstein, H. A. (1942), Formula for the transportation of bed load, *Trans. Am. Soc. Civ. Eng.*, *107*, 561–597.

Einstein, H. A. (1950), The bed-load function for sediment transportation in open channels, *Department of Agriculture Technical Bulletin*.

Fan, N., D. Zhong, B. Wu, E. Foufoula-Georgiou, and M. Guala (2014), A mechanistic-stochastic formulation of bed load particle motions: From individual particle forces to the fokker-planck equation under low transport rates, *Journal of Geophysical Research: Earth Surface*, *119*(3), 464,482, doi:10.1002/2013JF002823.

Fathel, S., D. Furbish, and M. Schmeeckle (2016), Parsing anomalous versus normal diffusive behavior of bed load sediment particles, *Earth Surface Processes and Landforms*, pp. n/a–n/a, doi:10.1002/esp.3994.

Fathel, S., D. Furbish, and M. Schmeeckle (in prep.), Experimental exploration of elements of sediment entrainment and disentrainment.

Fathel, S. L., D. J. Furbish, and M. W. Schmeeckle (2015), Experimental evidence of statistical ensemble behavior in bed load sediment transport, *Journal of Geo-*

physical Research: Earth Surface, *120*(11), 2298–2317, doi:10.1002/2015JF003552, 2015JF003552.

Fenton, J., and J. Abbott (1977), Initial movement of grains on a stream bed: The effect of relative protrusion, *352*(1671), 523537, doi:10.1098/rspa.1977.0014.

Foufoula-Georgiou, E., and C. Stark (2010), Introduction to special section on stochastic transport and emergent scaling on earth's surface: Rethinking geomorphic transport-Stochastic theories, broad scales of motion and nonlocality, *Journal of Geophysical Research*, *115*, doi:10.1029/2010JF001661.

Frey, P., and M. Church (2009), How rivers move, *Science Magazine*, *325*(5947), 1509–1510, doi:DOI:10.1126/science.1178516.

Furbish, D., and P. Haff (2010), From divots to swales: Hillslope sediment transport across divers length scales, *Journal of Geophysical Research*, *115*(F3), doi:10.1029/2009JF001576.

Furbish, D., and M. Schmeeckle (2013), A probabilistic derivation of the exponential-like distribution of bed load particle velocities, *Water Resources Research*, *49*(3), 15371,551, doi:10.1002/wrcr.20074.

Furbish, D., A. Arnold, and S. Hansard (1990), The species censorship problem: A general solution, *International Association for Mathematical Geology*.

Furbish, D., P. Haff, J. Roseberry, and M. Schmeeckle (2012a), A probabilistic description of the bed load sediment flux: 1. theory, *Journal of Geophysical Research*, *117*(F3), doi:10.1029/2012JF002352.

Furbish, D., A. Ball, and M. Schmeeckle (2012b), A probabilistic description of the bed load sediment flux: 4. fickian diffusion at low transport rates, *Journal of Geophysical Research*, *117*(F3), doi:10.1029/2012JF002356.

Furbish, D. J., J. C. Roseberry, and M. W. Schmeeckle (2012c), A probabilistic description of the bed load sediment flux: 3. the particle velocity distribution and the diffusive flux, *Journal of Geophysical Research*, *117*(F3).

Furbish, D. J., S. L. Fathel, and M. Schmeeckle (2016a), *Particle Motions and Bed Load Theory: The Entrainment Forms of the Flux and the Exner Equation*, John Wiley and Sons.

Furbish, D. J., M. Schmeeckle, R. Schumer, and S. L. Fathel (2016b), Probability distributions of bed-load particle velocities, accelerations, hop distances and travel times informed by Jayness principle of maximum entropy, *Journal of Geophysical Research: Earth Surface*, doi:10.1002/2016JF003833.

Ganti, V., M. M. Meerschaert, E. Foufoula-Georgiou, E. Viparelli, and G. Parker (2010), Normal and anomalous diffusion of gravel tracer particles in rivers, *Journal of Geophysical Research: Earth Surface*, *115*(F2), doi:10.1029/2008JF001222.

Gibbs, J. W. (1902), *Elementary Pinciples in Statistical Mechanics*, Yale University Press.

Gomez, B., and M. Church (1989), An assessment of bed load sediment transport formulae for gravel bed rivers, *Water Resources Research*, *25*(6), 1161–1186, doi:10.1029/WR025i006p01161.

Grass, A. J. (1970), Initial instability of fine bed sand, *Journal of the Hydraulics Division*, *96*(3), 619–632.

Grass, A. J. (1971), Structural features of turbulent flow over smooth and rough boundaries, *Journal of Fluid Mechanics*, *50*, 233–255, doi:10.1017/S0022112071002556.

Habersack, H. (2001), Radio-tracking gravel particles in a large braided river in new zealand: A field test of the stochastic theory of bed load transport proposed by einstein, *Hydrological Processes*, *15*(3), 377–391.

Hassan, M., H. Voepel, R. Schumer, G. Parker, and L. Fraccarollo (2013), Displacement characteristics of coarse fluvial bed sediment, *Journal of Geophysical Research: Earth Surface*, *118*(1), 155,165, doi:10.1029/2012JF002374.

Hassan, M. A., M. Church, and A. P. Schick (1991), Distance of movement of coarse particles in gravel bed streams, *Water Resources Research*, *27*(4), 503–511, doi:10.1029/90WR02762.

Hassan, M. A., et al. (2008), Salmon-driven bed load transport and bed morphology in mountain streams, *Geophysical Research Letters*, *35*(4), doi:10.1029/2007GL032997.

Heyman, J. (2014), A study of the spatio-temporal behaviour of bed load transport rate fluctuations, Ph.d. thesis, École Polytechnique Fédérale de Lausanne.

Heyman, J., and C. Ancey (2014), *Tracking bed load particles in a steep flume: methods and results*, CRC Press.

Heyman, J., F. Mettra, H. B. Ma, and C. Ancey (2013), Statistics of bedload transport over steep slopes: Separation of time scales and collective motion, *Geophysical Research Letters*, *40*(1), 128–133, doi:10.1029/2012GL054280.

Heyman, J., H. B. Ma, F. Mettra, and C. Ancey (2014), Spatial correlations in bed load transport: Evidence, importance, and modelling., *Journal of Geophysical Research: Earth Surface*, doi:10.1002/2013JF003003.

Hill, K., L. DellAngelo, and M. M. Meerschaert (2010), Heavy-tailed travel distance in gravel bed transport: An exploratory enquiry, *Journal of Geophysical Research*, *115*, doi:10.1029/2009JF001276.

Hirano, M. (1971), River-bed degredation with armoring, *Proceedings of the Japan Society of Civil Engineers*, *1971*(195), 5565, doi:10.2208/jscej1969.1971.195_55.

Houssais, M., C. P. Ortiz, D. J. Durian, and D. J. Jerolmack (2015), Onset of sediment transport is a continuous transition driven by fluid shear and granular creep, *Nature Communications*, *6*(6527), doi:10.1038/ncomms7527.

Huang, R., I. Chavez, K. M. Taute, B. Lukić, S. Jeney, M. G. Raizen, and E.-L. Florin (2011), Direct observation of the full transition from ballistic to diffusive Brownian motion in a liquid, *Nature Physics*, *7*(7), 576–580, doi:10.1038/nphys1953.

Jackson, R. G. (1976), Sedimentological and fluid-dynamic implications of the turbulent bursting phenomenon in geophysical flows, *Journal of Fluid Mechanics*, *77*(03), 531–560.

Kidanemariam, A. G., and M. Uhlmann (2014), Direct numerical simulation of pattern formation in subaqueous sediment, *Journal of Fluid Mechanics*, doi:10.1017/jfm.2014.284.

Kittel, C. (1958), *Elementary Statistical Physics*, John Wiley and Sons.

Komar, P., and Z. Li (1986), Pivoting analyses of the selective entrainment of sediments by shape and size with application to gravel threshold, *Sedimentology*, *33*(3), 425436, doi:10.1111/j.1365-3091.1986.tb00546.x.

Lajeunesse, E., L. Malverti, and F. Charru (2010), Bed load transport in turbulent flow at the grain scale: Experiments and modeling, *Journal of Geophysical Research*, *115*(F4), doi:10.1029/2009JF001628.

Lajeunesse, E., O. Devauchelle, M. Houssais, and G. Seizilles (2013), Tracer dispersion in bedload transport, *Advances in Geosciences*, *37*(37), 16, doi:10.5194/adgeo-37-1-2013.

Lamb, M. P., W. E. Dietrich, and J. G. Venditti (2008), Is the critical shields stress for incipient sediment motion dependent on channel-bed slope?, *Journal of Geophysical Research: Earth Surface*, *113*(F2), n/a–n/a, doi:10.1029/2007JF000831, f02008.

Laronne, J., and M. Carson (1976), Interrelationships between bed morphology and bed-material transport for a small, gravel-bed channel, *Sedimentology*, *23*(1), 67–85.

Li, T., S. Kheifets, D. Medellin, and M. G. Raizen (2010), Measurement of the instantaneous velocity of a Brownian particle, *Science*, *328*(5986), 1673–1675, doi: 10.1126/science.1189403.

Martin, R., P. Purohit, and D. Jerolmack (2014), Sedimentary bed evolution as a mean-reverting random walk: Implications for tracer statistics, *Geophysical Research Letters*, doi:10.1002/2014GL060525.

Martin, R. L., D. J. Jerolmack, and R. Schumer (2012), The physical basis for anomalous diffusion in bed load transport, *Journal of Geophysical Research: Earth Surface (2003–2012)*, *117*(F1).

Mazumder, R. (2000), Turbulence–particle interactions and their implications for sediment transport and bedform mechanics under unidirectional current: some recent developments, *Earth-Science Reviews*, *50*(1), 113–124.

Nelson, J. M., R. L. Shreve, S. R. McLean, and T. G. Drake (1995), Role of near-bed turbulence structure in bed load transport and bed form mechanics, *Water Resources Research*, *31*(8), 2071–2086.

Nezu, I., H. Nakagawa, and G. Jirka (1994), Turbulence in open-channel flows, *Journal of Hydraulic Engineering*.

Nikora, V., H. Habersack, T. Huber, and M. Ian (2002), On bed particle diffusion in gravel bed flows under weak bed load transport, *Water Resources Research*, *38*(6), 17–11, doi: 10.1029/2001WR000513.

Paintal, A. (1971), A stochastic model of bed load transport, *Journal of Hydraulic Research*, *9*(4), 527–554.

Paola, C., and R. Seal (1995), Grain size patchiness as a cause of selective deposition and downstream fining, *Water Resources Research*, *31*(5), 1395–1407, doi:10.1029/94WR02975.

Papanicolaou, A., P. Diplas, C. Dancey, and M. Balakrishnan (2001), Surface roughness effects in near-bed turbulence: Implications to sediment entrainment, *Journal of Engineering Mechanics*, *127*(3), 211–218.

Papanicolaou, A., P. Diplas, N. Evaggelopoulos, and S. Fotopoulos (2002), Stochastic incipient motion criterion for spheres under various bed packing conditions, *Journal of Hydraulic Engineering*, *128*(4), 369–380, doi:10.1061/(ASCE)0733-9429(2002)128:4(369).

Parker, G. (1991), Selective sorting and abrasion of river gravel. i: Theory, *Journal of Hydraulic Engineering*, *117*(2), 131–147, doi:10.1061/(ASCE)0733-9429(1991)117:2(131).

Parker, G., G. Seminara, and S. Luca (2000a), Bed load at low Sheilds stress on arbitrarily sloping beds: Alernative entrainment formulation, *Water Resources Research*, doi:10.1029/2001WR001253.

Parker, G., C. Paola, and S. Leclair (2000b), Probabilistic Exner sediment continuity equation for mixtures with no active layer, *Journal of Hydraulic Engineering*.

Pelosi, A., G. Parker, R. Schumer, and H. Ma (2014), Exner-based master equation for transport and dispersion of river pebble tracers: Derivation, asymptotic forms, and quantification of nonlocal vertical dispersion, *Journal of Geophysical Research: Earth Surface*, doi:10.1002/2014JF003130.

Powell, D. M., and P. J. Ashworth (1995), Spatial pattern of flow competence and bed load transport in a divided gravel bed river, *Water Resources Research*, *31*(3), 741–752, doi:10.1029/94WR02273.

Prancevic, J. P., and M. P. Lamb (2015), Particle friction angles in steep mountain channels, *Journal of Geophysical Research: Earth Surface*, *120*(2), 242–259, doi: 10.1002/2014JF003286, 2014JF003286.

Radice, A., V. Nikora, J. Campagnol, and F. Ballio (2013), Active interactions between turbulence and bed load: Conceptual picture and experimental evidence, *Water Resources Research*, *49*(1), 9099, doi:10.1029/2012WR012255.

Raudkivi, A. J., and R. Ettema (1982), Stability of armour layers in rivers, *Journal of the Hydraulics Division*, *108*(9), 1047–1057.

Recking, A. (2012), Influence of sediment supply on mountain streams bedload transport, *Geomorphology*, *175*, 139–150, doi:doi:10.1016/j.geomorph.2012.07.005.

Rickenmann, D. (2001), Comparison of bed load transport in torrents and gravel bed streams, *Water Resources Research*, *37*(12), 3295–3305, doi:10.1029/2001WR000319.

Roseberry, J., M. Schmeeckle, and D. Furbish (2012), A probabilistic description of the bed load sediment flux: 2. particle activity and motions, *Journal of Geophysical Research*, *117*(F3), doi:10.1029/2012JF002353.

Sayre, W. W., and D. W. Hubbell (1965), Transport and dispersion of labeled bed material: North Loup River, Nebraska, *United States Geological Survey Professional Paper*, *433*(C).

Schmeeckle, M. (2014a), The role of velocity, pressure, and bed stress fluctuations in bed load transport over bed forms: numerical simulation downstream of a backward-facing step, *Earth Surface Dynamics Discussions*, *2*(2), 715–732, doi: 10.5194/esurfd-2-715-2014.

Schmeeckle, M., and D. Furbish (2007), A Fokker-Planck model of bedload transport and morphodynamics, paper presented at the stochastic transport and Emerging Scaling on

Earth's Surface (stress) work group meeting, *Natl. Cent. for Earth-Surf. Dyn., Univ. of Ill. and Desert Res. Inst., Lake Tahoe, Nev*.

Schmeeckle, M. W. (2014b), Numerical simulation of turbulence and sediment transport of medium sand, *Journal of Geophysical Research: Earth Surface*, doi:10.1002/2013JF002911.

Schumer, R., M. M. Meerschaert, and B. Baeumer (2009), Fractional advection dispersion equations for modeling transport at the earth surface, *Journal of Geophysical Research: Earth Surface*, *114*(F4), doi:10.1029/2008JF001246.

Seizilles, G., E. Lajeunesse, O. Devauchelle, and M. Bak (2014), Cross-stream diffusion in bedload transport, *Physics of Fluids*, *26*, doi:10.1063/1.4861001.

Seminara, G., L. Solari, and G. Parker (2002), Bed load at low shields stress on arbitrarily sloping beds: Failure of the bagnold hypothesis, *Water resources research*, *38*(11), 31–1.

Shields, A. (1936), Anwendung der aehnlichkeitsmechanik und der turbulenzforschung auf die geschiebebewegung, *Tech. rep.*, Preussischen Versuchsanstalt für Wasserbau.

Singh, A., E. Foufoula-Georgiou, F. Porté-Agel, and P. R. Wilcock (2012), Coupled dynamics of the co-evolution of gravel bed topography, flow turbulence and sediment transport in an experimental channel, *Journal of Geophysical Research: Earth Surface (2003–2012)*, *117*(F4).

Stelczer, K. (1981), *Bed Load Transport: Theory and Practice*, Water Resources Publishing.

Sumer, B. M., L. H. Chua, N.-S. Cheng, and J. Fredsøe (2003), Influence of turbulence on bed load sediment transport, *Journal of Hydraulic Engineering*, *129*(8), 585–596.

Taylor, G. (1922), Diffusion by continuous movements, *Proceedings for the London Math Society*, *20*, 196–212.

Tolman, R. C. (1938), *The Principles of Statistical Mechanics*, Oxford.

Turowski, J. M. (2010), Probability distributions of bed load transport rates: A new derivation and comparison with field data, *Water Resources Research*, *46*(8), n/a–n/a, doi: 10.1029/2009WR008488, w08501.

Viswanathan, G., E. Raposo, F. Bartumeus, J. Catalan, and M. Da Luz (2005), Necessary criterion for distinguishing true superdiffusion from correlated random walk processes, *Physical Review E*, *72*(1), 011,111, doi:10.1103/PhysRevE.72.011111.

Voepel, H., R. Schumer, and M. A. Hassan (2013), Sediment residence time distributions: Theory and application from bed elevation measurements, *Journal of Geophysical Research: Earth Surface*, *118*(4), 2557–2567, doi:10.1002/jgrf.20151, 2013JF002816.

Voller, V., and C. Paola (2010), Can anomalous diffusion describe depositional fluvial profiles?, *Journal of Geophysical Research: Earth Surface*, doi:10.1029/2009JF001278.

Vollmer, S., and M. Kleinhans (2007), Predicting incipient motion, including the effect of turbulent pressure fluctuations in the bed, *Water Resources Research*, *43*(5), doi:10.1029/2006WR004919.

von Smoluchowski, M. (1906), Zur kinetischen theorie der brownschen molekularbewegung und der suspensionen, *Annalen der physik*, *326*(14), 756–780.

Wilcock, P. (2001), Toward a practical method for estimating sediment transport rates in gravel-bed rivers, *Earth Surface Processes and Landforms*, *26*, 1395–1408, doi:10.1002/esp.301.

Wong, M., G. Parker, P. DeVries, T. Brown, and S. Burges (2007), Experiments on dispersion of tracer stones under lower-regime plane-bed equilibrium bed load transport, *Water Resources Research*, *43*(3), doi:10.1029/2006WR005172.

Yager, E. M., J. W. Kirchner, and W. E. Dietrich (2007), Calculating bed load transport in steep boulder bed channels, *Water Resources Research*, *43*(7), n/a–n/a, doi:10.1029/2006WR005432, w07418.

Zanke, U. (2003), On the influence of turbulence on the initiation of sediment motion, *International Journal of Sediment Research*, *18*(1), 17–31.